Characterization of transport properties of bacterial porins : a study of internal dynamics-function relationship.

Cécile Bon[#], Christophe Danelon[#], Franck Gabel*, Mathias Winterhalter[#], Giuseppe Zaccaï*.
[#]Biophysique membranaire, Institut de Pharmacologie et de Biologie Structurale, 205 route de Narbonne, 31077 Toulouse Cedex, France.
* Biophysique moléculaire, Institut de Biologie Structurale, 41 rue Jules Horowitz F-38027 Grenoble Cedex 1 France.

Introduction

Gram-negative bacteria such that Escherichia Coli are surrounded by two lipid bilayer membranes, which confine the periplasmic space containing the murein cell wall. The outer membrane protects the bacteria against a harsh environment. At the same time, the embedded proteins fulfil a number of tasks that are crucial to the bacterial cell, such as solute and protein translocation, as well as signal transduction. Known integral membrane protein of the outer membrane all consist of anti-parallel beta-barrels, whereas membrane proteins from all other source consist of the alpha helix bundle, represented by the bacteriorhodopsin. These two structural families of integral proteins display distinctive biological functions, which are very likely to be associated with distinctive dynamics.

Porins are integral membrane proteins of the outer membrane of bacteria, that create transmembrane channels. They all fold in a closed β-sheet, exposed to a hydrophobic environment on one side and an aqueous channel on the other, with short turns at the periplasmic side and large loops at the outside of the cell [1]. They can be divided into three classes according to their function: i) general diffusion pores ii) specific channels containing a binding site for a certain solute. iii) active transporting, energy-consuming, channels. All these porins have their specific features and can serve as models for other channel forming proteins or peptides (eukaryotic channels, toxins, bacteriocins…). Benefits to choose these proteins as model are several : most of them can be overproduced to give high yields, and are extremly stable. The structure at atomic resolution has became known for several porins of each class [2,3], while the detergent distribution was revealed by neutron diffraction, using contrast variation [4,5]. Many mutants have been characterized.

OmpF is a trimer and belongs to the general diffusion class of porins [1]; it allows the diffusion of hydrophilic molecules accross the outer membrane with molecular weights up to approximatively 600 Da. It is believed to be the principal pathway for β-lactam antibiotics. OmpF has no specificity, and a weak selectivity towards cations. Moreover it exhibits an intriguing phenomena as reconstituted into lipid bilayers, the channel can be closed at a certain potential. The significance of this voltage gating is still not clear since the potentials needed to close the pores (about 150 mV) are larger than the naturally occuring Donnan potential across the outer membrane. It has been shown that naturally occuring components in the periplasm (membrane-derived oligosaccharides) or outer membane associated compounds (polyamines) are able to close the pores [6,7], and this could at least partly explain the discrepancy between OmpF behaviour *in vitro* and *in vivo*.

The OmpF exclusion limit and selectivity are attributed to one of the external loop, L3. Unlike the other loops, L3 is not exposed at the cell surface but folds into the barrel, forming a constriction zone at half the height of the channel. At the constriction zone, a strong transverse electrostatic field exists that is caused by acidic residues in loop L3 and a cluster of basic residues in the barrel wall opposite to the internal loop. L3, on the other hand, seems to have a stabilizing function in porin integrity, as many interaction occur between L3 and the barrel wall. A proposed mechanism of voltage gating is that voltage induces a movement of the complete L3 [8] and a subsequent blocking of the channel, but this seems very unlikely since this loops has many interactions with the channel wall. Smaller conformational changes in loop L3 seem more likely to be involved. An alternative mechanism of voltage gating may be the screening-unscreening of the charges in the channel. At the constriction zone, the water shell of entering molecules has to be stripped and/or the water molecules interacting with the peptide structure in the channel has to be removed to allow the passage of the entering molecule. The removal of the hydration shell, probably aided by the strong transversal electric field, followed by redistribution of the water molecules (and/or counter-ions) in the channel may result in unscreening of the charges in the channel and additionally increase the strength of the electrical field [9]. This may induce re-orientation of side-chains in the channel, resulting in closing of the pore.

We propose to study the function-dynamics relationship of OmpF using neutron scattering experiments, crystallography and electrophysiological methods. In a first step, we will investigate of the dynamics-secondary structure relations for membrane proteins and compare the dynamics of OmpF embedded in the outer membrane

with the dynamics of bacteriorhodopsin (BR) embedded in the purple membrane. In a second step, we will focus on the correlation of OmpF dynamics with modulations in the pore characteristics. Effect of the naturally occuring components that induce a closure of the channel (membrane-derived oligosaccharides, polyamines…) will be investigated. In addition, we will search for flexible zones near the constriction zone, especially in the L3 loop.

Methods

Elastic Incoherent Neutron scattering experiments (EINS):

Incoherent neutron scattering experiments take advantage of the large incoherent cross section of protons to follow the dynamics of the molecules by following the dynamics of the proton they contain [10]. In an EINS study, the dynamic information is obtained from the elastic scattering, which can be used to derive the cross-section weighted average mean-square displacement <u_> of the atoms. The <u_> contains contributions from all motions resolvable within the resolution of the spectrometer used, typically on timescales smaller than a few nanoseconds.

Electrophysiological study on planar lipid bilayer

A lipid bilayer is formed over an aperture located in a septum seperating two chambers. Each chamber is filled with a buffered ionic solution and contains an electrode which is used to detect any movement of ions through the bilayer. These electrodes are also used to maintain the transmembrane potential to a fixed value, independently of the ionic movement. In the absence of added channel proteins, the conductance, i.e. the ease of flow of current across the bilayer, is very low. Measure are usually made when an equilibrium of the channel insertion in the membrane is reached, and the conductance increase due to the presence of ion-conducting 'holes' in the membrane. When a compound is added in one chamber and is translocated through the channel, one then observes a decrease of the conductance due to the blocage of the channel. In our experiments, typically, membrane bilayers are made by 'painting' the aperture with lipids dissolved in an organic solvent (like n-decane) and subsequent evaporation of the solvent. Very dilute purified detergent solution of OmpF is then added to one chamber, so that only one trimer of OmpF ('**single-channel**') is sponteanously inserted in the membrane. The advantage of doing a single-channel experiment is that one obtains unaveraged signal, which give information about the kinetics of translocation of the compounds trough the channel, on a timescale of less than 1 ms [11] .

Figure 1: Black-lipid Membrane experiment : blockage of a single maltoporin trimer in presence of various concentrations of maltohexaose.

Typical results

Previous neutron studies of the light activated proton pump retinal-binding protein, BR, established the dependence of thermal dynamics on structural environment (lateral packing in the membrane and hydration) and its importance for biological activity [12]. In the BR structure, seven alpha helices are packed fairly tightly around a pocket containing the retinal chromophore and a proton channel. Hydration around the polar head-groups provides the necessary fluidity in the lipid environment around BR to permit high amplitude motions [13]. These motions have the same dependence on hydration as various aspects of BR function, such as the photocycle or proton pump activity [14]. Dynamical heterogeneities have been shown in the BR, using specific deuterium labelling : for instance, it appears that the cytoplasmic half of BR is softer than the extra-cellular half [15, 16, and figure 2].

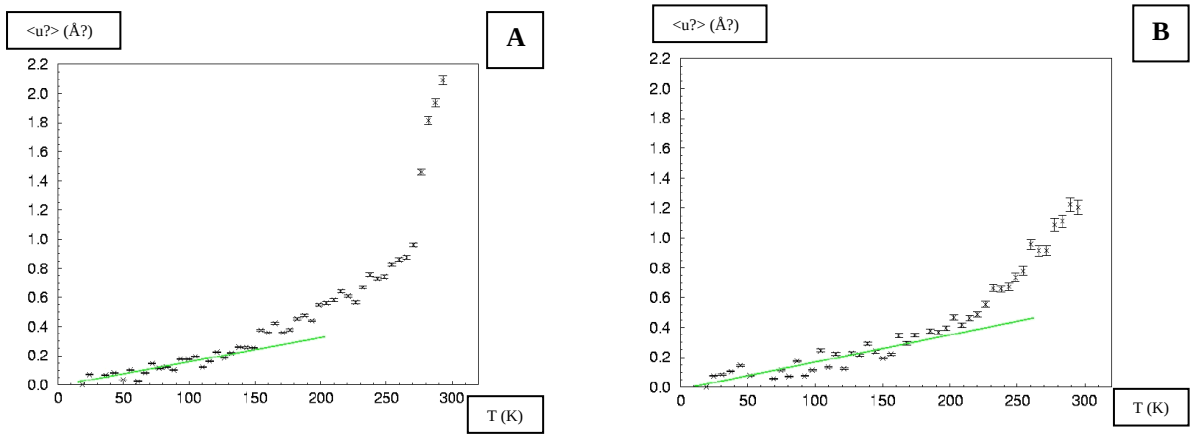

Figure 2: Hydrogen mean square amplitudes u2 - u2(Tmin) plotted as function of temperature for the hydrogenated wet PM and labelled (hydrogenated amino acids are located mainly in the retinal pocket and the extracellular half of the BR helices) wet PM. The solid lines correspond to linear fits of the data points for Tmin < T < 150 K. Taken from [15].

No other type of biological membrane have been studied so far using neutron experiments. In a first set of experiments on OmpF-enriched outer membrane of E. Coli, mean square fluctuations have been measured on IN13 spectrometer. Hydrogenated samples were used, which mean that the dynamics of lipids and proteins was probed.

Perspectives

Preparation of specifically deuterated samples are under way, so that the contribution of OmpF and outer-membrane lipids will be discriminated in subsequent IENS experiments. Dependence of thermal dynamics on the environment (hydration, lateral packing, effect of polyamines and membrane-derived oligosaccharides) will be probed. Several approaches will follow in order to investigate the molecular mechanism of voltage gating and ion selectivity :

- Black lipid membrane measurements of immobilised L3 mutants of OmpF channels and OmpF in interaction with membrane-derived oligosaccharides or polyamines, will be carried out.
- Crystallographic studies are under way.

References

1- Koebnik R, Locher KP, Van Gelder P. (2000) Structure and function of bacterial outer membrane proteins: barrels in a nutshell. Mol Microbiol. 37(2):239-53.
2- Weiss, M.S., Kreusch, A.., Schilz, E., Nestel, U., Welte, W., Weckesser, J. and Schulz, G.E. (1991) The structure of porin from Rhodobacter Capsulatus at 1.8Å esolution. Febs. Lett 280 (2), 379-382.
3- Cowan, S.W., Schirmer, T., Rummel, G., Steiert, M., Ghosh, Pauptit, R.A., Jansonius, J.N. & Rosenbusch, J.P. Detergent structure in tetragonal crystals of Ompf porin. Structure, 3, 1051-1059.
4- Pebay-Peyroula,E., Garavito, R.M.,Rosenbusch, J.P., Zulauf, M. and Timmins, P.A. (1995) Detergent structure in tetragonal crystals of Ompf porin Structure 3, 1051 – 1059.
5- Penel, S. Pebay-Peyroula, E., Rosenbusch, J., Rummel, G., Schirmer, T. and Timmins, P.A. (1998) Detergent binding in trigonal crystals of OmpF porin from Escherichia coli. Biochimie 80, 543 – 551
6- Delcour AH, Adler J, Kung C, Martinac B. (1992) Membrane-derived oligosaccharides (MDO's) promote closing of an E. coli porin channel. FEBS Lett. 304(2-3):216-20.
7- Basle A, Delcour AH. (2001) Effect of two polyamine toxins on the bacterial porin OmpF. Biochem Biophys Res Commun. 285(2):550-4.
8- Watanabe M, Rosenbusch J, Schirmer T, Karplus M. (1997) Computer simulations of the OmpF porin from the outer membrane of Escherichia coli. Biophys J. 72(5):2094-102.
9- Bjorksten J, Soares CM, Nilsson O, Tapia O. (1994) On the stability and plastic properties of the interior L3 loop in R. capsulatus porin. A molecular dynamics study. Protein Eng. 1994 Apr;7(4):487-93.
10- Bon C, Dianoux AJ, Ferrand M, Lehmann MS. (2002) A model for water motion in crystals of lysozyme based on an incoherent quasielastic neutron-scattering study. Biophys J. 83(3):1578-88.

11- Nestorovich EM, Danelon C, Winterhalter M, Bezrukov SM. (2002) Designed to penetrate: time-resolved interaction of single antibiotic molecules with bacterial pores.Proc Natl Acad Sci 99(15):9789-94.
12- Zaccai G. (2000). Moist and soft, dry and stiff: A review of neutron experiments on hydration-dynamics-activity relations in the purple membrane of Halobacterium salinarum. Biophys. Chem.
13- Ferrand M., Dianoux A.J., Petry W., Zaccai G. (1993). Thermal motions and function of bacteriorhodopsin in purple membranes: effects of temperature and hydration studied by neutron scattering. Proc. Natl. Acad. Sci. (USA). 90:9668-9672.
14- Lehnert U., Réat V., Weik M., Zaccai G., Pfister C. (1998). Correlation between thermal motions and functional conformational changes in bacteriorhodopsin: a neutron scattering study at different hydration levels. Biophys. J. 75:1945-1952.
15- Réat V., Patzelt H., Pfister C., Ferrand M., Oesterhelt D., Zaccai G. (1998). Dynamics of different functional parts of bacteriorhodopsin: H-2H labelling and neutron scattering. Proc. Natl. Acad. Sci. (USA). 95:4970-4975.
16- Zaccai G. (2000). How soft is a protein? A protein dynamics force constant measured by neutron scattering. Science. 288:1604-1607.

Towards the study of larger systems by high-resolution powder X-ray diffraction

A. N. Fitch, ESRF, BP 220, F-38043 Grenoble Cedex, France

Introduction

Powder diffraction is rarely the method of first choice to study the crystal structure of a large molecular system. The single-crystal approach is so much more powerful, because the individual Bragg reflections from the three-dimensional crystal lattice are resolved, leading to the unambiguous measurement of the intensities. From such information, crystal structures are solved, and accurately refined, (usually routinely), from small molecules to biological macromolecules. With powders, the collapse of the diffraction pattern onto a single dimension leads to overlap of diffraction peaks. The larger a structure or the lower its symmetry, the greater the number of reflections and the worse the overlap problem becomes. Peak overlap means that the individual peak intensities are obscured, and with severe overlap, even the 2θ positions of the reflections may be unresolvable. This limits the size of the structures that can be solved and, because of the resulting correlations, lowers the accuracy of structural parameters extracted by refinement.

Rather than using a powder, it is sometimes preferable to work with a very small single microcrystal, as is now feasible exploiting the brilliant X-ray beams of modern synchrotron-radiation sources, and large two-dimensional detector systems. However, the handling of such small crystals can be a major challenge, and powder specimens may be the only practical approach, when not even a microcrystal can be obtained. This can occur in the study of metastable phases or specific polymorphs, where only powder specimens exist. This is particularly important in the pharmaceuticals sector, where different formulation conditions may lead to the production of different crystalline forms of a biologically-active compound. Polymorphs, with different molecular packing, and pseudo-polymorphs, with different numbers of solvent molecules, may have different physical properties, so it is essential to characterise and understand the nature of the various forms. Powders are easier to use when studying destructive phase transitions of a compound that cause a single crystal to fragment, or when investigating difficult materials such a volatile liquids or gases, though improvements in handling and crystal-growing techniques are still being made. Powders are also used to study real materials under realistic operating conditions, such as *in-situ* catalytic reactions, solid-state synthesis, etc. In the area of structural biology, growing crystals of the appropriate quality for full structural characterisation is often a limiting step, and it may be that powders could serve a role in a more-limited exploration.

Recent progress

To advance in the field of powder diffraction, the effects of overlap must be reduced. Modern instruments harness the highly collimated nature of synchrotron radiation to yield diffraction patterns with the narrowest peak widths, thus reducing the overlap. However, it is rare, even from the best data, to solve by direct methods simple organic structures with many atoms. Fluorescein diacetate with 31 carbon and oxygen atoms is one of the biggest [1]. Larger structures can be solved by exploiting the molecular structure, which is normally known. The appropriate number of independent molecules (or fragments of molecules) are placed in the unit cell. The

molecules are translated and rotated within the cell, and for non-rigid molecules the torsion angles can be varied, to obtain the best agreement between the calculated and the measured diffraction data, under the control of a global minimisation technique such as a genetic algorithm or simulated annealing[1]. The size of the structure is then limited more by the total number of degrees of freedom, rather than the size of the molecules themselves.

One way of alleviating the peak overlap is to make the sample more like a single crystal. Thus Wessels *et al*. [2] studied zeolite UTD-1 with deliberately induced texture. From measurements of pole figures, the orientation distribution of the crystallites was obtained and this was used to help partition the intensity amongst the overlapping reflections. The crystal structure was solved with 69 non-hydrogen atoms in the asymmetric unit.

If a crystalline solid expands anisotropically with changes in temperature, then this can help to reduce the effects of peak overlap. Owing to the anisotropic expansion of the lattice, peaks overlapped at one temperature may be better resolved at another. The method was recently proposed by Shankland *et al*. [3] in the solution of the crystal structure of chlorathiazide. The first experiment on the new powder diffraction beam line ID31 at the ESRF exploited anisotropic thermal expansion to solve with direct methods the (centrosymmetric) crystal structure of an organic compound with 48 C and O atoms in the asymmetric unit. Previous attempts to solve the structure using the original BM16 beam line had failed. Further improvements in the data-collection strategy and data analysis are expected, which will push still higher the sizes of structures that can be solved. However it seems unlikely that truly large organic structures with several hundred atoms will be accessible without further innovation. An additional issue is that to study systems with many overlapping reflections the crystallinity of the sample itself can play a limiting role. Poorer crystallinity leads to broadening of the peaks from the sample itself, reducing the effectiveness of strategies such as the use of anisotropic thermal expansion.

Von Dreele [4] has studied the structures of proteins from high resolution powder diffraction data collected with synchrotron radiation. The samples are highly crystalline and give narrow diffraction peaks. By combining the diffraction data with stereochemical restraints for bond distances, angles, torsion angles, planar groups etc. he has shown that Rietveld refinement of protein crystal structures is feasible, showing good agreement with the known crystal structures. For chicken egg lysozyme, the precision on the lattice parameters, which is much better from powders than usually obtained from single-crystal measurements, was sufficiently good to reveal a subtle structural transition depending on the pH of the buffer solution used to precipitate the sample. This structural change has a strong effect on the ability of lysozyme to bind N-acetylglucosamine [5], with the ligand binding only to the structure grown at higher pH. In another study, a phase change to a metastable form was seen on grinding the T_3R_3 form of Zn-insulin, with a doubling of the *c*-axis of the unit cell with respect to the single-crystal structure [6]. The structure was solved by a molecular replacement technique. Two T_3R_3 complexes from the single-crystal structure were included in the doubled unit cell, defining each as a rigid body. Two

[1] Such an approach can also be envisaged to locate molecules adsorbed inside a host of known structure such as a zeolite, allowing also the occupancy of a molecule to vary.

rotations and a translation along the *z*-axis for each unit were sufficient to find a suitable starting model for subsequent Rietveld and stereochemical refinement.

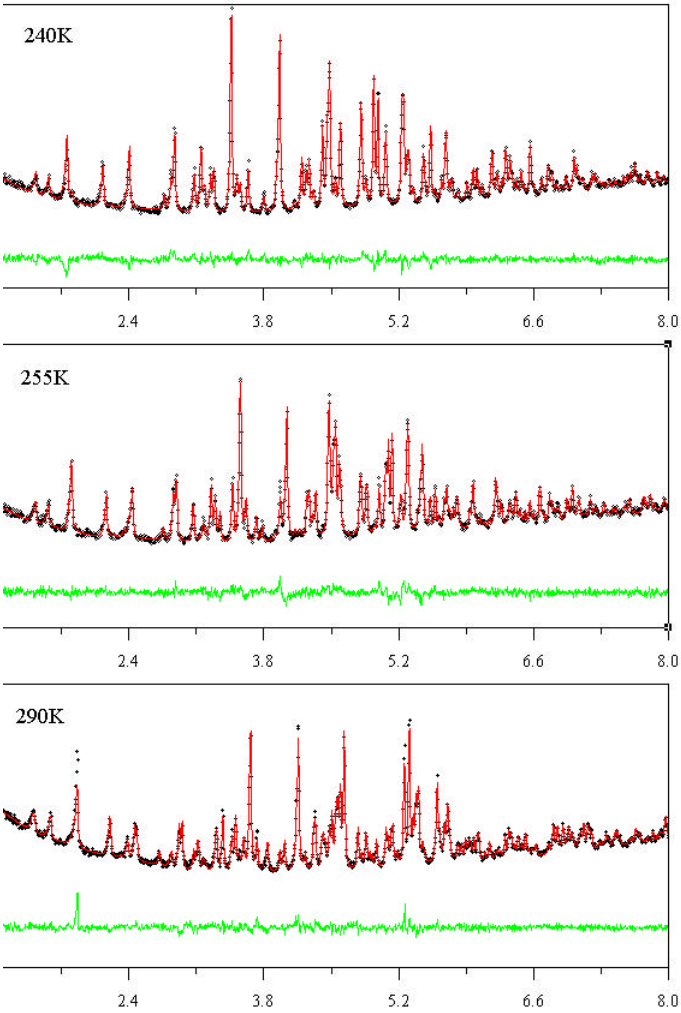

Figure 1: Powder diffraction patterns of myoglobin.

Measurements using powder diffraction have recently been made at ESRF on myoglobin [7]. To try to assess the impact of anisotropic thermal expansion on the effective resolution, patterns were collected at different temperatures, Fig 1. It is apparent that myoglobin undergoes phase transitions with temperature, Fig. 2, in a manner analogous to many small-molecule systems. Refinement of the lattice parameters show that the phase changes involve small distortions to the unit cell without any gross change in structure. All the patterns can be fitted with a single set of peak intensities. Temperature jump experiments can be carried out to investigate the kinetics of the evolution of one form to another.

Perspectives

Although limited by the problems of peak overlap, it is still often surprising how much new information can be obtained from a high resolution powder diffraction pattern. Where overlap is not severe, the peak positions show great sensitivity to subtle distortions in the lattice and this can reveal unsuspected phase transitions. Even with overlap, a powder pattern can contain enough information to allow moderately complex crystal structures to be solved, and much larger structures to be refined when combined with stereochemical restraints. The technique is simple to apply, and a series of measurements, varying some external quantity, such as temperature or composition, can uncover trends in the behaviour of a system, reflecting its inner microscopic chemical interactions.

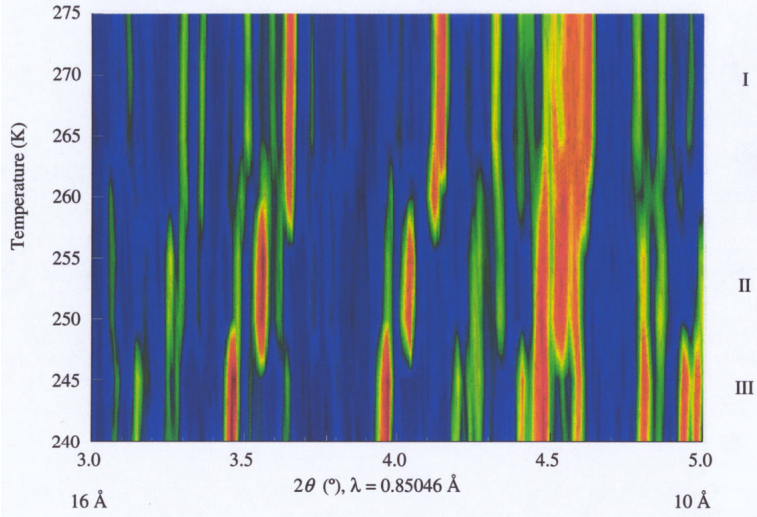

Figure 2: Phase transitions in myoglobin.

[1] *Solution of the crystal and molecular structure of complex low-symmetry organic compounds with powder diffraction techniques: fluorescein diacetate.* K.D. Knudsen, P. Pattison, A.N. Fitch and R.J. Cernik, Angew. Chem. Int. Ed., 37 (1998) 2340.

[2] *Single-crystal-like diffraction data from polycrystalline materials*. T. Wessels, Ch. Baerlocher and L.B. McCusker, Science, 284 (1999) 477.

[3] *Routine ab-initio structure determination of chlorothiazide by X-ray powder diffraction using optimised data collection and analysis strategies*. K. Shankland, W.I.F. David and D.S. Sivia, J. Mater. Chem., 7 (1977) 569.

[4*] Combined Rietveld and stereochemical restraint refinement of a protein crystal structure*. R.B. Von Dreele, J. Appl. Cryst., 32 (1999) 1084.

[5] *Binding of N-acetylglucosamine to chicken egg lysozyme: a powder diffraction study.* R.B. Von Dreele, Acta Cryst. D57 (2001) 1836.

[6] *The first protein crystal structure determined from high-resolution X-ray powder diffraction data: a variant of T_3R_3 human insulin-zinc complex produced by grinding.* R.B. Von Dreele, P.W. Stephens, G.D. Smith and R.H. Blessing, Acta Cryst., D56 (2000) 1549.

[7] *To be published.* J.P Wright.

Nucleic acid structure and transitions: a methodological challenge

V.T. Forsyth

Institut Laue Langevin, BP 156, 38042 Grenoble, France
and
Lennard Jones Laboratories, School of Chemistry and Physics, Keele University, UK

Nucleic acids (DNA and RNA) exist in nature as long polymer molecules in a highly condensed state. In the past there has been a considerable amount of work on sequence dependent structural variation in single crystal diffraction studies of short oligonucleotide sequences. However nucleic acid polymers well beyond the length of such oligonucleotides have remarkable cooperative properties. This behaviour depends critically on factors such as ionic strength and hydration in the environment of the molecule and can be investigated by the study of highly concentrated fibres, gels, and solutions. Notable in this are the observation of structural transitions between DNA conformations and the involvement of water in mediating these. Both X-ray and neutron diffraction can play a vital role; so too can other methods that can make a link between structural observations and molecular dynamics.

1. Introduction. The deoxyribonucleic acid (DNA) double helix can adopt one of five major variants depending on base-pair sequence, hydration and the nature of its ionic environment. The A [1], B [2], and C [3] conformations were first identified in natural DNA but are also observed routinely in a wide range of synthetic polynucleotides. Two-stranded synthetic DNA polymers having regular repetitive base-pair sequences can in addition adopt novel conformations such as the D conformation [4] which is adopted by DNA polymers containing an alternating A-T base-pair repeat, and the left-handed S (or Z) conformation [5] which has been most commonly reported in alternating G-C base-pair repeats of the double helix. Of

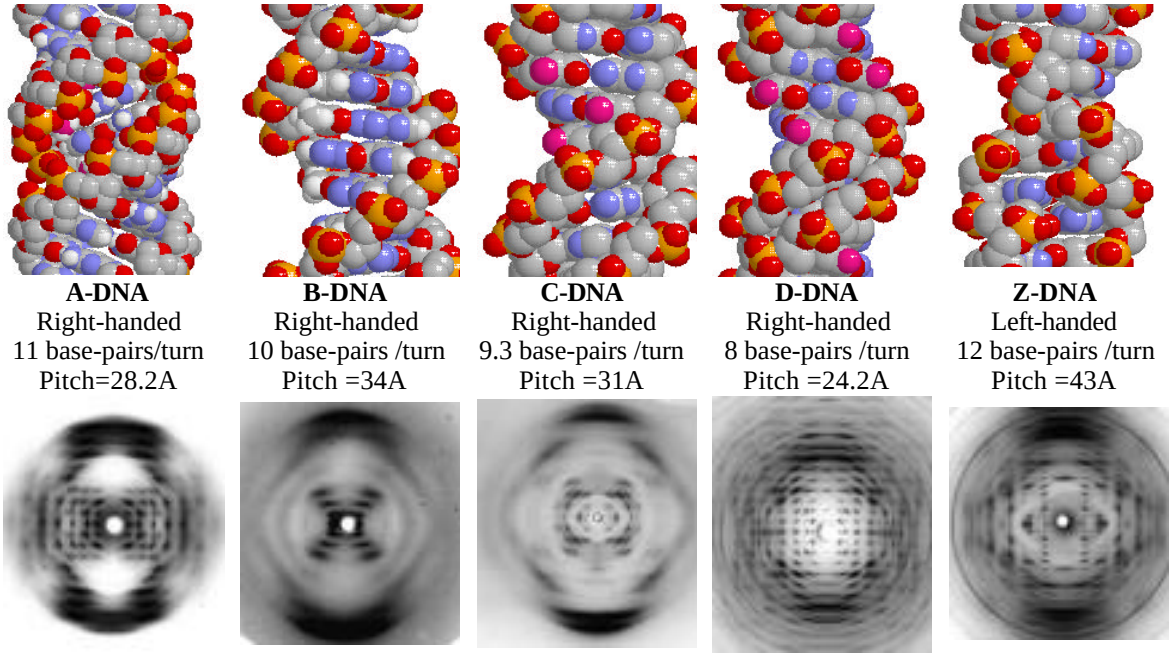

A-DNA	**B-DNA**	**C-DNA**	**D-DNA**	**Z-DNA**
Right-handed	Right-handed	Right-handed	Right-handed	Left-handed
11 base-pairs/turn	10 base-pairs /turn	9.3 base-pairs /turn	8 base-pairs /turn	12 base-pairs /turn
Pitch=28.2A	Pitch =34A	Pitch =31A	Pitch =24.2A	Pitch =43A

Figure1: *The five major conformational variants of the DNA double helix, their helix parameters, and the x-ray fibre diffraction patterns recorded from them.*

1 W. Fuller, M.H.F. Wilkins, H.R. Wilson, L.D. Hamilton, and S. Arnott, *J. Mol. Biol*. 12, 60 (1965).
2 R. Langridge, D.A. Marvin, W.E. Seeds, H.R. Wilson, C.W. Hooper, M.H.F. Wilkins and L.D. Hamilton, *J. Mol. Biol.* 2, 19 (1960).
3 D.A. Marvin, M. Spencer, M.H.F. Wilkins and L.D. Hamilton, *J. Mol. Biol*. 3, 547 (1961).
4 D.R. Davies and R.L. Baldwin, *J. Mol. Biol*. 6, 251 (1963).
5 S. Arnott, R. Chandrasekaran, D.L. Birdsall, A.G.W. Leslie and R.L. Ratliff, Nature 283, 743 (1980).

these five principal conformations of DNA, the A, B, C, and D conformations were all first determined by x-ray fibre diffraction. The left-handed S conformation was first discovered as the Z conformation in an x-ray single-crystal analysis of an oligonucleotide [6] and then subsequently reported in x-ray fibre diffraction studies where it was designated S-DNA. Figure 1 shows a summary of the five major families of DNA structure, along with examples of the type of x-ray fibre diffraction patterns that are recorded from them.

Figure 2 summarises the structural polymorphism observed in DNA polymers having various simple base-pair repeats. As mentioned above, two novel conformations not observed in natural "random sequence" DNA occur in alternating A-T and G-C sequences (*ie* D-DNA and Z-DNA respectively). These two structures can undergo conformational transitions involving B-DNA. Also evident from figure 2 is the unique behaviour of the two G-C and A-T *homopolymers* – these have remarkable preferences for A-DNA and B-DNA respectively.

NATURAL DNA	ALTERNATING A-T	ALTERNATING G-C	HOMOPOLYMER G-C	HOMOPOLYMER A-T
"Random" sequence	A - T T - A A - T T - A A - T T - A A - T T - A A - T T - A	G - C C - G G - C C - G G - C C - G G - C C - G G - C C - G	G - C G - C G - C G - C G - C G - C G - C G - C G - C G - C	A - T A - T A - T A - T A - T A - T A - T A - T A - T A - T
C ✿ A ✿ B	D ✿ B	Z ✿ B	A	B

Figure 2: *Diagram summarising the structures adopted in simple polymeric DNA sequences, as observed by fibre diffraction. The top part of the diagram shows the repeat in the polymer; the bottom shows the structures adopted. Where they occur, transitions that occur as a function of the fibre environment are indicated.*

It would be very surprising if the ability to adopt these very different structures they was not exploited in biological function. However, their biological significance is by no means clear. The A conformation is adopted by RNA double helices and by DNA:RNA hybrid molecules - this has resulted in persistent speculation about a possible role for A-DNA in transcription. Immunological work suggests that both B-DNA and Z-DNA have been identified *in vivo* [7]. It is known also that the structural transition to Z-DNA for appropriate sequences causes a number of fundamentally important effects [8, 9] and also that there are a large number of proteins that recognise Z-DNA [10, 11].

2. Methods for structure.

6 A.H.J. Wang, G.J. Quigley, F.J. Kolpak, J.L. Crawford, J.H. van Boom, G. van der Marel and A. Rich, Nature 282 680 (1979).
7 Jaworski *et al*, Science 238, 773 (1987).
8 Wolfl *et al.*, *Proc. Natl. Acad Sci. USA*, 93, 3664 (1996)
9 Muller *et al.*, *Proc. Natl. Acad Sci. USA*, 93, 780 (1996)
10 Herbert and Rich, Nuc. Acids Res. 21 (21), 4886 (1993)
11 Berchert at al, J. Biomol. Str. Dyn. 12(3), 605 (1994).

2.1 X-ray diffraction. X-ray fibre diffraction was pivotal in the discovery of the DNA double helix [12] and subsequently in the definitive structure determinations of the A, B, C, D, and Z conformations of the molecule. Since then there has been extensive work on a wide range of oligonucleotide single crystals. The two diffraction methods (single crystal and fibre diffraction) are highly complementary. Single crystal oligonucleotide methods offer *direct* structure determination at good/high resolution and the reward of possible information on sequence dependent local variation. The results from such studies do however have to accommodate the influence of crystal packing effects as well as end effects arising from the limited length of the oligonucleotides. Fibre diffraction experiments offer information, usually (but not always) at lower resolution (2-3A) and do not permit direct structure determination; structures are analysed by model building methods and assessed using rigorous validation methods. The critical advantage of fibre diffraction is that it offers a direct structural probe of the behaviour of the intact *polymer* molecule; all of the five major DNA structural variants can be observed in fibres (compared to the three – A, B, C - that can be seen in single crystals) and there exists furthermore the possibility of observing structural transitions between these conformations.

2.2 Synchrotron x-ray fibre diffraction – time resolved studies of structural transitions. Structural transitions in DNA fibres are typically observed as a function of water content in the sample and are regulated by adjusting the relative humidity of the sample environment. The availability of intense synchrotron x-ray sources and modern detecting systems means that it is now possible to study these transitions in real time. The first such transitions were recorded at the Daresbury synchrotron radiation source (SRS) [13,14]. Although these experiments were limited by the intensity of the source and by the use of early detecting systems, they showed the presence of structural intermediates and appeared (within the limited time resolution available) to be continuous in character. In later experiments at Daresbury, on-line image plate detectors improved this situation very significantly. Figure 3 shows the water driven transition between the D and the B forms of DNA. The degree of cooperativity is very striking - it is clear that during the experiments coordinated changes involving extended regions of the fibre sample are occurring. The particular transition shows how the conformation of the DNA undergoes a gradual (and as far as can be seen, continuous) change in which the pitch of the DNA changes from ~24A in D-DNA to ~34A as in B-DNA.

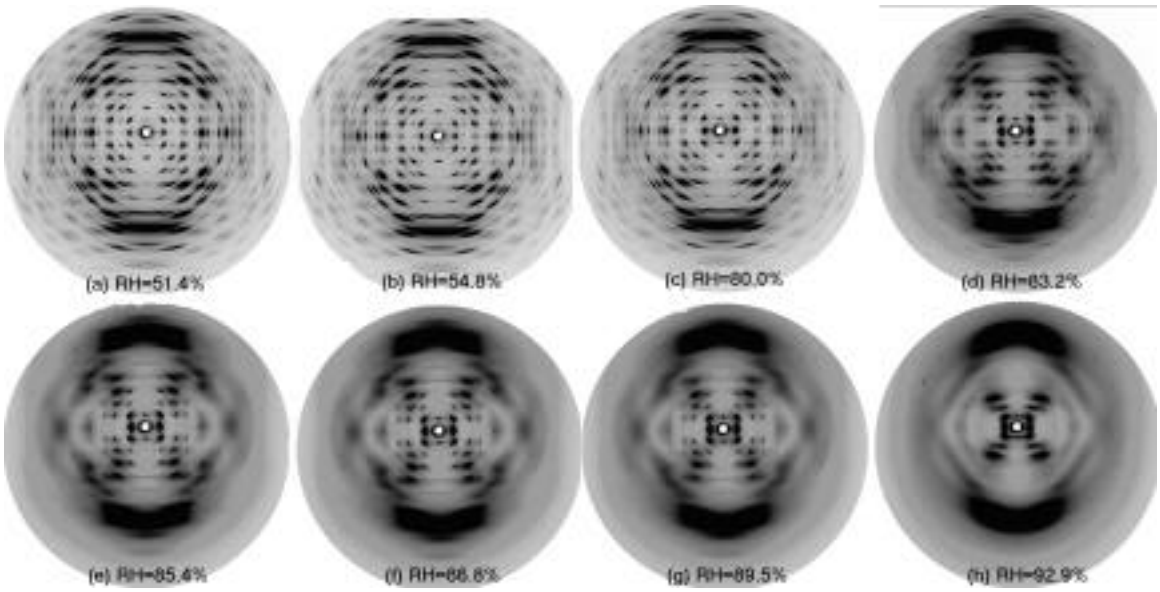

Figure 3: *Water driven transition between the D and the B conformations of DNA*

12 J.D. Watson and F.H.C. Crick, Nature 171, 737 (1953).

13 A. Mahendrasingam,V.T. Forsyth, W. Fuller *et al, Science* 233, 195-197 (1986).

14 V.T. Forsyth, R.J. Greenall, R. Hussain, A. Mahendrasingam *et al, Biochemical Society Transactions* 14, 553-557 (1986).

The advent of 3rd generation synchrotron radiation sources such as the ESRF has further widened the scope for this sort of work. It is now possible to obtain sub-second time resolution for experiments of this type. The ability to do this owes much to recent advances in detector technology and also the availability of large quantities of computer memory that allow data to be written directly to memory and stored for the duration of an experiment. Beamlines such ID2 at the ESRF [15] offer the ability carry out such experiments in a way that allows both low and high angle data to be recorded simultaneously. The power of experiments such as these has been demonstrated in recent studies of the transition between the A and B forms of *E. Coli* chromosomal DNA. This has shown clear evidence of a continuous pathway of conformational intermediates connecting the A and the B conformations of DNA. The experiment shows clearly why in previous experiments on 2nd generation sources it has not been possible to observe anything other than diffraction patterns that contain a simple mixture of the start and end states (ie A and B) – the most significant region of the transition occurs over a period of a few seconds, well beyond the time resolution available in previous work on this transition.

2.2 Neutron fibre diffraction. The results summarised in the previous sections illustrate the significance of water in stabilising DNA conformations and mediated transitions between these conformations. Indeed it has been suggested on numerous occasions that water and cations should be regarded as two genuinely integral components of DNA structure in addition to the bases, sugars and phosphates [16,17].

Although x-ray fibre diffraction is a very powerful technique for the study of DNA conformation and for the study of conformational transitions, it is less well suited to the study of water around DNA polymers as studied in fibres. The data are dominated by scattering from the electron-rich phosphates and attempts to extract information on structured water have not been very successful, mainly because of the relatively low scattering power. For this reason, neutron fibre diffraction was developed as a method that proved to be better suited to the investigation of the location of water around polymeric DNA [18]. The ability to isotopically replace H_2O in the DNA sample by D_2O allows the large coherent scattering length of deuterium to be utilised in imaging the water distribution around DNA. Neutron beam sources however have the disadvantage of relatively low flux, with the consequent requirement for large samples and counting times.

Figure 4 summarises the results obtained from a neutron fibre diffraction study of hydration in A-DNA. This work was carried on at the Institut Laue Langevin (ILL) on instrument D19 [19]. The study illustrated the presence of hydration sites in the asymmetric unit of the A-DNA molecule. The first is located in the major groove, bridging phosphate oxygen atoms on the same strand. The second was located at the centre of the opening of the major groove at equal distances from phosphates on either strand – the distances involved are such that it is likely that cations are involved in a zig-zag network across the opening of the major groove. The third is in the centre of the major groove and may also be associated with a string of cations along the centre of the groove. The fourth site appeared as a continuous core of density running along the helix axis in front of the bases in the major groove. It is likely that the appearance of this site in the Fourier maps arises from sequence dependent hydration features that are averaged in this "sequence averaged" sample.

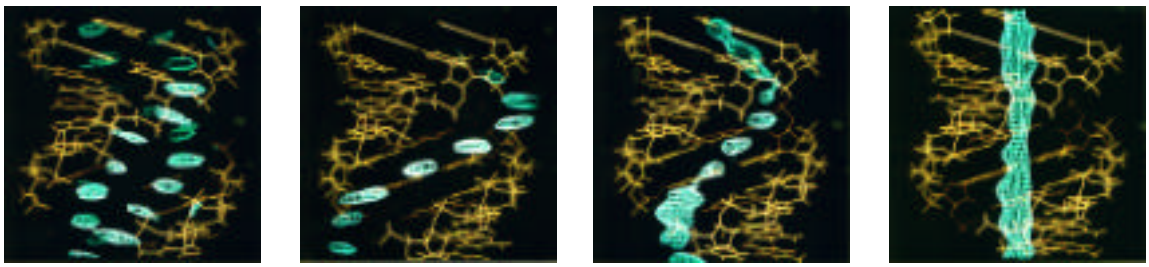

Figure 4: *Pictures showing the results of a neutron diffraction analysis showing 4 ordered water sites in A-DNA.*

This information on nucleic acid hydration is of course of central importance in modelling the structural transitions that can be followed by x-ray diffraction. Although it is not possible with neutron diffraction to follow the transitions with anything approaching the time resolution possible using synchrotron x-ray sources, information on water structure for the start and end points of these transitions is extremely valuable for the modelling of the detailed x-ray data.

15 ESRF Highlights *Introduction to soft condensed matter*, pg 35 (2001).
16 Prive *et al, J. Mol. Biol*. 217, 177 (1991)
17 Westhof and Patel, *Curr. Opin. Struct. Biol*. 5, 279 (1995)
18 V.T. Forsyth *et al, Fibre Diffraction Review* 7, 52 (1998)
19 M.W. Shotton, L.H. Pope, V.T. Forsyth, P. Langan, R.C. Denny, U. Giesen, M.-Th. Dauvergne, W. Fuller, *Biophysical Chemistry* 69 (1) , 85-96. (1997)

3. Perspectives

All of the work described here for studies of DNA can in one way or another be applied to a wide variety of polymer systems. Studies of this type face important methodological challenges. It is clear that synchrotron x-ray and neutron beam facilities, used together, can provide structural information that is not available by either technique alone, and that such information may be important in establishing structure-function/property relationships. Furthermore, it is essential to recognise that as more and more information becomes available on structural analyses of static or changing systems, there will be an increasing need to consider dynamic aspects.

Some of the most important challenges are technical. Synchrotron x-ray sources are steadily improving the time resolution that can be attained for work involving structural changes. Although new synchrotron sources are being built, it is likely that in the short/medium term the main changes will occur through the development/availability of better detecting systems. New investments at neutron beam sources are gradually demonstrating the gains that can be made if existing infrastructure is properly developed – both from the point of view of sample preparation and instrument/detector efficiency. Some of these developments may be of considerable importance in the study of the dynamics of polymer systems. For example, the ability to deuterate samples, either selectively or non selectively, could be very powerful in inelastic scattering and elastic incoherent scattering studies. Likewise it is important to recognise that investment in the development of methods for the production of large samples can pay handsome rewards.

Modelling of Solution Speciation

Julian D. Gale,
Department of Chemistry, Imperial College, South Kensington, SW7 2AY, UK.

Introduction

The nature of species in contact with solution is fundamental to many processes, from biological ones to issues in minerals processing. In particular, it is important to understand the different states in which species exist, in terms of protonation/deprotonation, as a function of conditions such as pH. The natural starting point for this is to be able to understamd dilute solutions, though ultimately we have to recognise that most chemical environments deviate from this ideal situation. Theoretical modelling provides one tool to assist in the interpretation of experimental data and to provide insight. Here we provide a perspective on what can be achieved and what are the limitations.

Methods

In this work, we shall focus primarily on the application of *ab initio* methods to solution speciation, though this also applies to the solvation of interfaces. Here results will be presented based on two differing approaches to the treatment of condensed phases. In the first, we consider the species as discrete entities embedded in an environment. For this situation, it is appropriate to use the standard machinary of molecular quantum mechanics, based on Gaussian basis sets (specially results at the B3LYP/6-311++G**//B3LYP/6-31G** level). In the second approach, we use a supercell approach through the application of periodic boundary conditions, in order to avoid surface effects. Given that such models need to be as large as possible, we employ the SIESTA methodology[1] in order to calculate the total energy and derivatives. Here the wavefunctions of the system are expanded in a basis set of numerical atomic orbitals that correspond to the solutions of the pseudopotential for the isolated atom. Flexibility is introduced by dividing the basis set into multiple-zetas and adding polarisation functions. The basis decays to zero at a specific distance, decided according to the increase in energy of the orbital. This truncation allows the Hamiltonian to be constructed in a manner whose cost scales linearly with increasing system size, thus making it feasible to study larger systems than with planewave approaches. The results reported here correspond to a DZP basis set, using Troullier-Martins pseudopotentials and the Perdew-Burke-Ernzerhof GGA.

Typical Results

To illustrate the application of theoretical methods to speciation we will consider the case of aluminium in solution. Under acidic conditions, this is of relevance to anti-perspirants and ground water contamination. However, here we will focus on basic conditions. Ultimately the aim is to understand the Bayer process by which aluminium is extracted from the mineral bauxite. Here the raw material is dissolved in caustic soda (Na(OH)) to form a so-called Bayer liquor from which aluminium slowly crystallises as the gibbsite polymorph of aluminium hydroxide. This process has very poor kinetics, and so an understanding of Bayer liquor chemistry is fundamental to accelerating it, with potentially enormous cost savings.

Before attempting to consider Bayer liquor, we turn to the case of the dilute alkaline solution of aluminium. The dominant solution species is believed to be the tetrahedral aluminate

---

[1] "*The SIESTA method for ab initio order-N materials simulation*", J.M. Soler, E. Artacho, J.D. Gale, A. Garcia, J. Junquera, P. Ordejon, D. Sanchez-Portal, J. Phys. C Cond. Matter, 14 (2002) 2745.

anion based on NMR and vibrational spectroscopy. We can postulate a large number of possible equilibria of which the simplist sequence is:

$$Al(OH)_3 + 3(OH)^- \rightleftharpoons Al(OH)_4^- + 2(OH)^- \rightleftharpoons Al(OH)_5^{2-} + (OH)^- \rightleftharpoons Al(OH)_6^{3-}$$

Calculating the energetics for these processes, using a continuum solvation model to represent dilute solution, yields reaction energies of –252, +11 and +107 kJ/mol, respectively, thus confirming that the monoanion is the preferred species.[2] This can also be validated by examining the infra-red spectra of the various possible anions. The experimental spectrum can be rationalised in terms of the monomer, if each hydroxyl group is explicitly solvated by a single water molecule.

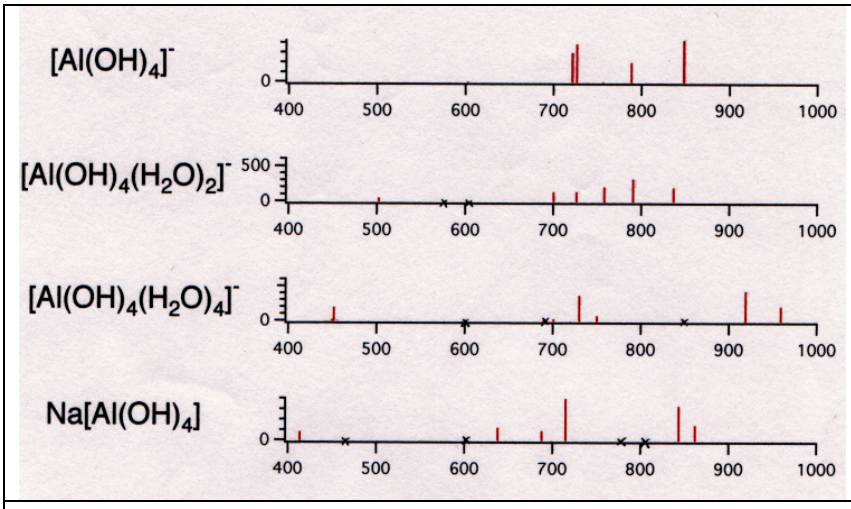

Figure 1. The calculated IR spectra for tetrahedral monomeric aluminate species. Experimentally, the spectrum consists of a peak at 720 cm^{-1} and a broad band above 900 cm^{-1}, but no intensity between 800 and 900 cm^{-1}.

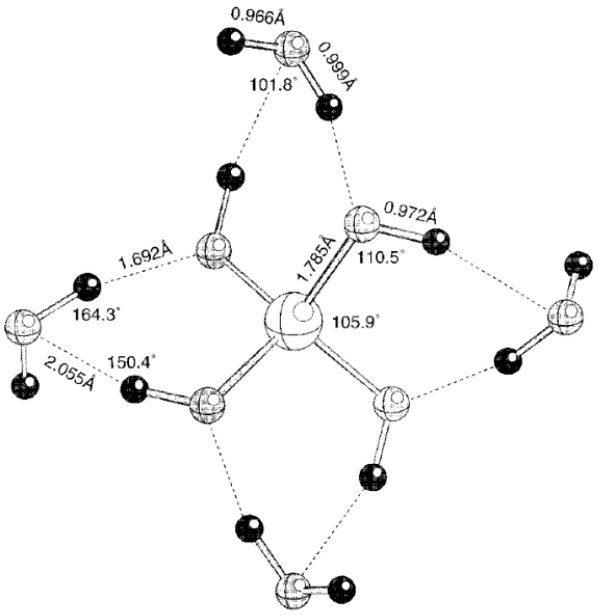

Figure 2. Solvated aluminate anion species predicted to correspond to the experimental IR spectrum.

[2] "*Theoretical Investigation of the Nature of Aluminum-Containing Species present in Alkaline Solution*", J.D. Gale, A.L. Rohl, H. Watling and G.M. Parkinson, J. Phys. Chem. B, 102 (1998) 10372.

In many cases it is now quite feasible to obtain good results for the characterisation of aqueous species at the dilute solution limit, either by using a cluster approach with explicit hydration for the first solvent shell and continuum solvation further out, or through supercell methods. What is more complex is to look at higher concentrations were condensation begins to occur and ion-pairing cannot be ignored. Bayer liquor provides perhaps the most extreme case of this situation where there are only 4 water molecules per solution species. Here the medium is more akin to an amorphous material than a dilute solution. Consequently, electrostatic interactions between ions are important and the dielectric behaviour no longer resembles water, rendering the continuum approaches less useful.

As an example, we have considered the nature of the aluminate monomers and one of the proposed dimer structures, in which a single hydroxyl bridging group exists, within a Bayer liqour model. A supercell is constructed containing of the order of 200 atoms, consisting of 56 water molecules, 2 aluminiums, and 4 Na(OH) molecules, giving a base concentration of 3.63M and an overall composition typical of such a system. Given that almost nothing is known about the structure of the system, first classical molecular dynamics was performed to generate a sensible initial configuration, and then 2 ps of *ab initio* molecular dynamics was performed at 353 K. Snapshots of both systems are shown in Figures 3 and 4.

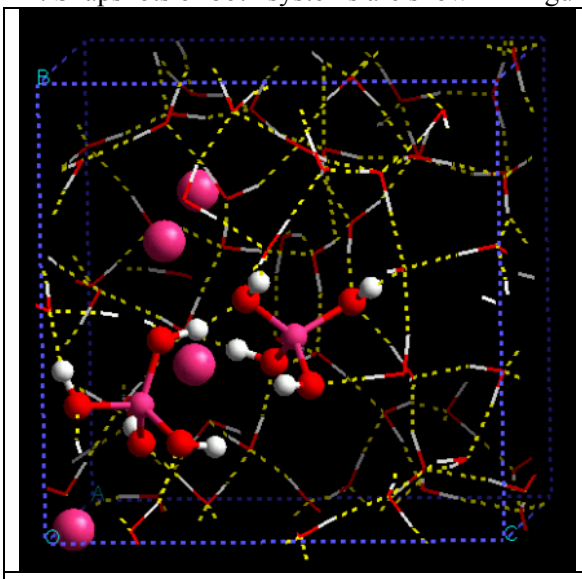

Figure 3. One configuration from an *ab initio* MD run on a Bayer liquor model containing two monomeric anions (ball and stick representation. Large pink spheres indicate sodium cations, oxygen is red and hydrogen white.

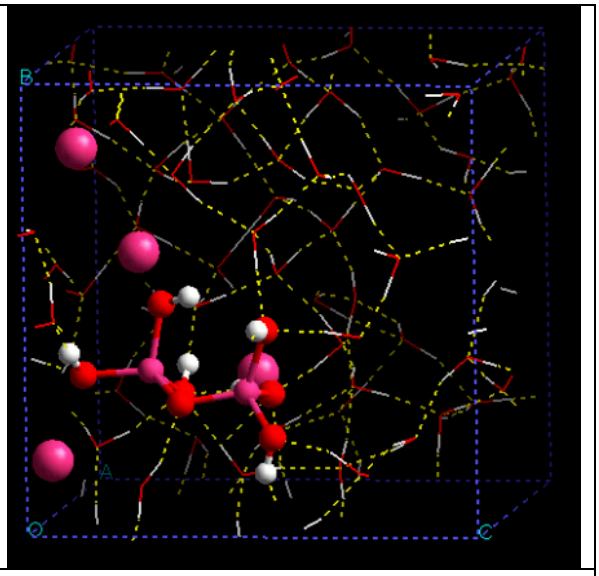

Figure 4. One configuration from an *ab initio* MD simulation of a hydroxo-bridged aluminate dimer in a Bayer liquor model. The yellow dot lines are an indication of hydrogen bonding contacts within the system.

While these simulations are very preliminary, since it is impossible to sample sufficient of configuration space to make definitive statements, they do offer some insights as to what is occuring in such complex systems. A general observation is that proton transfer appears to be quite facile and occurs frequently between hydroxide anions, waters and aluminate species, though the terminal groups of the later only ever act as acceptors. In the simulation of the two monomers, initially there appeared to be a tendancy for one hydroxyl group to begin to bridge between the aluminiums, though it never remained there for more than a few vibrational oscillations. As the simulation progresses the two anions even begin to diffuse apart slightly. For the dimer, the bridging Al-(OH)-Al link is never broken, but the proton is occasionally lost to form a bridging oxo-group. Intramolecular hydrogen bonds are also formed and broken through

out. All observations are consistent with a picture of the initial condensation being difficult to achieve, but thermodynamically favourable, such that once it has occurred and the vibrational energy dissipated then it is hard to reverse.

Typical Problems

The simulation of complex systems of high ion strength, such as the Bayer liquor shown above, is highly problematic. Because little is known about the real structure, it is necessary to virtually guess at feasible starting models and then to anneal the system. Due to the significant cost of *ab initio* dynamics, it is only possible to simulate a few picoseconds of real time, which is clearly inadequate to achieve any kind of meaningful statistical sample of a viscous liquid. Hence, we can only typically obtain insight, rather than anything quantitative, and even the insights may be questioned as to whether they are truly representative. Furthermore, since hydrogen transfer appears to be important we ideally should correct for the quantum behaviour of protons. While this is possible through path-integral techniques, this adds considerably to the computational cost of an already expensive task. The same observation also implies that classical forcefield methods cannot be reliably employed for these systems. However, there is some hope here since models are now emerging that allow for the transfer of protons within water simulations.[3]

Perspectives

In the context of the problem of speciation, dilute solutions can be considered as model ones that can be relatively readily simulated using present methods. More complex solutions require explicit simulation of large numbers of ions and molecules. Significant progress in this direction is being made for insulators where linear scaling makes calculations on many thousands of atoms possible, if not quite routine. However, the largest problem is one of reliable statistical sampling, since the number of states to be sampled increases rapidly with the size of system and it is impossible to enumerate or systematically consider these. The challenge of solvation is well illustrated by recent work on DNA.[4] It has been a significant achievement to be able to perform an *ab initio* calculation on a strand of this *in vacu*, but the ultimate success will be to model the same system in solution, thereby providing insight into the protonation state.

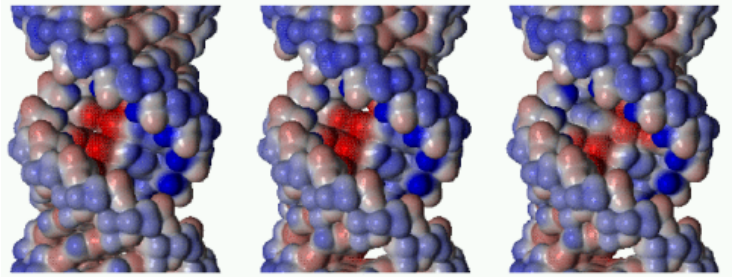

Figure 5. Electrostatic potential on isodensity surface of a 1-D DNA from *ab initio* calculation (from work of E. Artacho and co-workers)

Finally, we have to consider the accuracy of the underlying theoretical method. While DFT is a very useful method, there are clear limits to its accuracy. Furthermore, there is no immediate prospect of a significant improvement in the quality of the results. As a result, reliably going beyond model solutions is likely to remain a challenge for a considerable time.

---

[3] "*A multi-state empirical valence bond model for acid-base chemistry in aqueous solution*", M. Cuma, UW Schmitt and G.A. Voth, Chem. Phys., 258 (2000) 187.

[4] "*Absence of DC-conductivity in λ-DNA*" P.J. de Pablo, F. Moreno-Herroro, J. Colchero, J.G. Herrero, P. Herrero, A.M. Baro, P. Ordejon, J.M. Soler and E. Artacho, Phys. Rev. Lett., 85 (2000) 4992.

Extended abstract for ESF workshop: Bridging the gap in molecular science between model systems and real systems

Vibrational dynamics of nucleic acids, peptides and their building blocks in aqueous solution and solid phase

Mahmoud Ghomi, LPBC/CSSB (UMR CNRS 7033, Universités Paris 6 et Paris 13),
UPMC, case 138, 4 Place Jussieu, 75252 Paris cedex 05, France

Introduction

About thirty years of investigations by different groups through the world were necessary in order to emphasise the capability of vibrational spectroscopy in elucidating the structural and conformational properties of nucleic acids and proteins. In aqueous solutions, biomolecular dynamics is first characterized by Raman scattering and IR absorption in the spectral region of 3000-600 cm^{-1} (energy range: 400 to 80 meV), as far as their *fast motions* arising from the variation of valence bonds and angles are concerned. This spectral region corresponds to a 10^{-14} to 0.5 10^{-13} second time scale. These spectroscopic techniques allow to recognize, by means of adequate vibrational markers, the conformational information, such as alpha-helix and beta-sheet structures of proteins and peptides, double helix conformations (A, B and Z forms) in nucleic acids. Recent results show that there are still many interesting examples which can be studied by optical techniques, such as the conformational properties of ultrastable tetraloop hairpins in RNA and DNA [1-2]. The use of inelastic neutron scattering (INS) spectra recorded in solid phase and at low temperature on the polycrystalline powder samples of nucleic acid bases, nucleosides, nucleotides, amino acids and short peptides (building blocks of nucleic acids and proteins) could also reveal very promising results. For instance, it has been shown that NIS can be considered as a powerful tool in order to probe the condensed phase intermolecular hydrogen bonds in bases and nucleosides (see [3] and references therein). It is well known that intermolecular H-bonding plays a pivotal role in biomolecular recognition and interaction. In addition to the spectral range investigated by optical spectroscopy, NIS spectra permit exploration of the low frequency region (below 600 cm^{-1}: energy range from 80 meV to 25 meV) in which tosional motions dominate (*slow motions*, relative to the 10^{-13} second time scale range).

Methods and typical results

It should be emphasized that hairpins are elementary structural units responsible for nucleic acid folding. A hairpin consists of an intramolecular antiparallel double helix (stem) capped by a certain number of unpaired nucleotides (loop). In RNA (RiboNucleic Acid), hairpins allow this molecule to fold back on itself and to adopt its tertiary structures that are necessary for its function in various biological processes, such as translation and catalysis. In DNA (DeoxyriboNucleic Acid), hairpins participate for instance in the formation of cruciform units. Whatever the type of NA (RNA or DNA) is, the formation of hairpins leads to an increase of the structural and thermodynamic stability of the folded fragments. Hydrogen bonding between nucleotides and base stacking, are basically responsible for the structural and thermodynamic stability of hairpins. Furthermore, over 70% of the tetraloops belong to the UNCG and GNRA families (where N=U, A, C, G and R=A, G). Other minor tetraloops, such as UGAA, can also be found in the structure of 16S rRNA. For instance, the GAAA tetraloop participates in the long range tertiary interactions in catalytic RNAs; a toxin called ricin depurinates the second base (A) in the GAGA tetraloop; the third guanine (G) of this tetraloop (GAGA) takes part in this RNA/protein interaction; the GUGA tetraloop is conserved in ribozymes (catalytic RNAs). Up to now, the use of high resolution NMR spectroscopy permitted elucidation of the structural features of the GAAA, GCAA, GAGA, and UGAA tetraloops (RNA) formed in short synthetic oligonucleotides.

From the experimental point of view, Raman scattering and IR absorption have been used in order to analyse the vibrational features of nucleic acid and protein building blocks. In addition to these results, we have obtained the Raman and IR spectra of the short oligonucleotides (RNA or DNA) capable of forming ultrastable hairpins in aqueous solution (Figure 1).

---

1 *"Unusual nucleotide conformation in GNRA and UNCG type tetraloops formed in GNRA and UNCG type tetraloop hairpins: evidence from Raman marker assignments"*, N. Leulliot, V. Baumruk, M. Abdelkafi, P.Y. Turpin, A. Namane, C. Gouyette, T. Huynh-Dinh and M. Ghomi, Nucl. Acids Res. 27 (1999) 1398

2 *"Comparison between CUUG and UUCG tetraloops: Thermodynamic stability and structural features analysed by UV absorption and vibrational spectroscopy"*, V. Baumruk, C. Gouyette, T. Huynh-Dinh, J. S. Sun and M. Ghomi, Nucl. Acids Res. 29 (2001) 4089

3 *"Analysis of the Vibrational Spectra of RNA Building Blocks by NIS Spectroscopy and density functional calculations"*, M.P. Gaigeot, N. Leulliot, M. Ghomi, H. Jobic, C. Coulombeau and O. Bouloussa, Chem. Phys. 261 (2000) 217

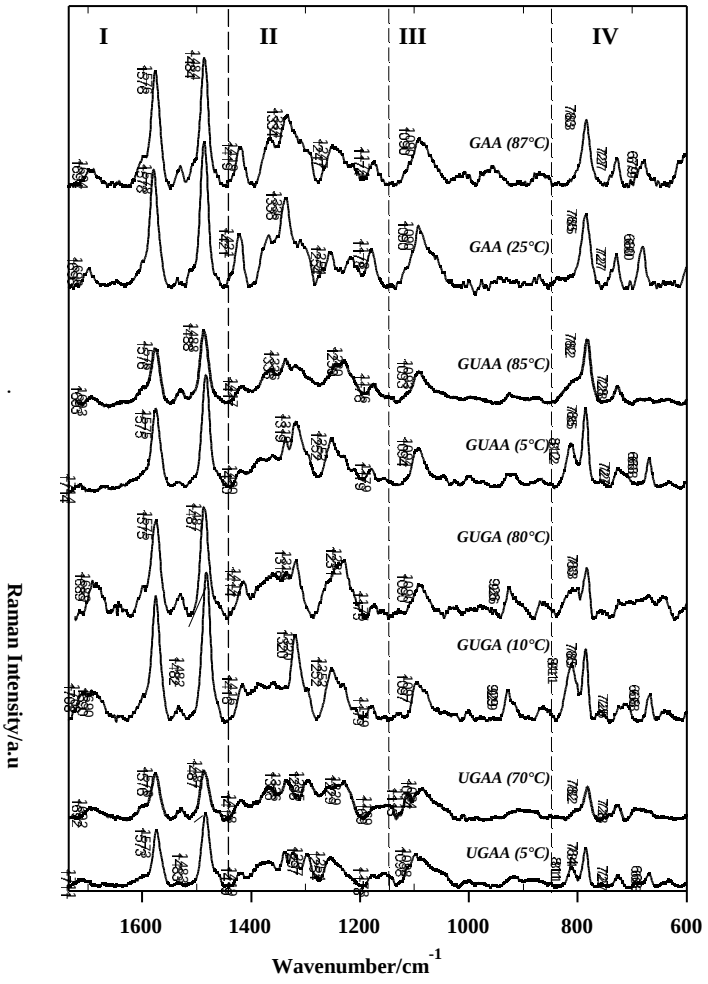

Figure 1. Raman spectra of a selection of the studied oligomers (UGAA, GUGA, GUAA, GAA) recorded in H_2O buffer (pH=6.8) at two ultimate temperatures (well below and well above the melting temperature (T_m) of each hairpin, respectively, Table 1)). Raman spectra are excited with 488 nm line (except for the GUAA hairpin, excitation at 514.5 nm), and displayed in 1725-600 cm^{-1} spectral regions. For abbreviations see Table 1.

*These spectra are divided into four contiguous spectral regions (**I** to **IV**), each of them bringing useful information on the order-to-disorder transition of the studied hairpins and the conformation of the nucleotides. For instance, In the region **I**, the downshift of the band at ~1710 cm^{-1} (low temperature), assigned to the base carbonyl stretch, to ~1690 cm^{-1} (high temperature) in RNA oligomers. This effect shows the breakdown of interbase H-bonds upon increasing temperature. The order to disorder transition can also be evidenced from the Raman hypochromism of several bands in the regions **I** to **IV**, consistent with the loss of stacking of the bases in the stem and loop of the hairpins.*

*Raman bands at ~811 cm^{-1} (A form helix marker in RNA) ~830 cm^{-1} (B form helix marker in DNA), both observed at low temperature (region **IV**), is consistent with the fact that the stem of the hairpins adopts a right-handed double helical conforamtion.*

The unusual stability of these hairpins has been evidenced by their high T_m (melting temperature) value obtained from the UV melting profile measurements, i.e. analysis of optical density (OD) at 288 nm (located in (the UV band relative to the π-π* electronic transition of the nucleic acid bases) as a function of temperature (Table 1).

Sequences	Abbreviation	T_m (°C)
Oligoribonucleotides Tetraloop hairpins		
5'-r(GCG-UGAA-CGC)-3'*	UGAA	46
5'-r(CGC-GAGA-GCG)-3'	GAGA	51
5'-r(CGC-GCGA-GCG)-3'	GCGA	56
5'-r(CGC-GGGA-GCG)-3'	GGGA	58
5'-r(CGC-GUGA-GCG)-3'	GUGA	58.5
5'-r(CGC-GGAA-GCG)-3'	GGAA	61
5'-r(CGC-GCAA-GCG)-3'	GCAA	62
5'-r(CGC-GUAA-GCG)-3'*	GUAA	63.6
5'-r(CGC-GAAA-GCG)-3'	GAAA	64
Oligodeoxynucleotide Triloop hairpin		
5'-d(GC-GAA-GC)-3'*	GAA	73.5

Table 1. T_m (melting temperature) values of the oligomer sequences forming stable hairpins, as obtained by UV absorption melting profiles in aqueous solutions.

T_m is the temperature value at which 50% of oligomers adopt an ordered conformation (hairpin); the rest of oligomers adopt a a disordered conformation (random coil).

*5' and 3' indicate the terminals of a given oligomer. The letter **r** designates an RNA oligomer, whereas the letter **d** refers to a DNA oligomer.*

Cantral sequences (underlined) refer to the loops (tetraloop in RNA and triloop in DNA) formed in these hairpins.

NIS spectra of the bases (U, C, A and G) and their parent ribonucleotides (rU, rC, rA and rG), all considered as the building blocks of RNA, obtained from the polycrystalline powder samples at T=15K, are shown in Figure 3.

The first advantage of the NIS spectra is that they provide interesting information on the vibrational modes which can be barely accessed by optical spectroscopy. For instance, those motions relative to the base N-H and C-H wagging motions of the bases (950-700 cm^{-1} spectral region), or those corresponding to the CCH, COH and OCH bending modes of the sugar observed in the 1550-1250 cm^{-1} spectral region (Figure 3, see the spectra of rU, rC, rG and rA).

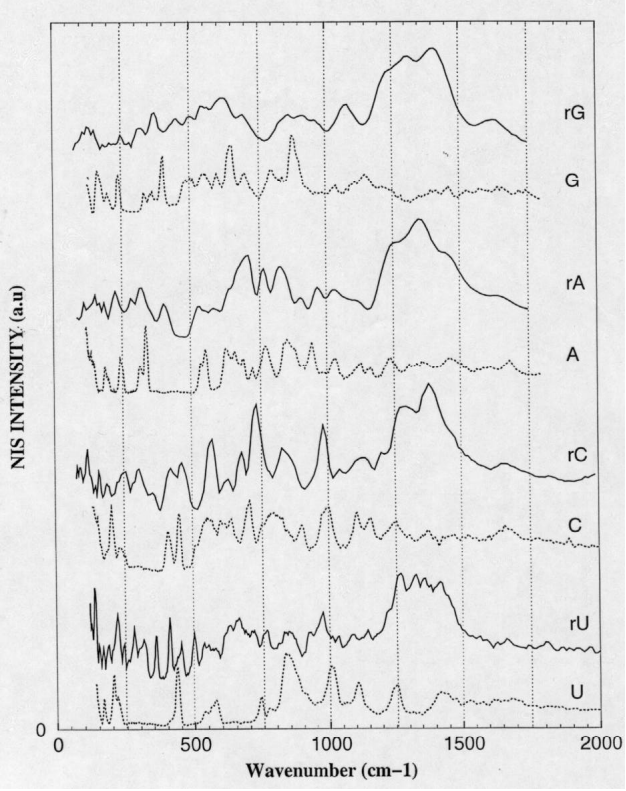

Figure 3. Neutron inelastic spectra of bases and ribonucleosides, recorded at 15K on the polycrystalline powder samples of these compounds. NIS spectrum of each base is compared to that of its parent nucleoside. This comparison permits the assignment of the modes between 1250 and 1550 cm^{-1}, to the vibrational motions of the ribose moiety included in each ribonucleoside. Other sugar modes can be detected in the spectral region below 900 cm^{-1}.
Many of the observed modes by NIS spectroscopy, cannot be accessed by traditional optical spectroscopy (Raman and IR).

Abbreviations:
U (uracil), C (cytosine), A (adenine), G (guanine).
Note that uracil is an RNA base, whereas the other bases (C, A, G) can be found in both RNA and DNA.
rU (uridine), rC (cytidine), rA (adenosine), rG (guanosine). r designates here a riboe (sugar) conjugated to a bas in a ribonucleoside.

In order to analyze the most prominent vibrational features of base and ribonucleosides and deoxyrobonucleosides (building blocks of DNA), as observed in optical and NIS spectra, we have carried out quantum mechanical calculations using the Density Functional Theory (DFT) method (GAUSSIAN Package from GAUSSIAN Inc. USA). Standard B3LYP/6-31G* level of theory has been used in order to estimate both the geometrical and vibrational properties of the analysed compounds.

Figure 4 (right) shows the optimised geometry of the lowest energy conformers of uridine (rU). They correspond to the C3'-endo/anti and C2'-endo/anti conformations, where C2'-rndo and C3'-endo refer to the ribose (sugar) conformations, and anti designates the orientation of the base (here uracil) with respect to the sugar. These two conformers differ one from the other by only 0.002 kcal/mol. They consequently represent two *nearly degenerate* conformers. The folding of RNA chain in UNCG and GNRA tetraloops (see above) is partially monitored by the C3'-endo/anti to C2'-endo/anti conformational transition of the sugars located in the middle ribonucleosides. The DFT calculations show that this transition can be done with a negligeable energy cost. Note the hydrogen bonds (broken lines) between the hydroxyl groups of the sugars as well as that of the C-H…O type H-bond between the sugar and the base.

In crystal phase uridine adopts a C3'-endo/anti conformation. In Figure 4 (right) we show the simulated NIS spectrum of uridine obtained by means of the calculated vibrational data of C3'-endo/anti uridine. Its comparison with the observed spectrum shows that below 900 cm^{-1}, many discrepancies occur in the simulated spectrum of the native species, whereas for the labile hydrogen deuterated species, the agreement between observed and simulated spectra is considerably improved. Hydrogen bonding in the crystal lattice of the bases and ribonucleosides generally occur on the labile hydrogens (relative to the N-H and O-H groups). The H-D exchange leads to the disappearance of the modes involving the labile hydrogens in NIS spectra (owing to the considerable difference between their incoherent cross section), especially those located below 900 cm^{-1}. We have also shown that by introducing explicit hydrogen bonds (for instance by means of water molecules) the agreement between the observed NIS spectra of these compounds and the simulated ones can be notably improved. The important conclusion that could be derived from these simple calculations (base or nucleoside

surrounded by water molecules) was that in solutions, the strength of the H-bonding with water molecules is comparable with the intermolecular ones, occurring in crystal phase.

Recent quantum mechanical (DFT) calculations on the crystal lattices of the bases and ribonucleosides [4], and the good quality of the simulated NIS spectra obtained at this level, could confirm all the assumptions based on our initial observations. They have also shown that the single molecule calculations provide calculated vibrational results that can completely deviate from those observed in solid phase, where the effect of the H-bonds on the vibrational modes cannot be neglected.

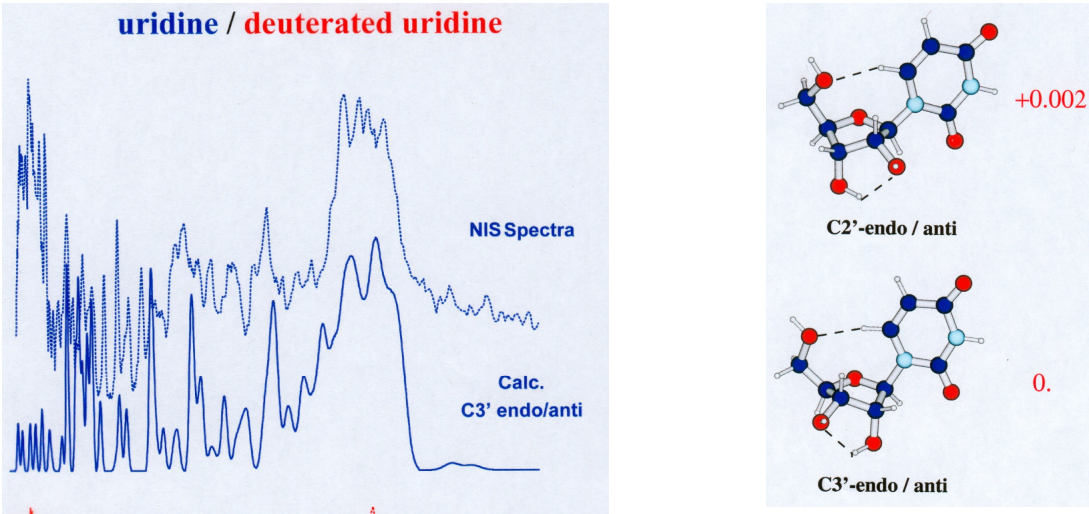

Figure 4
Left, Comparison between the calculated and observed NIS spectra of uridine (up) and its labile hydrogen deuterated species (bottom). Simulation has been made by means of the vibrational data obtained from a single moleculae model.
Right, Representation of the two lowest energy conformers of uridine.

Geometrical and harmonic vibrational calculations have been carried out at the DFT/B3LYP/6-31G level.*

Perspectives

All of the above mentioned results show that the dynamics (vibrational or large amplitude) of nucleic acids is still an active domain of research. This is also the case for peptides and proteins. Many other attractive examples can still be studied by the same spectroscopic techniques, such as biomolecular interactions. In the forthcoming years, the low frequency optical vibrational spectra merit to be carefully studied, in order to get information on the cooperative vibrational motion (large amplitude ones) of biopolymer chains. Quasi-elastic neutron spectroscopy (QENS) may also provide valuable information on the slower motions (larger time scale) of these molecules.

Acknowledgements

I would like to thank Belén Hernández, Nicolas Leulliot and Vladimir Baumruk for their help and discussions concerning the optical spectra. Hervé Jobic, John Tomkinson and Alexander Ivanov are gratefully acknowledged for their appreciable participation to the obtention of NIS at the Rutherford-Appleton (UK), and the institute of Laue Lagevin (France).

4 *"Modelling molecular vibrations in extended hydrogen-bonded network – crystalline bases of RNA and DNA and the nucleosides"*, M. Plazanet, N. Fukushima and M.R. Johnson, Chem. Phys. 280 (2002) 53

Microscopic dynamics and relaxation in a molecular-glass former

Miguel A. González
Institut Laue - Langevin, BP 156, 38042 Grenoble Cedex 9, France

1 Introduction

Dielectric relaxation constitutes a privileged technique in order to study the motions of molecular glass-formers, where the dynamics span many frequency decades. But the nature of the microscopic motions giving rise to low frequency relaxations in the dielectric spectra of molecular glass-formers in their normal or supercooled (SCL) liquid ranges still constitutes a controversial subject [1, 2, 3]. Among the existing molecular glass formers, small-chain alcohols are particularly good samples to study because of their easiness to form glasses, the relative long lifes of their SCL states as well as their simple molecular structures which makes them amenable to atomistic simulations using realistic interaction potentials.

Therefore we have explored the dynamics of two isomeric alcohols: 1-propanol (1Pr, $CH_3CH_2CH_2OH$) and 2-propanol (2Pr, $CH_3CHOHCH_3$). The chemical change of the OH hydroxyl group from the end to the middle of the three-carbon skeleton leads to remarkable differences in crystal and glass structures [4], thermal [5] (melting and glass-transition temperatures change from T_m = 148 K to 185 K and from T_g = 98 K to 115 K, respectively) and transport properties. However, basic molecular properties such as the dipole moment (1.7 Debyes) or the molecular volume do not change much. Moreover, the origin of the bands observed in the dielectric spectra of 1Pr has focussed many of the controversies mentioned above. Thus we intend to combine neutron spectroscopy and computer simulations to obtain a microscopic view or some hints above the nature of the motions giving rise to those bands.

2 Methods

As we said above, dielectric spectroscopy allows us to explore the dynamics of the system on a wide range of frequency decades. On the other side, the dynamic range explored with neutron scattering techniques is much more reduced, but neutrons provide a wealth of information on the nature of the motions observed (both space and energy are sampled). In particular, we have investigated the dynamics of both liquids (1Pr and 2Pr) by quasielastic neutron scattering using the IRIS spectrometer at the ISIS pulsed neutron source and the time-of-flight spectrometer IN6 at the ILL (Grenoble, France). Our main goal is to see wether rotational and mass-diffusion motions exhibit different temperature dependences, since mass-diffusion may be the main contributor to the viscosity $\eta(T)$ at high temperatures and rotations dominant at low temperatures. This would explain why $\eta(T)$ for 1Pr matches the T-dependence of the main dielectric relaxation time within a restricted temperature range only [1].

To help with data analysis, some quantities not directly amenable to experiment have been evaluated for both samples from computer Molecular Dynamics simulations. Those simulations were done using the DLPOLY package [6] and the potential employed in the simulations is the OPLS All-Atom force field [7]. This model includes all the molecular degrees of freedom (bonding, bending and torsions), so all the atoms of the molecules of 1Pr and 2Pr are treated explicitly. The interactions between nonbonded atoms are represented by a sum of Lennard-Jones and Coulomb terms. The simulated system consisted of 512 molecules of 1Pr or 2Pr. For both systems, the sample was equilibrated at 300 K and 1 bar during a period of 100 ps and then the temperature was reduced in a series of steps of 40 K. During each step the system was equilibrated for another period of 100 ps and the volume of the simulation box was allowed to change to keep the pressure close to 1 bar. In this way we quenched both isomers down to 60 K. The densities of the configurations thus obtained are 0.969 g/cm^3 (1Pr) and 0.970 g/cm^3 (2Pr). Then we simulated both alcohols at 60 K using the microcanonical ensemble (constant NVE) for a period of 100 ps. The first property calculated was the density of states (DOS), obtained as the Fourier transform of the velocity autocorrelation function. This quantity is directly comparable with the DOS obtained with NS and allows us to determine the validity of the simulations. Then

we computed the mean-square displacements for the molecular centers-of-mass and the orientational correlation functions in order to relate them with the findings obtained in the QENS experiments.

3 Typical results

The DOS, $G(\omega)$, computed for 1Pr and 2Pr are shown in Fig. 1. In order to be able to compare them with the experimental results, we have calculated the partial $G(\omega)$ for each atom and we have summed them weighted by their neutron cross section. Therefore the resulting curve contains basically only the contributions from the hydrogens of the molecule. This figure can be compared with the experimental DOS obtained in the QENS spectrometer and shown in Fig. 2.

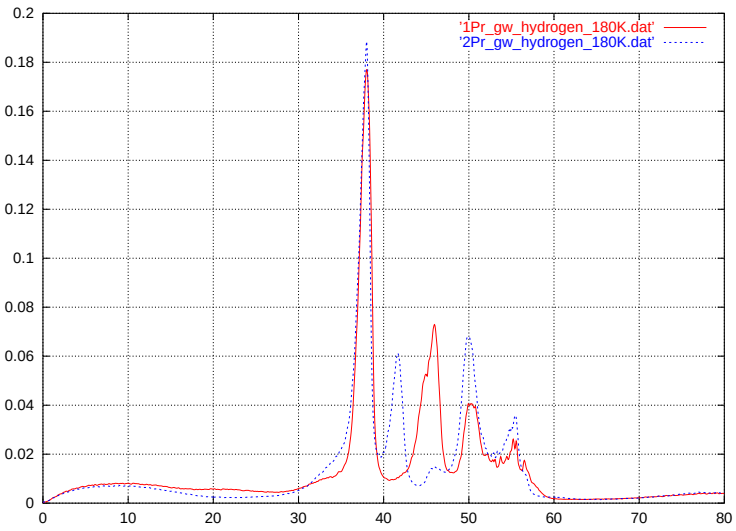

Figure 1: Simulated densities of states for 1-propanol (red continuous line) and 2-propanol (blue dotted line). Energy given in x-axis in meV units.

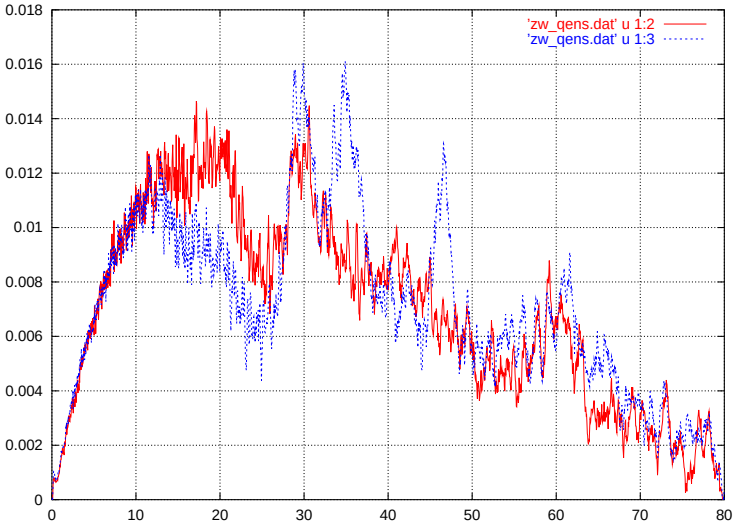

Figure 2: Experimental densities of states obtained in QENS for 1-propanol (red continuous line) and 2-propanol (blue dotted line). Energy given in x-axis in meV units.

We cannot expect a full agreement between experiment and a classical simulation. Nevertheless, the comparison of both figures shows that at a qualitative level the agreement between simulation and experiment is remarkably good. Thus, one sees that the first peak appearing at around 30 meV for both 1Pr and 2Pr appears also on the simulation (although shifted to 38 meV) and that the second peak at around 35 meV on 2Pr, which has no counterpart on 1Pr, is well reproduced in the simulated $G(\omega)$ of 1Pr (no peak) and 2Pr (shifted to 42 meV). The other clear peaks on the DOS of 2Pr at around 47 and 62 meV can be also tentatively assigned to the peaks obtained in the simulation at 50 and 55 meV. In the case of 1Pr there are no so clear peaks on the DOS obtained in QENS, so it is more difficult to do a similar assignment. One can tentatively make the correspondence between the small peaks at around 42 meV and the strong peak in the simulation at 46 meV and between the modes around 60 meV and the simulated peaks at around 55 meV (they appear in both isomers and in both experiment and simulation).

The information provided by the MD simulations allows to calculate also the partial DOS. They are shown in Fig. 3 and 4 for 1Pr and 2Pr respectively.

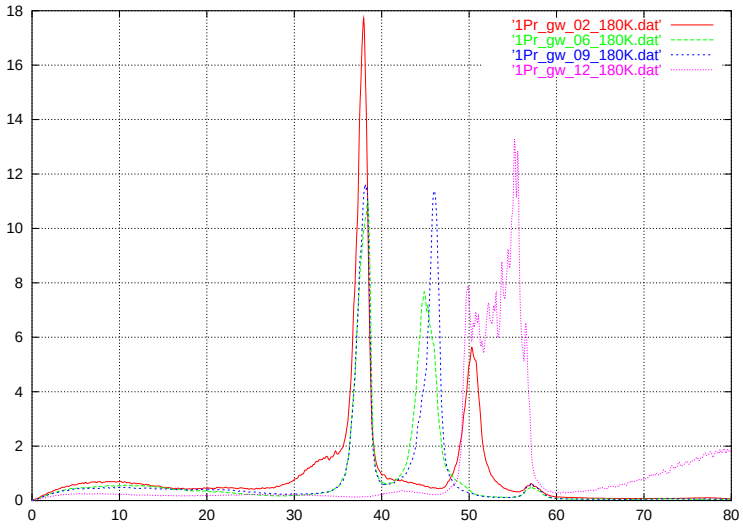

Figure 3: Partial densities of states simulated for 1-propanol.

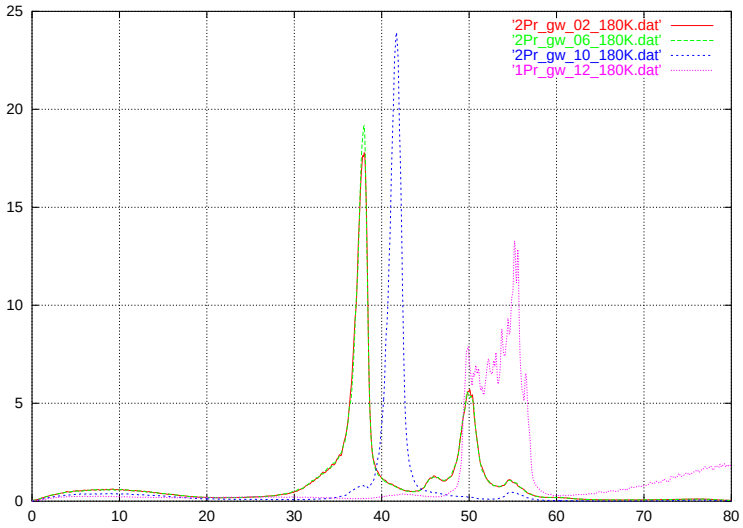

Figure 4: Partial densities of states simulated for 2-propanol.

It is possible to see that the first peak is mainly due to the hydrogens of the methyl groups. In the case of 1Pr there are also contributions from the hydrogens of the two CH_2 groups, while for 2Pr the hydrogen of the CH group contributes to the neighbour peak. The hydroxilic H contributes only above 50 meV and it is possible to see that it shows a bump around 80 meV which is due to the vibrations in an H-bond.

The low-frequency part of the DOS was obtained experimentally in IN6 and it is shown in Fig. 5. Comparing simulation and experiment we see that the simulation reproduces well the bump for 1Pr between 15 and 25 meV observed in QENS and also in IN6 but it does not a good job below 15 meV.

The final figure (Fig. 6) shows the results obtained for the center-of-mass and the reorientational motions in conjuction with the available experimental data. The agreement is again reasonably good.

4 Perspectives

One of the main problems found is the difficulty of calculating directly the dielectric spectrum. This is a collective properties and requires very long simulations (of the order of several nanoseconds) in order to be able to calculate it with enough accuracy. This problem becomes increasingly important as we cool our system and we approach to the glass-transition temperatures, as the relaxation times involved increase exponentially. It results clear that additional computing power together with new simulation methods are required to overcome this problem.

The other problem is on the empirical force field used. The applicable potentials have been developed over the years and they do a good job to calculate many properties, but they are not perfect. The comparison between the experimental and the simulated DOS is a clear example. It would be good to be able to use ab initio techniques to study the dynamics of these systems. However, the size and time scales involved seem to make this impossible at the moment.

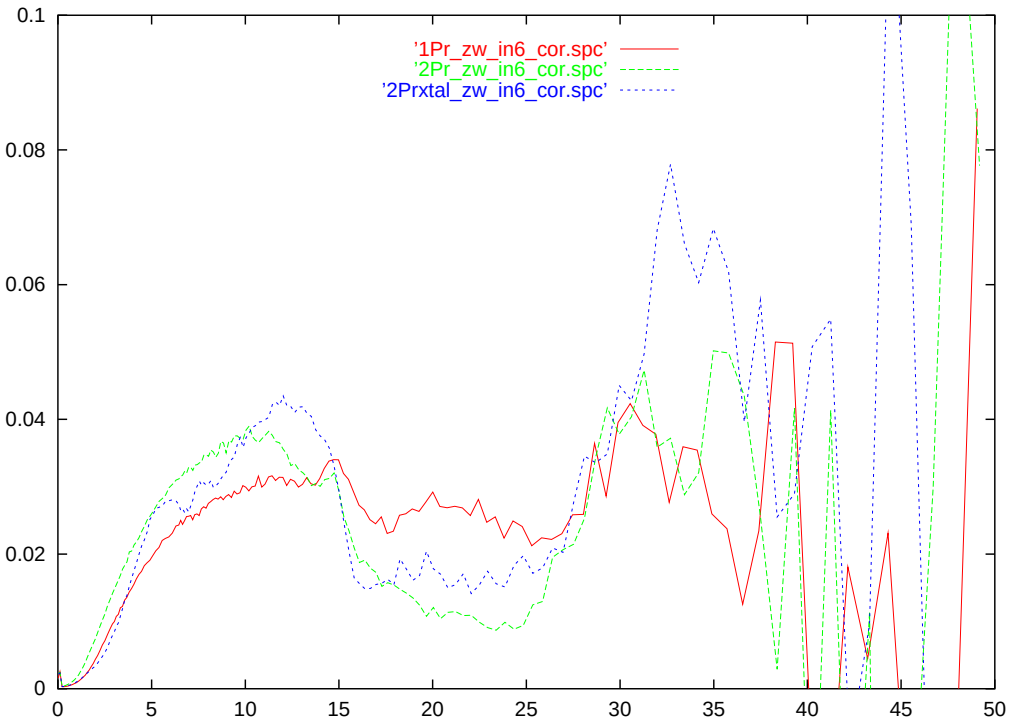

Figure 5: Low-frequency part of the densities of states obtained on IN6 for glassy 1-propanol (red line), glassy 2-propanol (green line) and crystalline 2-propanol (blue line).

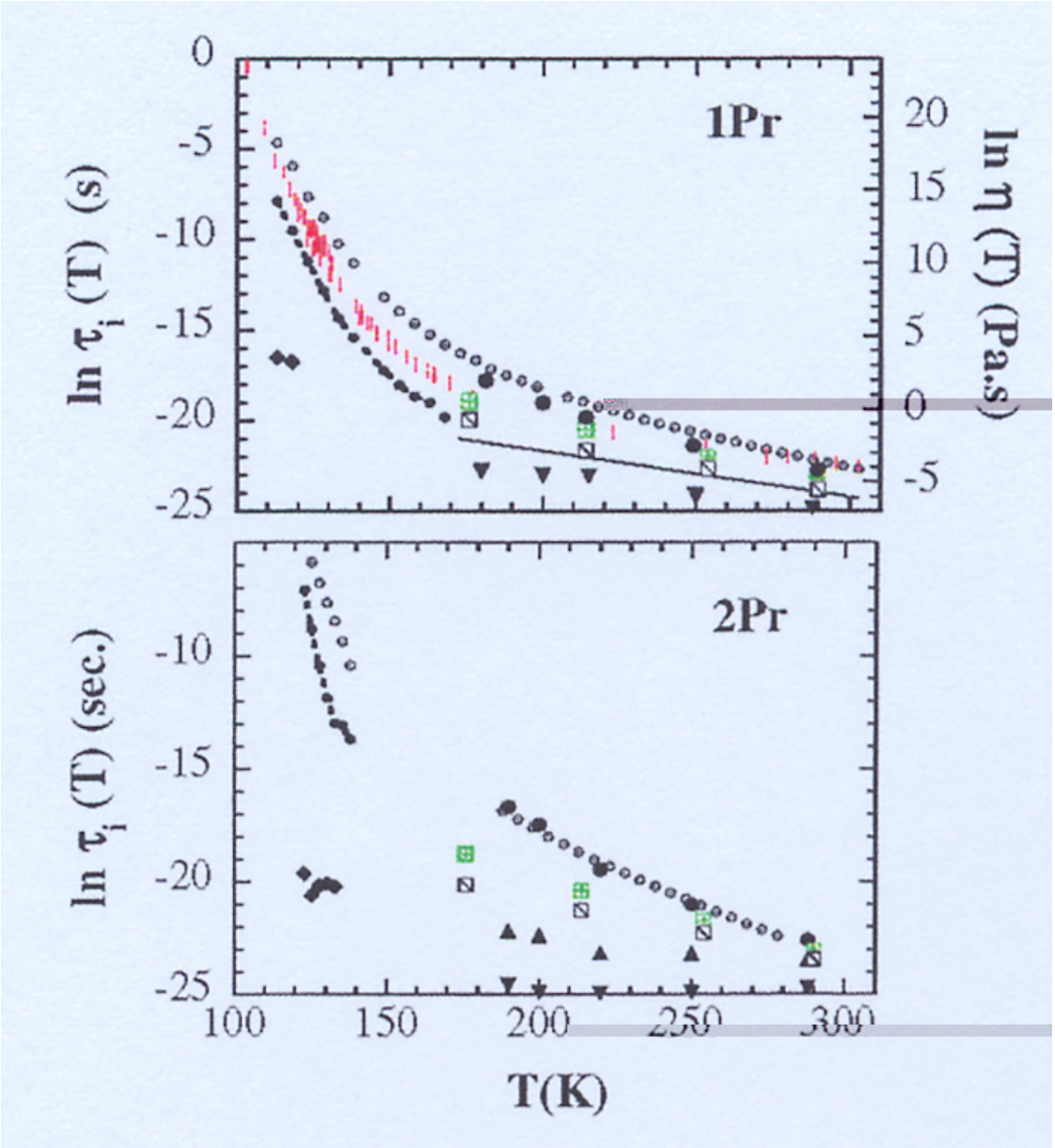

Figure 6: Relaxation times of 1-propanol (up) and 2-propanol (down). The open circles show dielectric data for the main peak, the thick dots display data for the secondary relaxation and the open lozenges stand for the relaxation time of the β-relaxation. The straight line correspond to ^{17}O NMR relaxation data. Red vertical bars show the temperature dependence of the viscosity. The solid circles (translation) and the inverted triangles (rotation) correspond to our quasielastic neutron scattering results. Simulation data are shown as squares: with a cross inside (for translational times) or a diagonal line (for rotational times derived from the long-time behaviour of $P_1(\cos\mu)(t)$.

References

[1] C. Hansen et al, *J. Chem. Phys.* **107**, 1086 (1997).

[2] M. Jiménez-Ruiz et al.c (submitted).

[3] G. Power et al., *J. Chem. Phys.* **116**, 4192 (2002).

[4] C. Talon et al., *Phys. Rev. Lett.* **88**, 115506 (2002).

[5] C. Talon et al., *J. Non-cryst. Solids* **287**, 226 (2001).

[6] DL_POLY is a package of molecular simulation routines written by W. Smith and T.R. Forester, copyright The Council for the Central Laboratory of the Research Councils, Daresbury Laboratory at Daresbury, Nr. Warrington (1996).

[7] W.L. Jorgensen, D.S. Maxwell, and J. Tirado-Rives, *J. Am. Chem. Soc.* **118**, 11225 (1996).

The dynamics of proton transfer studied by field-cycling NMR

A.J. Horsewill, School of Physics & Astronomy, University of Nottingham,
Nottingham, NG7 2RD, UK

Introduction

Hydrogen bonds and proton transfer are fundamental to many structures and processes in the molecular and life sciences. In recent years, field-cycling NMR has provided a sensitive technique for accurately measuring and characterising the proton transfer dynamics in model systems. Neutron scattering experiments have complemented this work and important progress has been reported in the literature in the sphere of theory and computational chemistry.

Experimental Methods

Historically, NMR has been one of the most proficient experimental techniques for studying the large amplitude dynamics of atoms and molecules. The molecular motion imposes characteristic features in both NMR spectra and NMR relaxation properties that can be analysed to reveal the dynamical rate and, in ideal cases, the structural geometry associated with the molecular rearrangement. In recent years, work in my laboratory has been concerned with the study of proton transfer in the hydrogen bonds of carboxylic acid dimers. Studied by many groups and a variety of experimental techniques, this is established as the model system for hydrogen bond dynamics. Investigations in Nottingham have been undertaken in the solid state at low temperature and measurements of the magnetic field dependence of the proton spin-lattice relaxation rate provide a direct measure of the spectral density function for proton transfer.[1] The width of this lineshape function provides a precise measurement of the inverse correlation time for the motion, τ_c^{-1}, Figure 1; the amplitude is determined by the structural geometry. This example is one of incoherent dynamics where the proton motion undergoes stochastic hopping between two sites with inequivalent energy. In cases where the proton exhibits coherent tunnelling, as in methyl rotation for example, then the spectral density possesses peaks centred at the tunnelling frequency. Experimentally these can be detected using level-crossing spectroscopy where enhanced nuclear spin relaxation is observed at magnetic field values where the tunnelling frequency matches a spin Larmor frequency. Common to investigations of both incoherent and coherent dynamics is the fact that the relaxation properties are studied as a function of magnetic field; since the detection of NMR signals is conventionally narrow band, to study broadband relaxation properties in this way invariably requires procedures that involve magnetic field-cycling.[2]

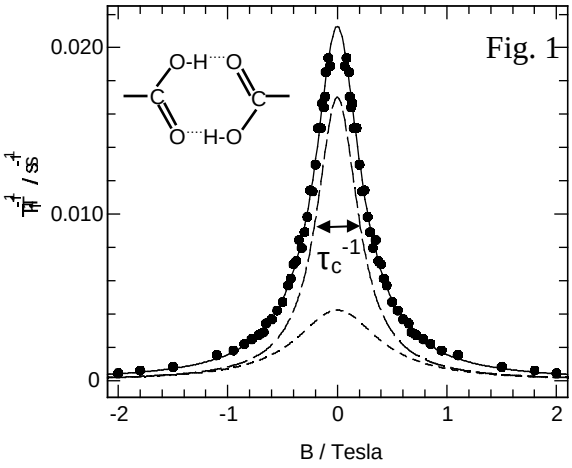

Figure 1 The spectral density for double proton transfer in the hydrogen bonds of benzoic acid. The linewidth provides a direct measurement of the inverse correlation time.

Typical Results

The inverse correlation time may be determined as a function of temperature as shown in Figure 2 where the proton transfer dynamics are recorded for three isotopologues of the benzoic acid dimer. The isotope mass effect is clearly apparent at low temperature where the ratio of the inverse correlation times are approximately 30:1 for HH and HD dimers and approximately 15:1 for HD and DD dimers. This, together with the characteristic plateau region where the correlation time is independent of temperature, reveals the contribution of quantum tunnelling to the dynamics. At low temperature the proton transfer motion is dominated by phonon assisted tunnelling, a barrier crossing mechanism that depends on the fundamental wave-like properties of the protons.

The benzoic acid samples are well ordered with a well-characterised crystal structure, furthermore, they are prepared with high purity. With only one mechanism driving the spin-lattice relaxation, assignments can be made with good confidence and measurements can be made with high precision. In Figure 3, an example is shown where more than one motional species is present; two correlation times characterises the sample. Here the contribution of each species to the overall proton spin-lattice relaxation rate is additive. Where the number of species is small there is a good chance of deconvolving the data to provide accurate measurements of the dynamics of the different species, however, with increasing complexity there may be no possibility of identifying the species separately.

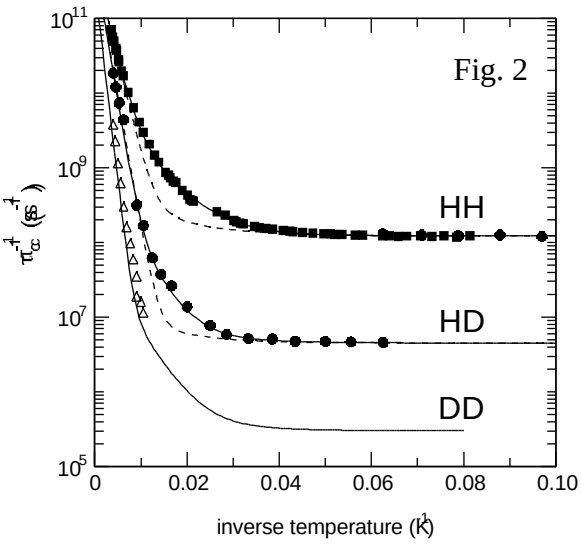

Figure 2 The dynamics for double proton transfer in three isotopologues of benzoic acid.

Perspectives

In recent years, field-cycling NMR relaxation measurements together with complementary quasi-elastic neutron scattering data have provided highly accurate data on the dynamics of proton transfer in model hydrogen bond systems in the solid state.[3] It is clear from these experiments that quantum tunnelling plays a pivotal role in the proton motion, particularly at low temperature. The dynamics are governed by a multi-dimensional potential energy surface (PES) reflecting the role of coupling to internal and external vibrational modes of the molecule. The experiments, particularly those at low temperature, can reveal limited information on the PES and some of its eigenstates. Neutron vibrational spectroscopy provides further insight into the modes which promote proton transfer, however, the complexity of the system is such that experiments alone are unlikely to be sufficient. Making controlled changes to the system, for example by deuteration or by application of pressure can be invaluable, however, sophisticated and intense *ab-initio* calculations are required to provide a more complete account of the mechanisms underlying the proton transfer motion. With the development of theoretical protocols such as the perturbative instanton approach of Benderskii[4], there is the possibility of modelling the behaviour in a satisfactory way for small model systems. These investigations are essential for providing us with a sound understanding of the fundamental aspects of tunnelling and molecular motion over a multi-dimensional potential energy surface. The foundations must be in place before tackling more complex molecular systems.

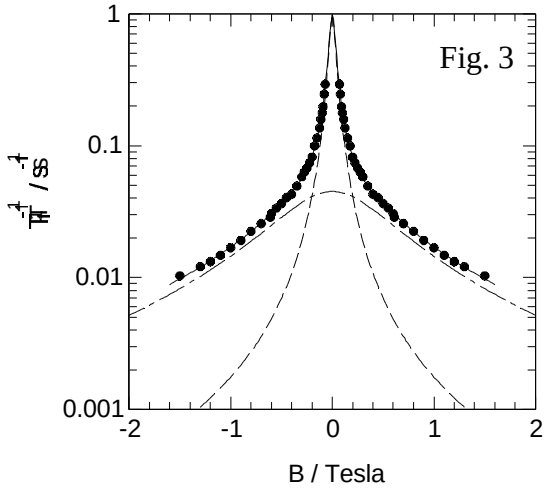

Figure 3 Two species contribute to this spectral density function and the two correlation times can be determined accurately. Simple deconvolution becomes impossible for complex systems.

Proton transfer is of fundamental importance to many structures and processes in the Life Sciences. Insight into the general principles and mechanisms can be gained from the study of small model systems like the carboxylic acid dimers. However, the study of specific processes in complex systems of biological importance is one faced with severe difficulties both experimental and computational. Clearly, where there is complexity we would like our experiments to have better discrimination in favour of the sites or functional moieties of interest. Increasingly there are ways being developed of designing more sophisticated NMR experiments that can give better specificity.

For example, multiple-quantum magic-angle spinning experiments[5] can be performed to determine the local molecular structure in systems with long-range disorder such as polymers.

Although NMR is very sensitive to magnetic interactions, the sensitivity of the measured NMR signal is rather poor and it is this limitation that inhibits many possibilities. The development of hyperpolarized nuclear spin systems offers the opportunity to overcome, partially at least, the problems of signal to noise ratio. Realistically, signal to noise improvements of order 10^4 may become possible, however, although it is currently possible to achieve large polarisations in ^{129}Xe and ^{3}He it is a more difficult and as yet largely unsolved problem to transfer this polarisation to nuclei of functional importance such as ^{1}H.

In the short term at least, it is likely that to obtain good signal to noise ratio and good specificity it will continue to be necessary to study crystalline materials with a high degree of order. Progress can still be achieved by selecting small molecular systems that possess functional groups that replicate the behaviour of 'real' systems. However, as is clear from protein folding, the substrate in which the molecule is contained may have as much influence on the behaviour as the protein molecule itself, in which case the study of the molecule in isolation of its environment may not entirely replicate the behaviour of real systems.

---

[1] D.F. Brougham, A.J. Horsewill & R.I. Jenkinson, Chem.Phys.Letters **272** (1997) 69
[2] A.J. Horsewill, Progr.Nucl.Mag.Res.Spectrosc. **35** (1999) 359
[3] M. Neumann, D.F. Brougham *et al* J.Chem.Phys. **109** (1998) 7300
[4] V.A. Benderskii *et al*, Chem.Phys. **262** (2000) 392 and refs therein
[5] I. Schnell, A. Watts & H.W. Spiess, J.Mag.Res. **149** (2001) 90 and refs therein

Extended abstract for the ESF workshop: Bridging the gap in molecular science between model systems and real systems

Electrostatic interactions and finite-size effects in molecular simulations.

Philippe H. Hünenberger, Laboratorium für Physikalische Chemie, ETH Zürich, CH-8093 Zürich, Switzerland

Introduction

Electrostatic interactions are of fundamental importance in determining the structure, dynamics, and function of biomolecules. In particular, they play a key role in protein folding and stability, pH-induced conformational changes, recognition of substrates by receptors and enzymatic catalysis. However, due to their magnitude and long-range nature, the accurate representation of electrostatic interactions in classical computer simulations is a difficult task. There is thus considerable effort in the scientific community towards the goals of (*i*) improving the representation of electrostatic interactions in biomolecular simulations, and (*ii*) understanding their specific role in biomolecular processes. The present abstract describes some of the work carried out in our group along the first of these lines.

From the point of view of quantum mechanics, chemistry can be described as the science of electrostatic interactions (between nuclei and electrons). However, to reach system-sizes and timescales compatible with the experimental world, most (bio-)molecular simulations rely on a classical description of molecular systems.[1] In this case, specific types of electronic effects (covalent, exchange-repulsion, dispersion, and long-range electrostatic interactions) are grouped into the different terms of a force field (potential energy function), and classical electrostatic interactions only encompass the long-range residual of quantum electrostatics. This long-range tail is usually represented by the Coulombic interaction between atomic partial charges located on the solute and solvent molecules. However, the accurate representation of long-range electrostatic interactions in classical computer simulations is a difficult problem.[2–5] In fact, the approximate treatment of these interactions in explicit-solvent (bio-)molecular simulations currently represents one of the principal bottlenecks in the accuracy of these methods.[2–5] This is because, due to computational costs, simulated systems are restricted to very small sizes (typically <1000 nm^3). As a direct consequence, the longest-range (>10 nm) component of intermolecular interactions can only be computed in an approximate manner. However, due to the magnitude and long-range nature of electrostatic interactions, uncontrolled approximations can give rise to important artifacts (so-called finite-size effects), which may strongly impair the reliability of many current simulations.

The majority of explicit-solvent biomolecular simulations are carried out under periodic boundary conditions. In this case, the solute biomolecule is placed into a computational box (space-filling shape, *e.g.* rectangular parallelipiped), and the empty volume filled by solvent molecules. The system considered in the simulation consists of the central box surrounded by an infinite array of periodic copies of itself,[2,6] which has the advandage of removing any distortion associated with a solvent/vacuum boundary. There are essentially three methods to handle electrostatic interactions in simulations under periodic boundary conditions (Figure 1). Straight truncation (ST) of the Coulomb interaction at a convenient (cutoff) distance,[2,6] in order to limit the computational costs and the effect of periodic boundary conditions, is often a very severe approximation, leading to important artifacts in many simulated properties.[7–13] Two alternative schemes are available to reduce these effects : the inclusion of a reaction-field (RF) correction[14,15] to the cutoff truncation, or the use of lattice-sum (LS) methods (Ewald,[16] P^{3}M,[17] PME[18]). These two types of methods also involve approximations, although presumably less drastic than the straight truncation of the long-range interactions. It is therefore of importance to carefully investigate and compare the accuracy of these different methods. Our strategy to analyze and improve electrostatic schemes for explicit-solvent molecular simulations is to use continuum electrostatics, with the goal of understanding, correcting, and ultimately eliminating finite-size effects.[5,12,13,19,20]

Method

Simulations of biomolecular systems (and in particular DNA, RNA, and proteins) using LS methods are beginning to abund in the literature. LS methods are formally exact for truly periodic systems (crystals), but only approximate for the simulation of real (non-periodic) solutions.[5] However, little work has been done

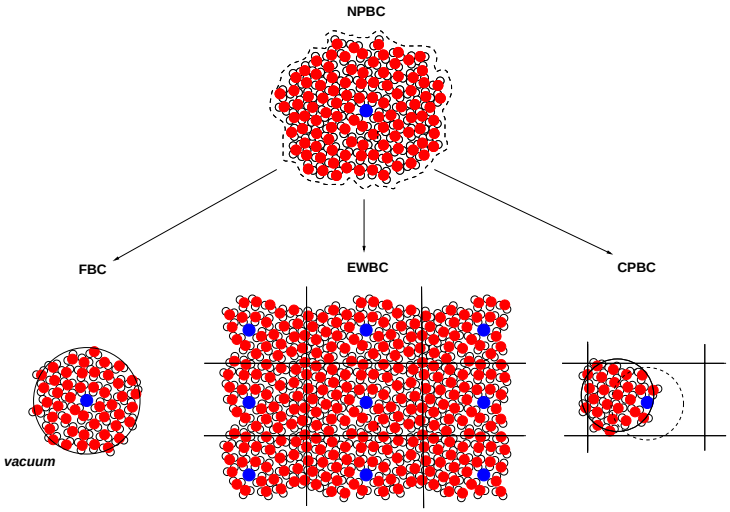

Figure 1: Possible choices of boundary conditions for molecular simulations using an explicit representation of the solvent. The solute is symbolized by a black sphere and the solvent (water) represented using a space-filling model. Non-periodic boundary conditions (NPBC) correspond to the ideal case of a macroscopic system, inaccessible to molecular simulations. Computationally tractable approximations are : Fixed boundary conditions (FBC), Ewald boundary conditions (EWBC; LS methods) and periodic boundary conditions with cutoff (CPBC; ST and RF methods). In the CPBC case, the dashed circle represents the solute-solvent cutoff of a solute atom (or charge group) and the solid circle the solvent-solvent cutoff of a solvent atom (or charge group). In the ST method, the medium outside the cutoff sphere is considered to be vacuum, while in the RF method, it is treated as a dielectric continuum with the same permittivity as the pure solvent.

to assess the nature and magnitude of the perturbation that arises from artificial periodicity. Our approach to study this perturbation based on continuum electrostatics is the following. The reaction potential (and solvation free energy) generated by the solvent around a solute of arbitrary shape and charge distribution can be determined by solving the Poisson equation using a finite-difference scheme.[21] This can be done both for non-periodic boundary conditions[21] and for periodic boundary conditions.[13] By comparing the two results, the effect of the artificially-imposed periodicity on the solvation free energy of a (bio-)molecule (in a given conformation) can be assessed quantitatively.[5,13,19,20] In cases where this perturbation is small (large computational box, solvent of high permittivity, solute with no net charge and of low polarity), the explicit-solvent simulation of the system using LS methods will be a reasonable approximation to the non-periodic case (macroscopic sample at infinite dilution). In other cases, the continuum method may be used to compute corrections for the finite-size effects affecting the simulated properties.

Continuum electrostatic methods can also be used to investigate finite-size effects linked with the ST and RF schemes, as well as some others (shifting and switching functions[2]). Although artifacts linked with the ST scheme are very important[7–13] , the RF method appears to be a viable alternative to LS methods for the simulation of biomolecular systems, and is also used by many research groups. As a first step in the continuum electrostatics analysis of the ST, RF, and related schemes, we considered the solvation of a spherical ion.[12] A generalized Born model was developed, where the r^{-1}-dependence of Coulomb's law is replaced by an arbitrary polynomial, truncated at a specified cutoff distance. It was possible to derive an analytical integral equation defining the polarization around the ion, and thus allowing to compute the ionic solvation free energy. This model was used to assess the quality of different approximations employed in explicit-solvent simulations, and derive corrections to ionic solvation free-energies calculated from these simulations.[12] It is also known from explicit-solvent simulations that cutoff truncation strongly affects the effective interaction (potential of mean force) between two solvated ions. Due to finite-size artifacts, this effective interaction may even become attractive over a certain range of distance for two ions of the same charge.[10] To tackle this problem, we have constructed a continuum electrostatics model[22] describing the interaction between two spherical ions in the presence of cutoff truncation (ST or RF). An alternative route is the use of a newly-developed algorithm for solving the Poisson equation for a solute-solvent system under periodic boundary conditions using fast Fourier transforms.[23] This method may be extended[24] to truncated Coulomb interactions (ST or RF), which should permit a systematic analysis (and possibly correction) of cutoff-linked finite-size effects in complex molecular systems.

Illustrative results

Three prototypical examples illustrate that the above considerations are far from being academic. The first example is the calculation of ionic solvation free energies. Values computed from explicit-solvent molecular dynamics simulations of the sodium cation (parameters from Straatsma & Berendsen[8]) range from -250 to -460 kJ/mol,[25] depending on the electrostatic scheme employed (LS, ST, or RF) and parameters used (edge of the cubic box in the range 1.2 to 4 nm, cutoff radius in the range 0.8-1.4 nm). However, when the appropriate corrections for finite-size effects based on continuum electrostatics are applied, all results converge to an estimate of -399±2 kJ/mol, in reasonable agreement with the experimental value of -370 kJ/mol (the slight discrepancy points towards the need of refining the force-field parameters determining the ionic radius).

The second example illustrates the influence of artificial periodicity on the conformational equilibrium of a polyalanine octapeptide (with charged termini) in water. Three explicit-solvent molecular dynamics simulations of this peptide were compared, using a LS method (P^3M[17]) for handling electrostatic interactions together with cubic periodic boxes of edges $L = 2$, 3, and 4 nm.[20] The α-helix was found to be stable and rigid in the smallest box, stable but less rigid in the medium box, and unfolding in the largest box (Figure 2). Only the latter behaviour agrees with experiment. The observed differences could be rationalized using a continuum electrostatics analysis of periodicity-induced artifacts (see above) based on configurations from the trajectories. These calculations show that the α-helical conformation is stabilized by artificial periodicity relative to any other configuration sampled during the simulations. This stabilization is due to the favorable interaction between the charged termini of the oligopeptide in the central computational box and those of its periodic copies in the adjacent boxes. This artifact increases in magnitude with decreasing box size, and is responsible for the absence of unfolding in the two smaller boxes and the reduced backbone fluctuations in the smallest box.

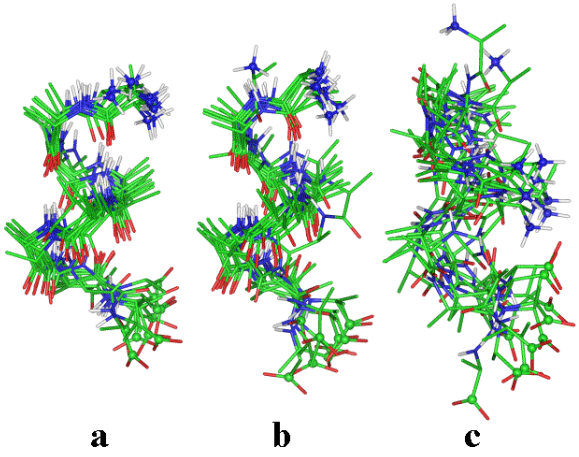

Figure 2: Ten configurations (superimposed on the C_α atoms) taken at 100 ps intervals from three molecular dynamics simulations (employing LS electrostatics) of a polyalanine octapeptide (charged termini) with cubic unit cells of edges $L = 2$ nm (a), $L = 3$ nm (b), and $L = 4$ nm (c).

These results suggest that electrostatic finite-size effects in explicit-solvent simulations of biomolecules may significantly perturb the potentials of mean force for conformational equilibria. The effect may be so strong as to invert the relative stabilities of the folded and unfolded states of a peptide.[20] Because of the potential implications of these findings for the reliability of many biomolecular simulations, we are currently performing a systematic study of finite-size effects in simulations of complex biomolecular systems, including an oligonucleotide (double-stranded DNA dodecamer), a small charged protein (insulin gene enhancer protein ISL-1), and a membrane patch (2×64 dipalmitoyl-phosphatidylcholine double layer), with different electrostatic schemes (SC, RF, or LS), parameters (cutoff distance, box size), and numbers of counter-ions (none, minimal set, or excess).

References

[1] P.H. Hünenberger and W.F. van Gunsteren, in *Computer simulation of biomolecular systems, theoretical and experimental applications*, Vol. **3**, van Gunsteren, W.F., Weiner, P.K. & Wilkinson, A.J., Eds., Kluwer/Escom Science Publishers, Dordrecht, The Netherlands, pp 3-82. (1997).

[2] W.F. van Gunsteren and H.J.C Berendsen, *Angew. Chem. Int. Ed. Engl.* **29**, 992 (1990).

[3] P.E. Smith and W.F. van Gunsteren, in *Computer simulation of biomolecular systems, theoretical and experimental applications*, Vol. **2**, van Gunsteren, W.F., Weiner, P.K. & Wilkinson, A.J., Eds., ESCOM Science Publishers, B.V., Leiden, The Netherlands, pp 182-212 (1993).

[4] R.M. Levy and E. Gallicchio, *Annu. Rev. Phys. Chem.* **49**, 531 (1998).

[5] P.H. Hünenberger, in : *Simulation and theory of electrostatic interactions in solution: Computational chemistry, biophysics, and aqueous solution*, Hummer, G. & Pratt, L.R., Eds., American Institute of Physics, New York, U.S.A, pp 17-83. (1999).

[6] M.P. Allen and D.J. Tildesley, *Computer simulation of liquids.* Oxford University Press, New York (1987).

[7] M. Neumann, O. Steinhauser, and G.S. Pawley, *Mol. Phys.* **52**, 97 (1984).

[8] T.P. Straatsma and H.J.C. Berendsen, *J. Chem. Phys.* **89**, 5876 (1989).

[9] H. Schreiber and O. Steinhauser, *Chem. Phys.* **168**, 75 (1992).

[10] G. Hummer, D.M. Soumpasis, and M. Neumann, *Mol. Phys.* **81**, 1155 (1993).

[11] R.H. Wood, *J. Chem. Phys.* **103**, 6177 (1995).

[12] N.A. Baker, P.H. Hünenberger, and J.A. McCammon, *J. Chem. Phys.* **110**, 10679 (1999).

[13] P.H. Hünenberger and J.A. McCammon, *J. Chem. Phys.* **110**, 1856 (1999).

[14] J.A. Barker and R.O. Watts, *Mol. Phys.* **26**, 789 (1973).

[15] I.G. Tironi, R. Sperb, P.E. Smith, and W.F. van Gunsteren, *J. Chem. Phys.* **102**, 5451 (1995).

[16] P.P. Ewald, *Ann. Phys.* **64**, 253 (1921).

[17] R.W. Hockney and J.W. Eastwood, *Computer simulation using particles.* Institute of Physics Publishing , Bristol (1981).

[18] U. Essmann, L. Perera, M.L. Berkowitz, T. Darden, H. Lee, and L.G. Pedersen, *J. Chem. Phys.* **103**, 8577 (1995).

[19] P.H. Hünenberger and J.A. McCammon, *Biophys. Chem.* **78**, 69 (1999).

[20] W. Weber, P.H. Hünenberger, and J.A. McCammon, *J. Phys. Chem. B* **104**, 3668 (2000).

[21] J.D. Madura, M.E. Davis, M.K. Gilson, R.C. Wade, B.A. Luty, and J.A. McCammon, in : *Reviews in computational chemistry*, Vol. **4**, Lipkowitz, K.B. & Boyd, D.B., Eds., VCH Publishers, Inc., New York, pp 229-267 (1994).

[22] M. Bergdorf, C. Peter, and P.H. Hünenberger, *Manuscript in preparation*

[23] C. Peter, W.F. van Gunsteren, and P.H. Hünenberger, *J. Chem. Phys.* **116**, 7434 (2002).

[24] C. Peter, W.F. van Gunsteren, and P.H. Hünenberger, *Manuscript in preparation*

[25] S. Sasso and P.H. Hünenberger, *Manuscript in preparation*

Dynamics of adsorbed molecules measured by neutron scattering techniques

H. Jobic
Institut de Recherches sur la Catalyse, 2 ave A. Einstein, 69626 Villeurbanne, France

Introduction

Adsorption phenomena operate in many physical, chemical, or biological systems. Some important applications are found in catalysis, separation or purification. This process may happen from either gaseous or liquid phases. With many catalysts, such as transition metals, a strong chemical bond is formed between the adsorbate and the surface, this is known as chemisorption. On the other hand, physisorption involves mainly van der Waals forces and electrostatic forces.

Hydrocarbons on metals

The inelastic neutron scattering (INS) data of benzene chemisorbed on Ni and Pt were amongst the first spectra to be quantitatively interpreted with a normal coordinate analysis [1]. It was found that benzene was adsorbed flat on the surfaces and a significant weakening of the C-C stretching force constant was observed, the perturbation being larger on bare Ni than on Pt or Ni precovered with H_2. The force field of a model molecule, $(\eta^6\text{-}C_6H_6)Cr(CO)_3$, was transferred to the case of adsorbed benzene by changing a few force constants. For the adsorption geometry, the benzene molecule was taken bound to only one metal atom (Fig. 1) because the electron energy loss spectra (EELS) obtained on Ni(111) and (100) are almost identical.

Figure 1

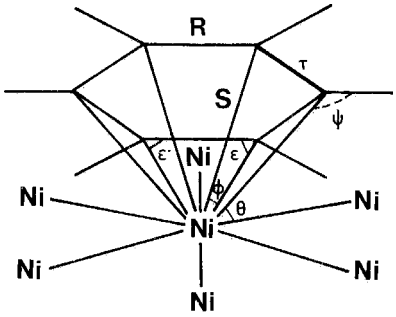

However, even if one may consider that the internal modes of benzene are reasonably assigned, all the vibrational modes of benzene relative to the surface could not be observed so that the bonding geometry could not be firmly established.

The adsorption of other hydrocarbons, mainly acetylene and ethylene, has also been studied by INS on different metals. The assignments are complicated because decomposition and rearrangement of the molecular fragments often occur after adsorption at room temperature.

At that time, first principles calculations could not be envisaged for such systems, this may now be possible with the DFT method.

Zeolitic systems

Comparisons between neutron scattering data and various simulation techniques have been performed for molecules adsorbed in zeolites. This concerns all types of molecular motion: vibrations, rotations, and translations.

One area is the acidity of zeolites and the interaction of probe molecules, such as water, with the acidic sites which are formed by bridging hydroxyl groups, i.e. OH groups bonded to Si and Al atoms. A few years ago, it has been much debated whether the Brönsted acidity of zeolites was high enough to protonate water. The experimental INS spectrum was compared to spectra simulated for the two possible structures: hydrogen-bonded water and hydroxonium ion [2]. The theoretical frequencies and atomic displacements were derived from ab initio MP2 calculations performed on small clusters. The comparison between theory and experiment clearly showed that the water

molecule was attached to an acid site via two hydrogen bonds, and that hydroxonium ions were not formed.

Periodic DFT calculations are limited in zeolites because of the huge number of atoms in the unit cell. Therefore, various force fields have been developed. These force fields are parameterized against structural and vibrational data. Since the low-frequency range (< 100 cm^{-1}) is difficult to access with ir or Raman, INS spectroscopy could be used as a critical test of the force fields.

For example, the external modes of benzene in NaY were computed from different force fields by Fourier transformations of velocity correlation functions [3]. Comparison with experiment (Figure 1) shows that librational modes are sometimes overestimated (Figure 1b). The JAV force field (Figure 1c) describes reasonably well the external modes below 100 cm^{-1}, but the first internal mode is badly reproduced (220 instead of 405 cm^{-1}).

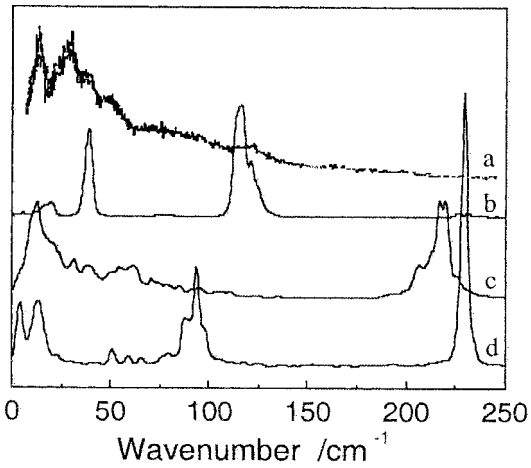

Figure 2. Low-frequency modes of benzene in NaY.

Comparison between experimental (a) and calculated spectra: CVFF (b), JAV (c), and HA (c) [3].

For simulations of long-range diffusion, these low-frequency modes partly control site-to-site jumps. Various jump types can be found in the regularly spaced cavities of zeolites. In the case of benzene in NaY, which was one of the first systems to be investigated by powder neutron diffraction [4], the molecule can jump from one SII adsorption site to another SII cation site, within the same supercage (Figure 3). In some simulations, these jumps have been assumed to be uncorrelated with intercage jumps, which involve SII and window sites [5]. Recent quasi-elastic neutron scattering (QENS) experiments are in contradiction with this approximation.

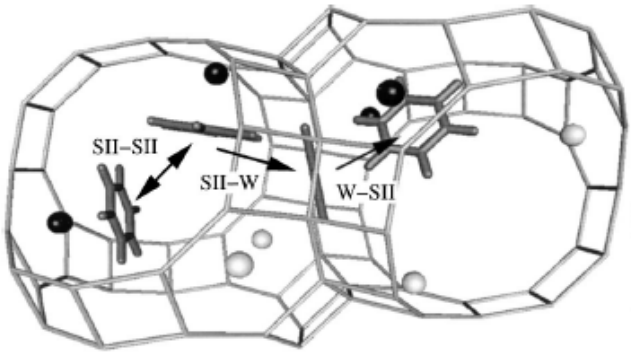

Figure 3. Elementary hopping processes for benzene in NaY zeolite [5].

At low benzene concentration, the self-diffusion coefficients obtained from experiment and various theoretical methods are however in reasonable agreement (Figure 4). The activation energies are also comparable, it is the loading dependence which still poses a problem. It can be noted that QENS is the only experimental method which allows to derive the diffusivity of benzene in this zeolite. When the number of cations increases, i.e. the NaX zeolite, simulations become much more difficult because the cation sites are not well determined and further all the sites are not fully occupied so that the jump types for benzene are not as simple as in Figure 3.

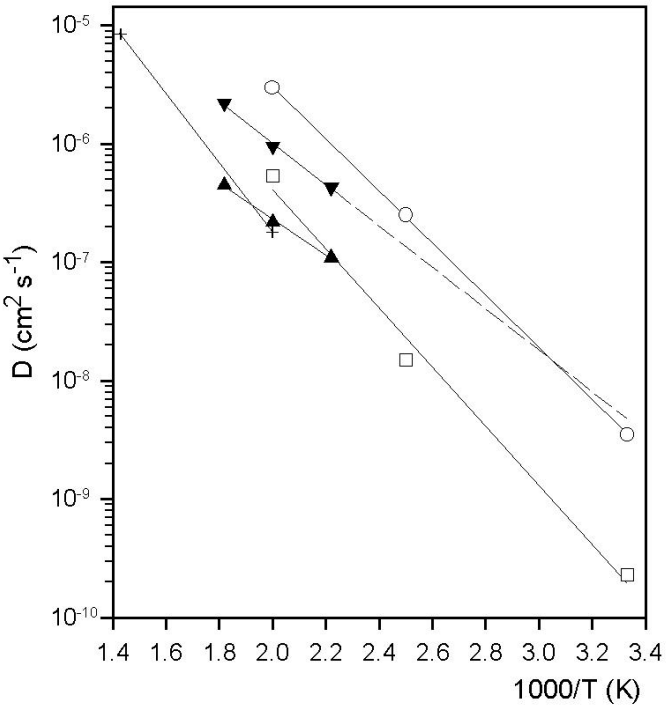

Figure 4. Self-diffusion coefficients of benzene in NaY obtained by different methods: (▼) QENS at a loading of 2 molecules per supercage; (▲) QENS for 4.5 molecules per supercage, on average; (○) kinetic Monte Carlo simulations; (□) constrained reaction coordinate dynamics; (+) MD simulations [6].

The diameter of the windows, in the NaY zeolite, is about 7.4 Å. This is larger than the kinetic diameter of benzene and for the simulations the approximation of a rigid framework does not give widely different results from a flexible lattice. However, in other zeolitic structures, the windows can be smaller. For example, in silicalite, the pores are about 5.5 Å in diameter. This complicates the determination of the diffusion coefficients of benzene, both experimentally and theoretically. With neutron scattering, one has to use the ultra high resolution of the spin-echo method. A molecular simulation performed with a flexible framework was found to be in agreement with experiment, but another simulation considering fixed atomic positions for the zeolite atoms yielded much lower diffusivities, by about 2 orders of magnitude (refs. given in [7]).

Conclusions

The space and time scales of neutron scattering techniques are unique, and comparisons with results obtained from molecular simulations are increasingly found in the literature. Following a catalytic cycle in real conditions (gas composition, pressure, temperature) is still impossible by neutron or simulation methods. However, results obtained on simple systems are already of great interest for the understanding of these complex phenomena. The new European Spallation Source (ESS), if it is built, would offer new instrumentation. Nothing will stop progress in simulations.

References

[1] H. Jobic, A. Renouprez et al. Surf. Sci. **95**, 496 (1980); **111**, 53 (1981); J. Catal. **74**, 296 (1982).
[2] H. Jobic, A. Tuel, M. Krossner, J. Sauer, J. Phys. Chem. **100**, 19545 (1996).
[3] F. Jousse, S. M. Auerbach, H. Jobic, D. P. Vercauteren, J. Phys. IV France **10**, Pr7-147 (2000).
[4] A. N. Fitch, H. Jobic, A. Renouprez, J. Phys. Chem. **90**, 1311 (1986).
[5] S. M. Auerbach, Int. Rev. Phys. Chem. **19**, 155 (2000).
[6] H. Jobic, A. N. Fitch, J. Combet, J. Phys. Chem. B **104**, 8491 (2000).
[7] H. Jobic, M. Bée, S. Pouget, J. Phys. Chem. B **104**, 7130 (2000).

Neutron scattering and numerical modelling studies of molecular vibrations in extended hydrogen-bond networks

M. R. Johnson, Institut Laue Langevin, BP 156, 38042 Grenoble, France

Introduction

Hydrogen bonds are of fundamental importance in determining the extended structure of molecular systems, be it motifs for packing of molecules (and polymers) or the folded structures of single polymers, like proteins. We have studied the structure and vibrational dynamics of a number of model, crystalline, hydrogen-bonded solids using neutron scattering and density functional theory-based first principles calculations. Vibrational dynamics provide sensitive information on local structure and the characterisation of modes is of fundamental importance in evaluating their contribution to processes like proton transfer in hydrogen bonds and ligand dissociation.

Methods

The starting point for any numerical investigation is a reliable structure. While many relevant structures can be found in the Cambridge Database, these often date back ~30 years for small molecule compounds, as is the case for the base molecules of DNA [1]. Reliable data, obtained by single crystal diffraction, preferably with neutrons which can offer a more favourable contrast than X-rays between light and heavy atoms, therefore exists for fewer systems. In certain cases we perform neutron powder diffraction on deuterated samples at low temperature (<10K) in order to obtain the required structural information.

Vibrational spectra are typically measured by optical methods like IR and Raman (IRR). However, inelastic neutron scattering (INS) offers the important advantage in the context of our work in that spectral intensities are simple to calculate, being directly proportional to normal mode atomic displacements. INS also has no selection rules (all modes are visible), but resolution is worse than for IRR and varies with energy transfer, and neutron flux is low so the best experiments are performed on samples at ~10K i.e. solids.

Accurate normal mode analysis, including dispersion and density of states calculations, in solids requires solid state first principles methods. The most appropriate is periodic DFT, which allows inter- and intra-molecular interactions to be treated on an equal footing. The principle limitation of DFT is the local density approximation (for electron exchange and correlation effects), which excludes dispersive interactions, these playing an important role in molecular solids. Since molecular vibrations depend on short-range forces (r ~6Å) the problem is most apparent in the correct determination of the equilibrium structure, in particular the unit cell shape and volume.

Typical results

We have applied periodic DFT methods, as embodied in the code VASP [2] to a large number of hydrogen bonded systems, ranging from dimers in benzoic acid [3], to one-dimensional chains of molecules in n-methyl acetamide [4], to higher dimensional networks, in the bases and nucleosides of DNA and RNA [5] (initially studied by Ghomi, Jobic and co-workers) and in molecular systems containing peptide groups, including polypeptides.

---

1 *"Modelling molecular vibrations in extended hydrogen-bonded networks – crystalline bases of RNA and DNA and the nucleosides"*, M. Plazanet, N. Fukushima and M.R. Johnson, Chem. Phys. 280(2002)53

2 http://cms.mpi.univie.ac.at/vasp/vasp/vasp.html)

3 *"The vibrational spectrum of crystalline benzoic acid: inelastic neutron scattering and DFT calculations"*, M. Plazanet, N. Fukushima, M.R. Johnson, A.J. Horsewill and H-P. Trommsdorff, J. Chem. Phys. 115 (2001) 3241

4 *"Structure and vibrational dynamics of the strongly hydrogen-bonded model peptide: n-methyl acetamide."*, G.J. Kearley, M.R. Johnson, M. Plazanet and E. Suard, J. Chem. Phys. 115 (2001) 2614

5 *"Modelling molecular vibrations in extended hydrogen-bonded networks – crystalline bases of rna and dna and the nucleosides"*, M. Plazanet, N. Fukushima and M.R. Johnson, Chem. Phys. 280(2002)53

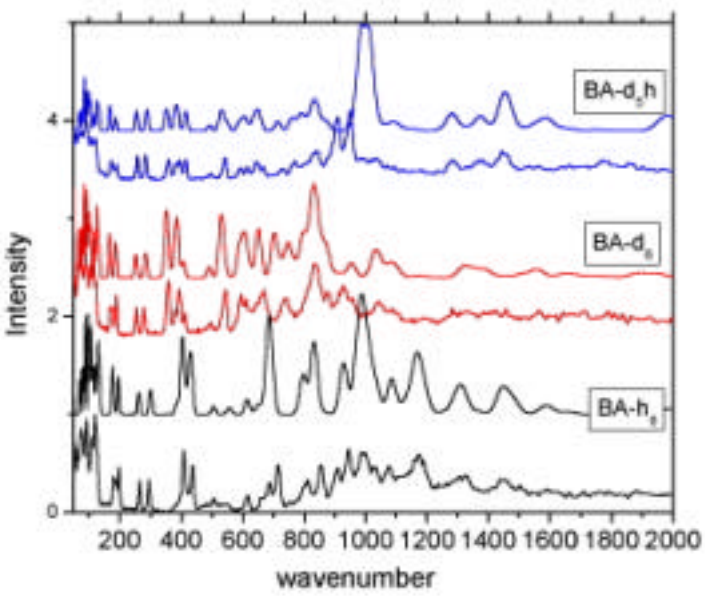

Figure 1: Vibrational spectra for benzoic acid for protonated (lower), deuterated (middle) and partially deuterated molecules. D5H denotes a deuterated phenyl ring so the most intense modes in the spectrum are due to the proton in the hydrogen bond. The lower spectrum in each pair is measured, the upper spectrum is the result of normal mode analysis for the gamma point. All calculated spectra are derived from the same force constant matrix.

In the best cases, such as benzoic acid (see figure 1), the agreement between calculation and mesurement, without any parameter refinement, is so good that an unequivocal assigment of all modes is possible. The spectra for isotopic derivatives are all calculated from the same matrix of force constants, that is a single set of DFT calculations of interatomic forces, illustrating the quality of the DFT results. The spectra shown are for the gamma point, calculated on a single unit cell (volume ~550Å3) containing 60 atoms. By taking a supercell composed of four unit cells, the forces induced on atoms at the edge of the supercell by an atom displaced from equilibrium at the centre are close to zero and the normal modes at finite wave vector can be calculated accurately. Figure 2 shows the dispersion and the density of states for modes close to 200cm^{-1} in benzoic acid, the interest in this result being that spectral intensity in this frequency range was recently, incorrectly assigned to proton tunnelling modes rather than vibrational modes. The effect of unit cell shape and size on vibrational modes is seen clearly in the case of uracil (figure 3). The out-of-plane N-H wags occur in the frequency range 800-1000cm^{-1} due to hydrogen bonding, for an isolated molecule they would be at about half this frequency. On optimisation of the unit cell, these modes shift to higher frequency by up to 50cm^{-1} and the spectral profile changes significantly. The hydrogen bonds shorten along with the a and b axes of the cell, which define the plane containing the hydrogen bonds, while the Van der Waals bonding between planes leads to expansion in the DFT calculation.

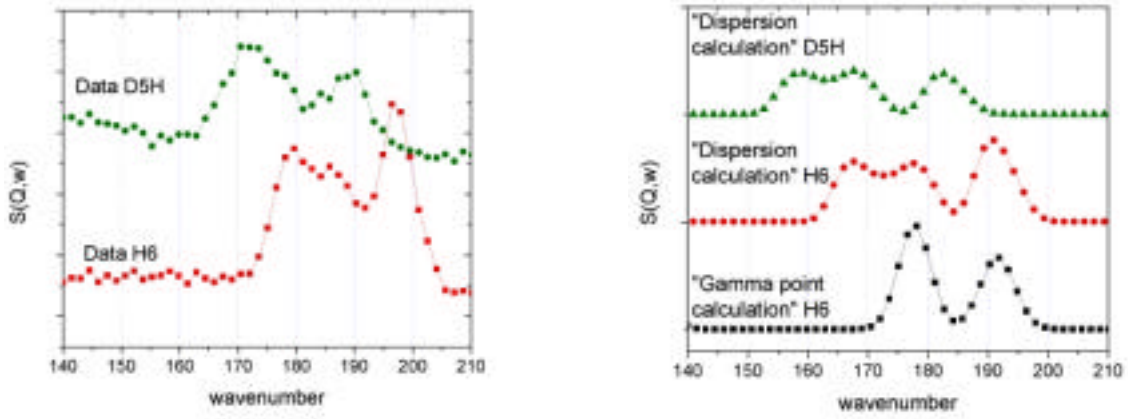

Figure 2: Measured spectra of benzoic acid at ~200cm^{-1}. The lower frequency gamma point mode shows significant dispersion that is correctly reproduced by the DFT-phonon calculation on 4 unit

Typical problems

The results shown in figures 1-3 are good, but they are not perfect. Furthermore the number of inequivalent atoms in each system is not greater than 15. All calculations are performed in the harmonic approximation and this is partly to blame for the overestimate in the prominent modes in the upper spectrum of figure 1, these are the out-of-plane wags of the O-H bonds. Anharmonicity is characterised by calculating the potential energy variation along the normal co-ordinate. The second contribution to the overestimate of this mode frequency is the optimised hydrogen bond length, which is about 0.05A shorter than the measured length, and the same effect was widely observed in the work on the bases and nucleosides of DNA/RNA Indeed different aspects of geometry optimisation are at the origin of a number of problems. The potential energy surface is complex for such molecular systems. While most minima give similar spectra, the variations become significant for congested spectra when peaks overlap. More seriously, certain minima can give a large number of negative frequencies. Another way of expressing the same problem is that geometry optimisation starting from different structures does not give a unique solution and a time-consuming simulated annealing procedure is required to explore the PES. Furthermore, since the total energy calculation does not include all interactions, the correct structure does not necessarily have the lowest energy. This type of problem is in fact most serious for hydrogen bond networks since these significantly perturb the single molecule approximation; if the hydrogen bonds are not correctly described the errors in the vibrational spectra are dramatic. Accordingly the worst results in this type of analysis have been obtained for an ice-methane clathrate, where the unit cell contains about 50 water molecules.

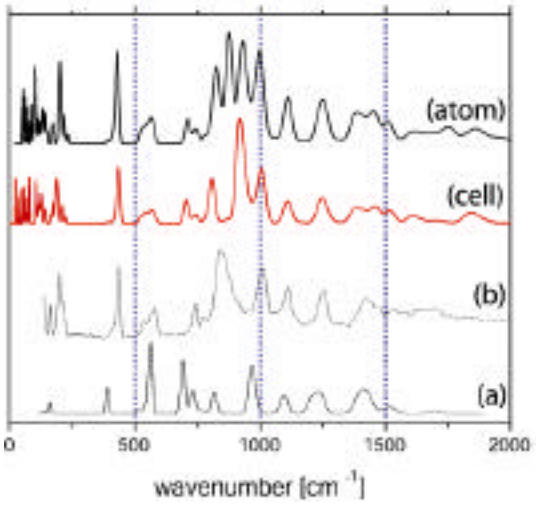

Figure 3: Vibrational spectra of uracil. The measured curve (b) is reasonably well reproduced by the periodic DFT calculations denoted "atom" and "cell". The central pair of the 4 peaks between 750cm^{-1} and 1000cm^{-1} in the upper curve, become a single peak when the unit cell is also optimised, geometry changes inducing peak 50cm^{-1} peak shifts. Curve (a) is the result of a single molecule calculation (M-P Gaigeot et al., Chem. Phys. 261 (2000) 217).

There are a number of limitations for INS and vibrational spectroscopy like the low flux, the limited energy resolution and the loss of information on increasing temperature. The strengths of a technique also become its limitations. The fact that all atoms are visible results in congested spectra for more complex systems and while partial deuteration can be used to target molecular groups, the background signal from the deuterated molecular groups cannot be ignored. The complementarity between INS and IRR should be exploited, the former for mode assignment, the latter for mode evolution under different experimental conditions.

Perspectives

In the future we would like to apply this combined numerical and experimental approach to more realistic model systems, like strands of DNA or RNA and polypeptides.

Currently the "reasonable" computational limit for this type of work, using plane-wave DFT, is a system of about 300 atoms with no symmetry. By using linear scaling methods, as for example embodied in SIESTA [6], systems of up to 1000 atoms may be possible. But is there a price to pay in precision in using these methods and moving on to bigger systems? Since vibrational spectroscopy is essentially a local probe, the experimental signal from an amorphous sample will be determined by the local structural order. In this case, the most appropriate numerical model may be a cluster calculation or cluster, treated at high precision with quantum chemistry methods, embedded in a larger model, treated with molecular mechanics. This latter approach is referred to as QM/MM. Again the question arises, to what extent is precision compromised?

Experimentally, samples could be optimised for this type of measurement. Fibres with a high degree of crystallinity, developed for fibre diffraction experiments, could be used. For INS, partial deuteration significantly reduces the scattering from the deuterated parts of the molecule, enabling specific regions of a polymer to be targeted. Of course such samples are more difficult and expensive to prepare. The validity of a numerical approach could also be tested experimentally by changing experimental conditions, for INS this would entail applying hydrostatic pressure. While pressure induced shifts may be smaller than the absolute precision of calculated frequencies, calculated shifts are often correctly reproduced, for example frequency shifts induced by $O^{16} - O^{18}$ substitution in benzoic acid.

Finally, as samples become bigger and more complex (i.e. real!), the quality of experimental information declines and ultimately lower precision calculations will reproduce the experimental data. However, we are not yet at the stage where all high-resolution data on moderately complex systems can be reproduced by quantum chemistry methods, so computational improvements should be sought here. Lower precision methods should then be evaluated and calibrated on these and other realistic model systems. The trap that one must avoid falling into with more complex systems is believing that a calculation correctly describes a system simply because it reproduces the experimental data.

---

6 http://www.uam.es/departamentos/ciencias/fismateriac/siesta

Scaling up molecular vibrations.

G. J. Kearley
Interfaculty Reactor Institute, Delft University of Technology, Mekelweg 15, 2629JB Delft, The Netherlands

Introduction.

Over the past ten years of so it has become almost routine to calculate vibrational spectra of modestly-sized molecular species from ***ab-initio*** methods, and a good number of these have been compared with inelastic neutron scattering (INS) data. The main advantage of neutrons in this respect is that the measured spectrum can be directly compared with the calculated spectrum, and this frequently resolves assignment ambiguities that would be difficult to resolve using frequency-data alone. In general, the agreement is good, although there are residual problems with solid-state effects, including dispersion. Occasionally the reason for disagreement between observed and calculated spectra remains unresolved – not everything is yet understood.

Small crystalline model systems usually give clean INS spectra with sharp well-separated peaks, but moves towards more complex molecules gives either an awesome forest of peaks (a "rich" spectrum!), or a few very broad featureless bumps. These spectra cannot be analysed in any detail, and consequently the main role INS for larger systems is via "passing up" of information from more tractable model-systems.

An alternative approach is to regard a large system as a distribution of well characterised small systems. Basically, the INS spectrum of a polymer is treated as the sum of spectra from some distribution of oligomers with different conformations. First we have to determine low-energy conformations of oligomers and compare these with the INS experiment in the normal way. We then find how these might be summed by comparison with the INS spectrum of the polymer. Can we then understand the origin of these conformations?

Oligomer conformations from vibrations.

The structure and dynamics of many large and complex systems is determined by a "difficult" potential-energy surface. The calculations themselves are very time-consuming, and approximations can introduce errors that are large compared with the energy difference between the many possible molecular conformations. Further, many of these systems are poorly- or non-crystalline, and the concept of minimum-energy conformation is not appropriate. The experimental determination of atomic positions by crystallographic methods is also difficult in these systems.

Notwithstanding the residual problems with calculating vibrational spectra, the method is now basically reliable enough to identify errors in proposed structures and assignments, and we are now beginning to elucidate molecular conformations in simple model systems. The idea here is to extend the use of the structural sensitivity of molecular vibrations in a way that is similar to polymorph-prediction (or proposal). Low-energy conformations are sought by calculation, but

then the observed and calculated vibrational spectra are compared, rather than the diffraction patterns. Calculating a vibrational spectrum has far higher overheads than calculating a diffraction patterns so clearly, this approach is only of interest in those cases where crystallographic information in unobtainable. This means poorly crystalline or amorphous systems, and in our particular case: polymers.

A simple example.

Dihedral angles are usually the most important degree of freedom in molecular conformation. The spectral sensitivity to this angle is about 10^{o}, as illustrated by the calculated INS spectrum as a function of the inter-ring angle in bithiophene shown below. In the gas-phase this angle is 27^{o} but in the solid the molecule is trans-planar as found by crystallography, calculation and the measured INS spectrum. The rotational potential for dihedral angles is often very soft for the isolated molecule and bithiophene is no exception. In the non-crystalline solid polymers there will be some distribution of inter-ring angles, and at present we are working up through other oligomers of thiophene with the aim of determining this distribution and understanding its origin.

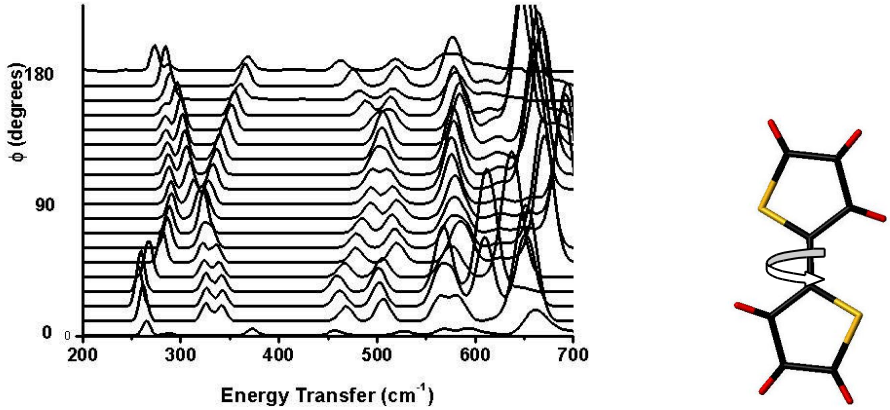

We are also investigating oligomers of other conjugated polymers and the model polymer electrolyte PEO (with salt), in each case regarding the polymers as the sum of oligomers that may have any one of a number of local structures.

Challenges.

1. We are working with distributions of orientations, each orientation imposing its effect on its neighbours, and ***vice versa***, and ultimately this is what we wish to understand. In the first instance we treat this as a sum of different oligomers, but in order to grasp the origin of the conformations (correlation between local structures) the oligomers may need to be quite large.
2. Clearly, there is vibrational coupling between the segments, and this will be sensitive to the relative conformations of the segments. Band-splittings introduced by this coupling must not be confused with different sites or

distributions. This effect can probably be elucidated qualitatively by rapid semi-empirical, or even empirical, method, although this has yet to be done.

3. It is not easy to control the amorphous fraction within the INS experiment, both sharp and broadened peaks being possible as a function of sample history.
4. It is worth noting that the INS intensity is “shared” between atomic displacements in a number of modes, and a serious error in a high-amplitude low-energy mode can have consequences for the calculated intensities elsewhere in the spectrum. Consequently, the effect of calculating vibrational spectra for molecules away from their minimum-energy conformation can have far-reaching effects on calculated intensities, and this needs to be recognised.
5. The number of local minima can be large, and it can also be that more than one of these provides acceptable agreement with the calculated spectrum. If required these can usually be distinguished by selective deuteration, the spectral effects of which can easily be calculated in advance.

Perspectives:

So far this approach seems to work, although we are still rising to the “challenges” above. There is an incentive to extend this to multicomponent systems in order to understand how additives such as salts, nanoparticles etc. change the local structures.

Perhaps the most serious constraint at present is the time taken to scan through the conformations and to produce calculated INS spectra for these. As we move to larger oligomers this problem will become more serious. Empirical force-constants derived from ***ab-initio*** calculations (including scaling methods) may have an important role to play in investigating these questions and also in increasing the speed of the whole process.

Studying relaxation processes in liquids and proteins by autoregressive modeling of Molecular Dynamics trajectories

Gerald R. Kneller
Centre de Biophysique Moléculaire, CNRS UPR 4301
Rue Charles Sadron, F-45071 Orléans Cedex 2, France.

1 Introduction

Molecular Dynamics simulations are widely used to study the structure and dynamics of condensed matter systems on the atomic scale. Their complementarity to spectroscopic techniques makes them a valuable tool for the interpretation of experimental data. On the other hand, a simulation approach can also help to develop theoretical models. In this contribution it is shown that autoregressive modeling of time series can be used to compute not only realistic spectra for comparison with experiments, but also quantities which are of interest for the model building process. These quantities are memory functions, friction coefficients and spectra of relaxation times. In contrast to correlation functions, their associated memory functions are not easy to calculate from simulation data. It will be shown that friction coefficients can be directly extracted from autoregressive models, without using mean-square displacements in conjunction with the Einstein law. In this way friction and diffusion can be given a meaningful interpretation in case that the Einstein law for diffusion does not apply.

2 Autoregressive model

Autoregressive (AR) modeling is a standard tool for the estimation of power spectra associated with discrete time series [1]. In physical applications it is often referred to as maximum entropy method. Within an AR model of order P the signal under consideration is described by the difference equation

$$x(t) = \sum_{n=1}^{P} a_n^{(P)} x(t - n\Delta t) + \epsilon_P(t), \tag{1}$$

where Δt is a sampling interval, $a_n^{(P)}$ are coefficients yet to determined, and $\epsilon_P(t)$ is a white noise process with zero mean and variance σ_P^2. On recognizes that $x(t)$ is modeled as a Markov process if $P = 1$. In the following it is

assumed that $x(t)$ is a *stationary* time series. The coefficients $\{a_n\}$ can be determined by various methods which use different explicit or implicit estimations of the autocorrelation function of the signal. In our studies we use the Burg algorithm which is efficient and yields also stable estimators of the autocorrelation function [1, 2, 3]. Taking a time series of equidistantly sampled values of $x(t)$ as input, the Burg algorithm yields estimations of the model parameters $\{a_n\}$ and σ_P^2. To omit technical details we will now assume that these parameters are known. Within the AR model, all physical quantities can be expressed in terms of the zeros of the characteristic polynomial

$$p(z) = z^P - \sum_{k=1}^{P} a_k z^{P-k}. \tag{2}$$

Using that the z-transform of the discrete autocorrelation function $r(n) \equiv \langle x(n\Delta t)x(0)\rangle$ has the simple "all-pole" form

$$R(z) = \sum_{n=-\infty}^{+\infty} r(n)z^{-n} = \frac{1}{a_P^{(P)}} \frac{-z^P \sigma_P^2}{\prod_{k=1}^{P}(z-z_k)\ \prod_{l=1}^{P}(z-z_l^{-1})}, \tag{3}$$

the autocorrelation function $r(n)$ and its Fourier spectrum are given by

$$r(n) = \sum_{j=1}^{P} \beta_j z_j^{|n|}, \tag{4}$$

$$\tilde{r}(\omega) = R(\exp[i\omega\Delta t]), \tag{5}$$

respectively. The coefficients β_j are defined as $\beta_j = \lim_{z\to z_j}(z-z_j)R(z)$. Eq. (4) shows that the AR model is stable if all poles are located inside the unit circle.

3 Memory functions

The key concept of the following studies is to model the velocity $v(t)$ of a tagged particle in a Molecular Dynamics simulation as an AR process. Fitting the model (1) to such discrete velocity "signals" yields a spectrum of P characteristic frequencies and relaxation constants which are derived from the poles $\{z_k\}$ defined in (2). As it has been shown in [4], these quantities allow not only to express the velocity autocorrelation function (VACF) and its Fourier spectrum, but also the associated memory function which is defined by

$$\frac{d}{dt}\psi(t) = -\int_0^t d\tau\, \xi(t-\tau)\psi(\tau). \tag{6}$$

Here $\xi(t-\tau)$ is the time-delayed memory kernel and $\psi(t)$ is the (normalized) autocorrelation function

$$\psi(t) = \frac{\langle v(t)v(0)\rangle}{\langle v^2(0)\rangle}. \tag{7}$$

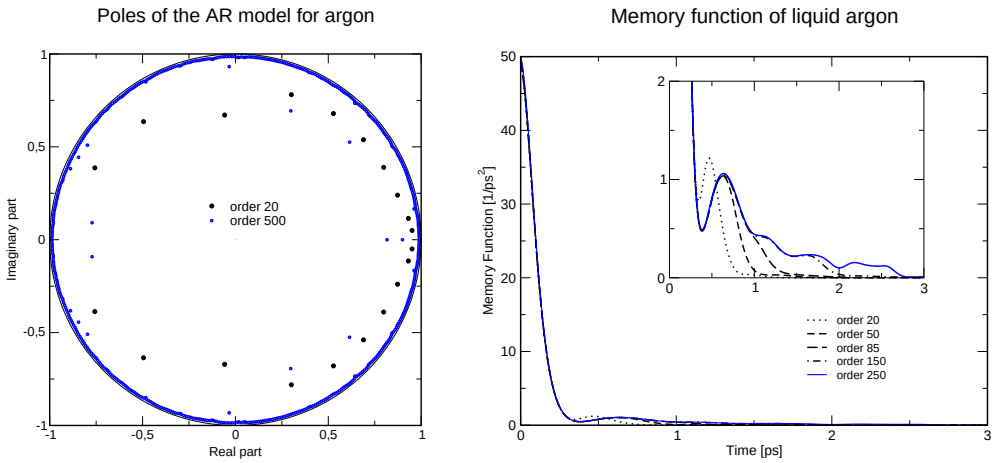

Figure 1: **Left:** Location of the poles obtained from an AR model for the velocities of liquid argon. The sampling step is $\Delta t = 10\,fs$. The black dots correspond to $P = 20$ and the blue dots to $P = 500$. **Right:** Memory functions of liquid argon for various orders of P.

To compute memory functions numerically, one uses the (one-sided) z-transform of the discretized form of (6),

$$\frac{\psi(n+1) - \psi(n)}{\Delta t} = -\sum_{k=0}^{n-1} \Delta t\, \xi(n-k)\psi(k), \tag{8}$$

which can be solved for the memory function in z-space

$$\Xi_>(z) = \sum_{n=0}^{\infty} \xi(n) z^{-n} = \frac{1}{\Delta t^2}\left(\frac{z}{\Psi_>(z)} + 1 - z\right). \tag{9}$$

Here $\Psi_>(z) = \sum_{j=1}^{P} \beta_j \frac{z}{z - z_j}$, where β_j are the same coefficients as those appearing in (4). $\Xi_>(z)$ is then transformed back into the time domain by polynomial division. For discrete functions the one-sided z-transform plays the same role as the Laplace transform for continuous functions. Fig. 1 shows the location of the poles obtained from the velocity trajectories of a simulation of liquid argon (left) and memory functions for different values of P (right).

4 Friction and diffusion

The friction constant of a *freely diffusing* particle is defined as integral over its memory function. The latter may be approximated as a sum over the sampled values of $\xi(t)$,

$$\gamma = \int_0^{\infty} dt\, \xi(t) \approx \Delta t \sum_{n=0}^{\infty} \xi(n). \tag{10}$$

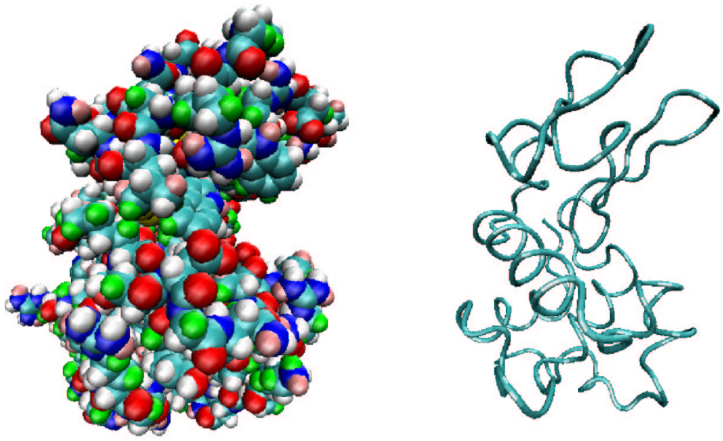

Figure 2: **Left:** All-atom model of Lysozyme. **Right:** The corresponding backbone formed by the C_α-atoms.

The discrete approximation may also be written as

$$\gamma = \Delta t \, \Xi_{>}(0), \tag{11}$$

using the definition of the one-sided z-transform. The above equation shows that the memory function needs not be calculated to obtain γ. This aspect of importance from a numerical point of view. For a particle whose motion is not confined, the friction constant may be obtained from the Einstein law which relates γ to the diffusion constant, D,

$$D = \frac{k_B T}{M\gamma}. \tag{12}$$

For simple liquids, such as liquid argon, the above relation can be well reproduced from simulation data, using γ from eq. (11). Since internal atomic motions motions in proteins are confined, the corresponding mean-square displacement tends to a plateau value and the diffusion constant becomes zero. Therefore the friction constant must tend to infinity. Our numerical studies for the C_α-atoms in the backbone of Lysozyme show indeed this trend. A graphical representation of Lysozyme and its backbone is given in Fig. 2. Fig. 3 oppses the mean-square displacement of Argon and the C_α-atoms in Lysozyme. The insets in the respective graphs show the evolution of the integral over the memory function. It can be seen that the latter stays almost constant in case of liquid Argon, whereas a clear increase can be seen for the C_α-atoms of Lysozyme. The divergence of the integral over the memory function can be used to describe the dynamics of the atoms in a confined system like a protein by an effective Langevin oscillator. The parameters of this model depend, however, on the observation interval of the motions. If the fundamental frequency of the oscillator is ω_0 and the friction constant is γ, the corresponding memory function has the form

$$\xi(t) = \gamma\delta(t) + \omega_0^2. \tag{13}$$

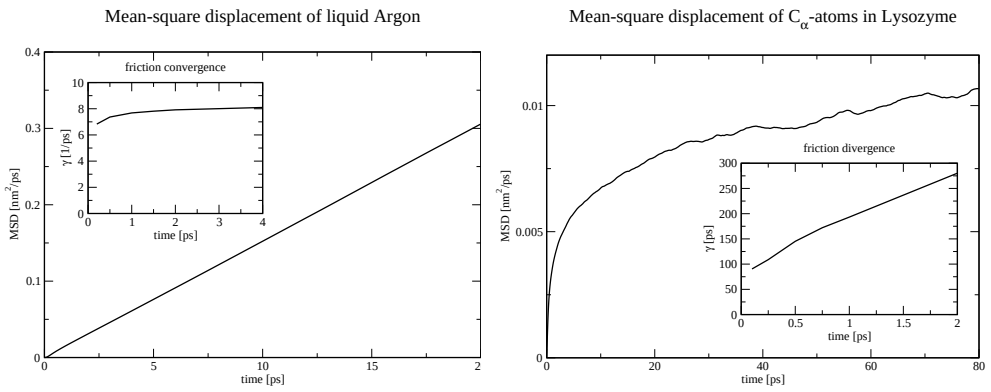

Figure 3: **Left:** Mean-square displacement of liquid argon and the evolution of γ with increasing the integration interval. **Right:** The corresponding plot for the C_α-atoms in Lysozyme.

From the Langevin model one obtains therefore a linear divergence of the time integral over the memory function,

$$\int_0^t d\tau\, \xi(\tau) = \gamma + \omega_0^2 t. \tag{14}$$

One notes that one has here a time-dependent friction constant which is composed of a "real" friction constant and a contribution from the repelling force which is reflected in an ever lasting memory.

The above consideration show how semi-analytical models can help understanding the potential energy landscape in liquids and proteins.

References

[1] A. Papoulis. *Probablity, Random Variables, and Stochastic Processes*. McGraw Hill, 3rd edition, 1991. CBM.

[2] J. Burg. *Maximum entropy spectral analysis*. PhD thesis, Stanford University, Stanford (CA), USA, May 1975.

[3] J. Makhoul. Stable and efficient lattice methods for linear prediction. *IEEE Transactions on Acoustics, Speech, and Signal Processing*, ASSP-25(5):423–428, 1977.

[4] G.R. Kneller and K. Hinsen. Computing memory functions from Molecular Dynamics simulations. *J. Chem. Phys.*, 115(24):11097–11105, 2001.

Fluorostyrenes and Numerical methods. A first approach to the real molecular structure?

A.Navarro, J.M. Granadino and M.Fernández-Gómez
Department of Physical and Analytical Chemistry, University of Jaén, 23071-J, SPAIN

Introduction

The original idea of this work was to obtain the force constant values of the torsion as well as other vibrations of the vinyl group of fluorostyrene derivatives. This is to search for a correlation between the properties of the closed shell compounds with the hyperfine parameters of the radicals formed by the process of muon implantation in these compounds. It has been shown that such relations are useful pointers towards mechanisms of hyperfine interaction.

At the present, the common way to obtain reliable force constants values is through the combined use of quantum mechanical calculations and vibrational analysis, using the secular equation of the theory of small vibrations, ***GFL=LL***. The starting point for any vibrational analysis is a reliable structure to calculate the kinematic coefficient matrix, ***G***, and the force constant matrix, ***F***. The last one can be obtained from quantum mechanical calculations, and fitted via refinement or scaling in order to reproduce the experimental vibrational wavenumbers.

Systems containing π-conjugation have attracted great attention for a long time. In fact, considerable number of experimental and theoretical studies have been devoted to styrene, and more recently to fluorostyrenes. In this work we have studied two different fluorostyrene derivatives: the 3-fluorostyrene (both *cis*- and *trans*- conformers) and the 4-fluorostyrene derivatives (see Figure 1). Due to their reactivity, the determination of the structure in this kind of compounds is difficult and no reliable experimental structure data are available. While all experiments have shown the conformation to be planar, from *ab initio* calculations the planar structures were found to be a first-order saddle point. DFT methods have shown impressive performance in the predictions of molecular properties especially, vibrational properties. In fact, they have been decisive in order to clarify the structure of styrene [1 and references therein]. In this work, we have applied them to the study of the fluorostyrene derivatives above mentioned, optimizing the molecular geometry and performing calculations for the internal barrier to rotation. In addition, the vibrational features of these compounds have been used to extract conclusions about the structural information, and the comparison among the force fields of these compounds and those for related molecules have been decisive in order to conclude that the conjugation between the vinyl moiety and the benzene ring is not as strong as expected for this kind of molecules.

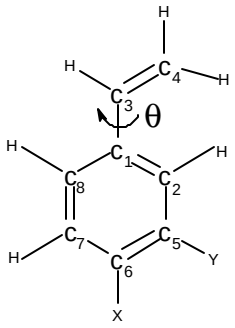

Figure 1. Molecular structure for 3-fluorostyrene (X=H, Y=F) and 4-fluorostyrene (X=F, Y=H).

Methods

The set of programs Gaussian 98 [2] was used to carry out the *ab initio* and DFT calculations running on a Digital Alpha Server 2000. Calculations were performed using standard gradient techniques at the MP2 and DFT levels using the 6-31G*, 6-311G** and 6-311++G** basis sets. As exchange functional, Becke´s hybrid exchange was used, B3, and as correlation functional Lee-Yang-Parr non-local functional, LYP. Vibrational wavenumbers were calculated from analytical second derivatives to check the minimum of the potential energy surface.

---

1 "*Conformational Information from Vibrational Spectra of Styrene, trans-Stilbene, and cis-Stilbene*", C.H. Choi and M. Kertesz, J. Phys. Chem. 191 (1997) 3823

2 J. A. Pople et al., *Gaussian 98* Revision A.7; Gaussian, Inc.: Pittsburgh, 1998

Infrared and Raman spectra were measured in the liquid phase at room temperature. The Raman spectra were recorded using a Bruker IFS16 spectrometer with a FRA 106 FT-Raman module. 1064 nm laser excitation of a diode laser was used with the spectra recorded at 1 cm^{-1} resolution, with a liquid nitrogen cooled germanium detector. The FT-IR spectra were recorded by using a FTIR Perkin Elmer 1760 X spectrometer, at 1 cm^{-1} resolution. The INS spectrum was obtained by using the TFXA spectrometer at the ISIS pulsed neutron source, in the Rutherford Appleton Laboratory, Chilton, U.K., which has an energy resolution <2%. The sample was loaded into a standard liquid-helium cryostat controlled at T<20K.

The force constant matrix in Cartesian coordinates from Gaussian was transformed into both internal and symmetry coordinates using several Fortran computer programs [3]. These molecular force fields were fitted, when using IR-Raman data, with the program ASYM40 [4] (for the scaling and refinement procedure), and, when using the INS spectrum, with the program CLIMAX [5] (only used for refinement). In the case of the force fields built up with ASYM40, the same uncertainty, 1 cm^{-1}, was assigned for all the wavenumbers.

Typical results

Geometry. We have optimized the structure for 4-fluorostyrene and 3-fluorstyrene (*cis*- and *trans*-conformers). From *ab initio* calculations at the MP2/6-31G* level, the planar structure (θ=180º in 4-fluorostyrene, and θ =0° and θ =180°, for the *cis* and *trans* conformers in 3-fluorostyrene, respectively, θ being the dihedral angle C_4-C_3-C_1-C_2, see Fig. 1) was found to be a first-order saddle point, with one imaginary wavenumber associated with the vinyl group torsion. In order to obtain a true minimum, it was necessary to carry out a partial optimization where the benzene ring was kept planar and using as starting point a non-planar structure where the vinyl moiety is located on a plane other than that of the benzene ring. These true minima are obtained for a *skew* ($\theta \approx 160°$) and *gauche* ($\theta \approx 20°$) forms, in the case of the 3-fluorostyrene, and for 153.0° in the case of 4-fluorostyrene. These results agree with the reported values from MP2/6-31G* calculations for styrene, which also yields a nonplanar conformation with a torsional angle of 27.2° [1]. On the other hand, DFT calculations, using the B3LYP hybrid functional and the 6-31G*, 6-311G** and 6-311++G** bases sets give the preferred conformation as the planar structures. This result is in agreement with the experimental studies for 3-fluorostyrene, the *cis* conformer being more stable than the *trans* conformer, irrespective of the basis set used for the calculation, and for 4-fluorostyrene.

Table 1 compares some structural parameters of 3- and 4-fluorostyrene with those reported for styrene. The C=C vinyl bond length and the phenyl-vinyl C-C bond length are very similar for all the molecules and even for both conformers of the 3-fluorostyrene. The value for the C=C vinyl bond length being close to the experimental value for the C=C bond length in ethylene, 1.334-1.339 Å. These results therefore lead to the conclusion that the fluorine atom ring-substitution should affect neither the strength nor the orientation of the vinyl group in a significant way.

Table 2 shows the barriers to internal rotation of n-butane, 1,3-butadiene, styrene, 3-fluorostyrene and 4-fluorostyrene computed at the B3LYP/6-311++G** level. Since in the systems 1,3-butadiene and styrene this internal rotation implies a partial break of the involved π bond these values can be taken as a measure of the π conjugation of the system. As can be seen the values of barriers to internal rotation for the styrenes are closer to the value for a typical sp^3 bond, 3.2 kcal mol^{-1}, than to the value for a typical conjugated system, 7 kcal mol^{-1}. It is well known that DFT methods overestimate the π stabilization. Some authors have found that for typical conjugated π systems DFT calculations obtain barriers to internal rotation as much as twice to that of the experimental. Within this context, the overestimation in the present calculations as shown by the difference between the experimental and the B3LYP/6-311++G** barriers to internal rotation leads to the conclusion that *the overestimation of planarity is not as significant as expected for this kind of systems* [6].

---

3 E. Martínez Torres, non-commercial programs

4 L. Hedberg and I.M. Mills, J. Mol. Spectrosc. 160 (1993) 117

5 G.J. Kearley, J. Chem. Soc. Faraday Trans. II, 82 (1984) 41

6 M.H. Gordon and J.A. Pople, J. Phys. Chem. 97 (1992) 1147

***Table 1**: Bond distances (in Å) for styrene, cis-3-fluorostyrene, trans-3-fluorostyrene and 4-fluorostyrene ([a] reference 1; [b] Experimental value for C=C in ethylnene is 1.334-1.339Å, J.L. Duncan, Mol. Phys. 28 (1974)1177.*

		C_1-C_3	C_3=C_4[b]	C_1-C_3-C_4
	styrene[a]	1.472	1.343	125.3
	cis-3FS	1.472	1.343	125.4
	trans-3FS	1.472	1.343	125.2
MP2/6-31G*	4FS	1.472	1.343	125.4
	styrene[a]	1.472	1.339	127.7
	cis-3FS	1.472	1.339	127.5
	trans-3FS	1.473	1.339	127.4
B3LYP/6-31G*	4FS	1.472	1.339	127.7
	styrene[a]	1.472	1.337	127.7
	cis-3FS	1.472	1.336	127.4
B3LYP/	trans-3FS	1.472	1.336	127.4
6-311++G**	4FS	1.471	1.337	127.7

***Figure 2.** Internal barrier to rotation at the B3LYP/6-311++G** level (kcal mol^{-1})*

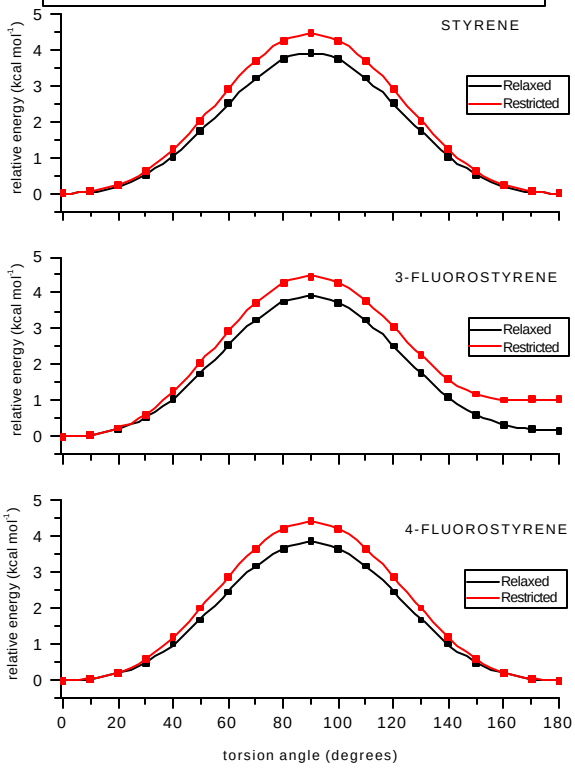

***Table 2.** Internal barrier to rotation at the B3LYP/6-311++G** level (kcal mol^{-1})*

System	Method	Barrier
Styrene	Relaxed	3.9
	Restricted	4.4
cis-3FS	Relaxed	3.9
	Restricted	4.5
trans-3FS	Relaxed	3.8
	Restricted	3.4
4FS	Relaxed	3.8
	Restricted	4.4
n-butane		3.2
1,3-butadiene		7.0

In Table 3 are listed the parameters for the torsional potential function in their ground electronic state and those from experimental techniques. The potential function has been found to be of the form:

$$V(q) = \sum_i \frac{1}{2} V_{Ni} \left[1 - \cos(iNq)\right]$$

where θ is the torsional angle. The corresponding curves are shown in Figure 2 for both relaxed and restricted calculations.

***Table 3**: Parameters {V_i} for the Fourier series in kcal/mol (experimental values from T. Schaefer and R. Sebastian, Chem.Phys. Lett. 163 (1989) 212, and references therein).*

System	Method		V_1	V_2	V_3	V_4	V_5	V_6
	Vibronic Fluorescence		-	3.06	-	-0.79	-	0.02
	Microwave		-	3.29	-	-0.79	-	-
		Relaxed		3.92	-	-0.59	-	-0.01
Styrene	This work	Restricted		4.48	-	-0.61	-	-0.05
	Supersonic jet fluorescence		0.63	3.00	-	-0.70	-	-
		Relaxed	0.10	3.86	0.06	-0.60	0.00	-0.02
3FS	This work	Restricted	0.71	4.01	0.27	-0.72	0.06	-0.08
	Supersonic jet fluorescence		-	2.71	-	-0.66	-	-
	Raman spectrum		-	1.58	-	-	-	-
	Electronic absorption		-	1.00	-	-	-	-
		Relaxed	-	3.88	-	-0.60	-	-0.03
4FS	This work	Restricted	-	4.47	-	-0.63	-	-0.06

Force Field Calculation. Assuming planar structure for these compounds, normal coordinates analysis have been performed by using the force fields calculated at the B3LYP/6-311++G** level and data from infrared, Raman and INS techniques in order to obtain reliable values for the diagonal force constants. Two different procedures were checked to fit the force fields: the traditional refinement method and the scaled quantum mechanical force field method.

Using the ASYM40 program, and experimental vibrational wavenumbers from infrared and Raman techniques, the force constant matrix (B3LYP/6-311++G**) for the *cis*- and *trans*-3-fluorostyrene and 4-fluorostyrene have been fitted. When the refinement method was applied, a set of independent symmetry coordinates (C_s symmetry) all of them orthogonal with all the redundancies of the molecule was used to block the secular equation. In the case of the scaling method, natural coordinates were used according to the Pulay's method, and the initial value for all the scale factors before refining was 0.928, as proposed by Rauhut et al. [7] for the B3LYP functional. As in the refinement procedure, no empirical correction of the theoretical geometry was used. In Table 4 the r.m.s. deviations for the frequencies obtained by the B3LYP/6-311++G** and using only the 0.928 scale factor, along with the r.m.s. deviations of the refinement and scaling procedure, are shown. As one can see, using only one scale factor decreases the r.m.s. deviations though it is clear that there is a better agreement with the use of multiple scale factors. Also, it can be seen that the deviations are much smaller in the refinement procedure than in the case of the

scaling method. However, while ~ 40 diagonal force constants were refined in the case of the refinement method, only a total of 19 scale factors were refined in the case of the scaling method.

Using the CLIMAX program, and experimental data from INS technique, intensities and vibrational wavenumbers, the force constant matrix (B3LYP/6-311++G**) expressed in independent symmetry coordinates for the 4-fluorostyrene have been fitted. The final INS profile after the fitting is shown in Figure 3. Figure 4 shows the calculated INS spectrum at the B3LYP/6-311++G** level for the *cis* and *trans*-3fluorstyrene without any fitting. In this case, it was impossible to fit the INS profile due to the presence of both conformers, cis and trans, in the INS spectrum.

In Table 5 are listed the force constants after the scaling corresponding to the C-C stretching, which are defined as valence internal coordinate in the case of the scaling method. One can appreciate that the values for the C_3-C_4 stretching force constant (8.777, 8.834, 8.783 and 8.636 aJ Å^{-2} for *cis*, *trans*-3-fluorostyrene, 4-fluorostyrene and styrene, respectively) are close to the typical value for a C-C double bond, 9.6 aJ Å^{-2}. These values are also in agreement with the values from the scaled force field of stilbene of 8.483 and 8.641 aJ Å^{-2} for the C_3-C_4 stretching force constant obtained by Arenas et al. [8]. By the other hand, the values for the C_1-C_3 stretching (4.860, 4.882, 4.884 and 4.987 aJ Å^{-2} for cis, trans-3-fluorostryene, 4-fluorostyrene and styrene, respectively) are close to to the typical value for a C-C single bond, 4.50 aJ Å^{-2}.

Table 4: *Initial and final r.m.s. (cm^{-1}) for the scaling and refinement methods.*

		cis-3FS	trans-3FS	4FS
B3LYP/ 6-311++G**	IR/Raman	59.1	58.6	57.7
	INS	-	-	18.4
Scale Factor 0.928		18.5	19.2	17.5
Scaling		5.0	5.0	5.2
Refinement	ASYM40	0.5	0.2	1.5
	CLIMAX	-	-	3.6

According to the philosophy of the canonical force field [9], only those force constants expressed in independent symmetry coordinates from the refinement method, using both ASYM40 and CLIMAX programs, have been transformed into pure vibrational form for comparison. Some of them are shown in Table 5 along with the values reported by Hargittai et al [10] for styrene, Goodman et al. [11] and Pulay et al.[12] for bencene. If we stare into the set of values $\{F_{i,i}\}$ i=1-8, it can be seen that the value of $F_{8,8}$ is almost twofold that of the rest. This may mean that the vinyl C-C bond is significantly localised. *The values for the C_1-C_3 stretching force constants from the refinement are farther from a single C-C bond stretching force constant than in the case of the scaling method.*

Figure 3. *INS spectrum for 4-fluorostyrene (¾ observed and ¾ calculated)*

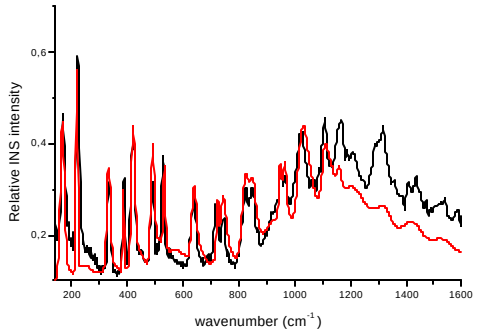

Figure 4. *INS spectrum for 3-fluorostyrene (¾ observed and ¾ cis and ¾ trans calculated)*

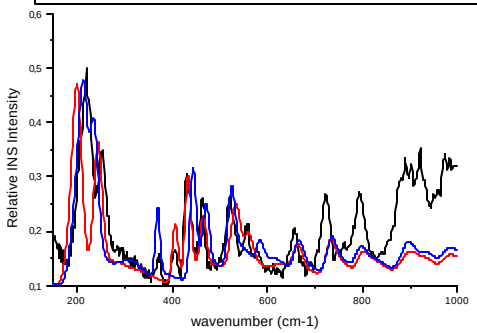

Furthermore the force constant value for the torsional motion of the C_1-C_3 group is more than double that for the C-C torsion within the benzene ring. All these results lead us to the conclusion that the conjugation between the vinyl moiety and the benzene ring is not as strong as expected for this kind of molecules.

***Table 5**: Scaled and refined force constants for the C-C stretching and C-C torsion* (*Units are consistent with the energy measured in aJ, bond lengths in Å and bond angles in radians*).

	SCALING				VIBRATIONAL PURE						Description
	cis-3FS	trans-3FS	4FS	Styrene[10]	cis-3FS	trans-3FS	4FS ASYM40	4FS CLIMAX	Bencene Goodman[11]	Bencene Pulay[12]	
$F_{1,1}$	6.299	6.193	6.171	6.282	5.518	5.382	4.525	4.681			
$F_{2,2}$	6.549	6.722	6.712	6.700	5.489	5.597	5.621	5.358			
$F_{3,3}$	6.607	6.500	6.614	6.535	5.087	5.031	5.393	5.403			
$F_{4,4}$	6.592	6.794	6.770	6.667	5.036	5.024	5.719	5.468			$C\text{-}C_{benc}$ stret.
$F_{5,5}$	6.832	6.742	6.587	6.603	4.681	4.431	4.991	5.197			
$F_{6,6}$	6.183	6.363	6.327	6.441	5.650	5.364	5.164	5.343	4.892	4.760	
$F_{7,7}$	4.860	4.882	4.884	4.987	6.004	5.292	5.317	5.596	-	-	C_1-C_3 stret.
$F_{8,8}$	8.777	8.834	8.783	8.636	8.088	9.088	8.655	8.491	-	-	C_3-C_4 stret
$F_{50,50}$					0.503	0.525	0.519	0.546	0.249		C_3-C_4 tors.

Typical Problems

Although it would be preferable to compare calculated harmonic frequencies with experimental harmonic frequencies, or calculated anharmonic frequencies with experimental fundamental modes, it is not routinely practicable for polyatomic molecules at the present. Therefore, the anharmonicity and intermolecular effects have been refined into the force constants, and in the same way, the scale factors have been fitted to observed frequencies (anharmonic) including into the final scaled factors values the anharmonic contribution.

It must be remarked, anyway, that in spite of the good results for the r.m.s., from both refinement and scaling methods, the experimental data have been taken from liquid and solid phases while the force fields have been performed in the isolated molecule approximation. As a probe of the non-negligible intermolecular interactions in this kind of compounds one can look at the weak INS intensity calculated from the DFT methods compared to the experimental one, even after refining (Figures 3 and 4).

According to the Pulay's method, bonds are described by individual stretching coordinates. This is suggested by a generally low coupling between bonds (even in conjugated systems) and the fact that the anharmonicity can be described in the most compact form in terms of individual bonds. Therefore, each stretching force constant is fitted using an individual scale factor for each one. In the case of the refinement method, the stretching force constants are combined, and then refined. The last ones must be transformed into the canonical form for comparison. As it can be seen in Table 5, the values for the C_1-C_3 stretching force constants from the refinement, using ASYM40 and CLIMAX, are further from a single C-C bond stretching force constant than in the case of the scaling method, while in principle, both *methods should produce similar results*. In addition, in some previous works when the scaling method was applied in the analysis of the INS spectrum of small systems, the authors pointed out that in order to reproduce the INS intensity the sign of some off-diagonal force constant might be changed, which is possible in the case of the refinement method, but not when using the scaling method.

Perspectives

Due to computational limitations, only MP2 with a moderate basis set, 6-31G*, was performed. It could be interesting to check if a increasing of the size of the basis set gives planar structures in spite of the high consuming time calculation. In this way, DFT has been gaining popularity in computational quantum chemistry for its computational speed and incorporation of electron correlation. However, there is not systematic way to improve the quality of a particular DFT calculation. Therefore, are DFT methods the *panacea*?

As it can be seen from the INS spectra, the INS intensity is not reproduced in all the INS profile probably due to the influence of the environment in the solid phase. In order to improve the results, periodic DFT calculation could be essayed. In addition, taking into account the final results for the force constants values from the refinement and the scaling methods, and the very different procedures to build the complex independent symmetry coordinates or the simple natural coordinates, it could be desirable to implement the scaling method to fit the INS spectrum and to compare the results from both methods.

A very particular situation occurs when two different conformers are present in the INS spectrum. At the present, it is not possible to fit the INS profile but it could be interesting in the future to implement this particularity in CLIMAX.

---

7 G. Rauhut and P. Pulay, J. Phys. Chem. 99 (1995) 3093

8 J.F. Arenas, I. López-Tocón, J.C. Otero, J.I. Marcos, J. Phys. Chem.99 (1995) 11392

9 E. Martínez Torres, J.J. López Gónzalez and M. Fernández Gómez, J. Chem. Phys. 110 (1999) 3302

10 R. Hargittai, P.G. Szalay, G. Pongor and G. Fogarasi, J. Mol. Struct. 306 (1994) 293

11 L. Goodman, A.G. Ozkabak and S.N. Thakur, J. Phys. Chem. 95 (1991) 9044

12 P. Pulay, G. Fogarasi and J.E. Boggs, J. Chem. Phys. 74 (1981) 3999

Dynamics of Polymers and Liquid Crystals

Stephen J. Picken, Delft University of Technology, Polymer Materials and Engineering (PME),
Julianalaan 136, 2628BL Delft, The Netherlands

Introduction

The work we are doing, at the section Polymer Materials and Engineering (PME) at the TU Delft, concerns itself among a variety of things with the task of trying to better understand the dynamics & ageing of complex polymer systems. Here the general strategy is to obtain additional or more detailed information by perturbing the equilibrium structure of polymeric materials. The various methods include the use of self-organisation, e.g. in liquid crystal polymers (LCP's) & block-copolymers, the concept of confinement, e.g. by adding nano-particles, and the investigation of the dynamics in (ultra)thin polymer films. In relation to this dynamics other related techniques are used including the study of the age-old problem of free-volume & ageing dynamics using positron annihilation lifetime spectroscopy (PALS), and the development of fluorescent probe molecules to monitor polymerisation and local dynamics using spectroscopic techniques. Finally, we are collaborating on the use of quasi-elastic neutron scattering (QENS) to investigate the local dynamics of discotic materials. In all these techniques of course we should realise that polymers tend to be slow – but we have time-temperature superposition to help us. Also, apart from having to bridge a wide range of time scales we should also be able to deal with the related length-scaled that govern the various processes. Without being able to really address the details of these topics in the following will try to give a flavour of what we think is interesting and where we hope to be heading.

Methods

In the presentation we will limit ourselves to LCP's, the dynamics in (ultra)thin polymer films, and free-volume & ageing dynamics.

The dynamics of LCP's is a typical example of the coupling between the dynamics and the self-organisation and anisotropy that can occur in complex polymer systems. Using standard thermal analysis, microscopy and x-ray diffraction (XRD) methods it is possible to accurately determine the structure property relations in a static sense i.e. what is relation between the structure and the phase diagram. From a dynamic point of view it is then possible to probe in detail what the effect of local structural changes is on the dynamics. The most frequently used technique at present is that of dielectric relaxation spectroscopy however other techniques including QENS may provide further information in future.

Apart from the effect of spontaneous self-organised structures on the dynamics, it is of interest to impose length scales onto polymeric systems e.g. by confining the chain-statistics by adding of a high volume fraction of nano-particles or by investigating the dynamics in ultra-thin polymer films. Using dielectric relaxation spectroscopy the dynamics of very thin polymer poly(methyl-methacrylate) (PMMA) films can be investigated, down to about 4 nm, and the effect on the polymer mobility can be rather striking. Related to this the concept of “collectively rearranging regions” or CRR's may be useful to describe the sequential nature of the processes required for a "single relaxation event".

Extending the dynamics of polymers to even longer time scales it is of interest to examine the present state of affairs in the field of physical-ageing dynamics. We have been performing a careful study on the physical ageing of polycarbonate using positron annihilation lifetime spectroscopy (PALS). Here the results indicate that the free-volume acts as a means to dramatically speed up the mobility of the polymers due to the steadily increasing excess free volume and that the observed dynamics can be successfully modelled using relatively simple equations.

Typical results

Concerning the dynamics of LCP's the most striking effects occur at phase transitions e.g. from nematic-discotic to nematic-columnar. Here, the discotic side groups initially are arranged as individual entities in the N_D phase, while in the N_{Col} phase the mesogens are aligned on short columns. The effect on the relaxation strength and the relaxation time then allows us to correlate the dynamics and the collectivity of the processes to the local structure as probed by XRD. In figure 1 we show the XRD patterns of a N_{col} and a N_D phase where the column length increases by about a factor 4 at the transition. In figure 2 we show the corresponding relaxation time and strength from dielectric relaxation spectroscopy, the observed slowing down nicely corresponds to the picture of a collective motion of the disks in the N_{col} phase while the increased relaxation strength by about a factor 4 agrees very well with the increasing correlation length as obtained from the line-width in XRD using the Scherrer equation.

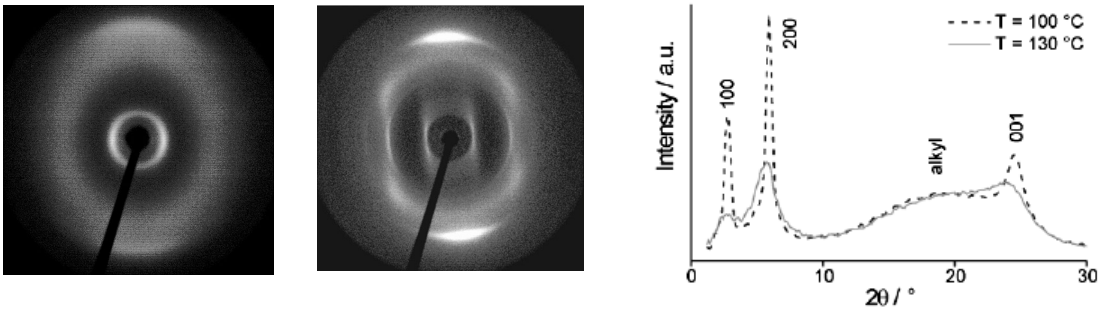

Figure 1: XRD patterns of the N_D (left) and N_{col} phase (middle), analysing the linewidth of the (001) reflection shows a fourfold increase of the columnar stacking length, via the Scherrer equation. As an example the right hand figure shows a radial scan for the N_D (130°C) and N_L (100°C) phase.

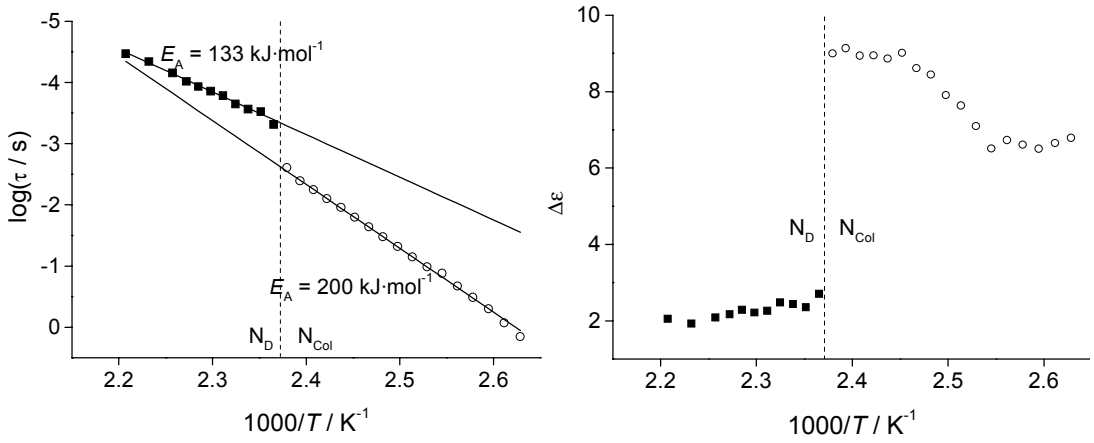

Figure 2: This shows the relaxation time τ and the relaxation strength Δε', as a function of reciprocal temperature, around the N_D to N_{col} transition. Note the 10 fold slowing down at the transition and an increase of the relaxation strength by a factor of 4, indicating a collective mode in the N_{col} phase

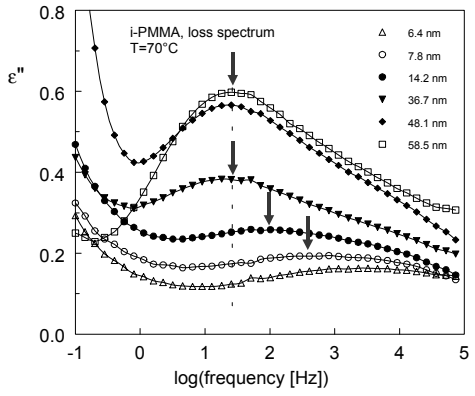

Figure 3: Shift of the α-peak versus film thickness in Isotactic PMMA, here shown in the frequency domain (d= 6.4 – 58.5 nm)

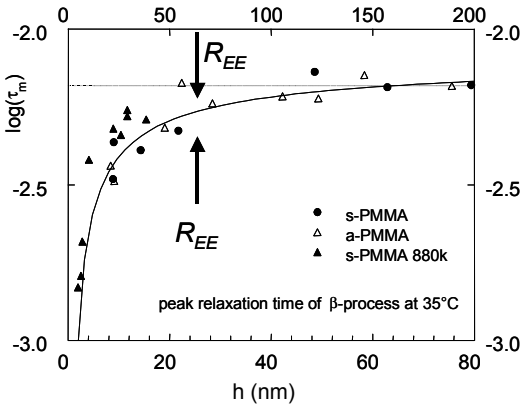

Figure 4: This shows the secondary β relaxation time versus film thickness for low (bottom) and high (top-scale) M_W PMMA samples.

In the dynamics of supported (ultra)thin films of PMMA there is a large effect of the film thickness on the α-process (i.e. the glass transition) of the polymers, where a substantial shift to lower temperatures (by 10-20 K) can be observed at low film thickness. This is shown in figure 3. In addition there appears to be a coupling of the secondary β relaxation time to both the molecular weight and the film dimensions via the average endpoint distance $\langle R^2 \rangle$. Figure 4 shows how a "master-curve" can be constructed for the β-relaxation, by scaling the film thickness to the polymer endpoint distance $\langle R^2 \rangle$.

Finally in the field of physical ageing the PALS technique allows us to determine the average size of the free-volume voids (via the relaxation time τ) and their number (via the intensity). We find that the average size of the free-volume voids remains invariant during physical ageing (see figure 5), while the number decreases as a function of time. This occurs at various rates depending on the temperature used for the ageing of the samples (see fig.6 as an example, using a single exponential to fit the data), the PALS measurement itself is always performed at room-temperature where for each data point a separate sample is used to avoid the effect of charging that also influences the intensity. The results can be interpreted using a very simple expression proposed before by Struik that describes how the relaxation time is related to the temperature and the excess free-volume. This gives rise to a strong self-retardation process during physical ageing where the rate of relaxation is a highly non-linear function of time and effectively the equilibrium will never be reached.

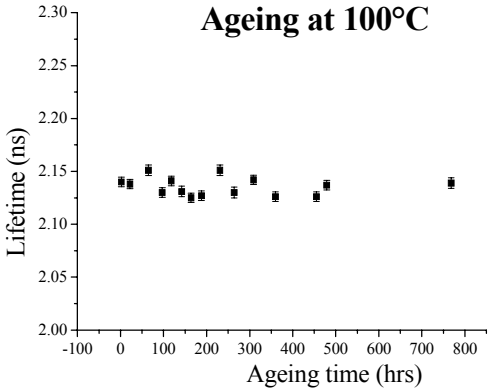

Figure 5: O-Ps lifetime (measured at RT) versus ageing time at 100°C for PC from PALS. The lifetime is a measure for the average void size.

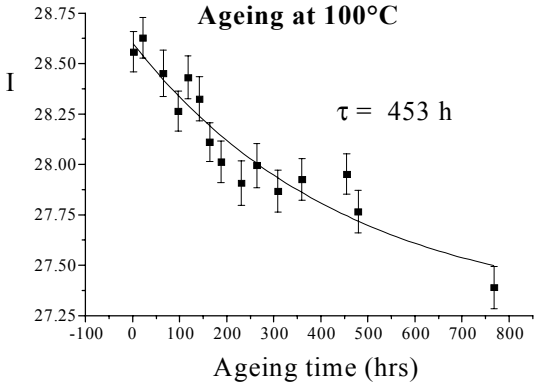

Figure 6: O-Ps intensity (measured at RT) versus ageing time at 100°C for PC from PALS. The intensity is a measure for the number of voids.

Perspectives

The work so far indicates that there is still scope for further investigation of polymer dynamics using a variety of techniques. The effect or self-organisation and confinement can be investigated usefully by considering the effect of spontaneous self-organisation using LC phases and via confinement, either as thin films or by using nano-sized fillers. Regarding the long-standing problem of physical-ageing it appears that there may be scope for the introduction well defined "entities' with a well defined size that govern the ageing process. Clearly this has implications both for our understanding of the relaxation phenomena on the molecular scale as well as for the practical application and optimisation of polymer materials. From a practical point of view the challenges will be to identify materials and techniques that remain tractable as the topic is already more than complicated enough. This means that we need to have well defined polymer materials that are well characterised and that can be modified e.g. using specific deuteration without a too large synthetic effort being involved. Via this route it will be possible to involve techniques like SANS and QENS for further probing of the structure and extending the dynamic range to even shorter time scales. Indeed recent results using QENS on model discotic materials show interesting results in the dynamics, which is related to the molecular organisation both in the columnar and in the isotropic phase. Also, clearly for the probing of the effects of confinement via the study of (ultra)thin films it is necessary to produce nice clean samples which implies the need for good film making facilities. It would seem to be the case that an integrated approach, where both fast (ps) and slow (Ms) time-scale phenomena are being investigated, may indeed lead to a more complete understanding of the dynamic processes that govern the properties of polymeric materials.

Extended abstract for ESF workshop: Bridging the Gap in molecular science between model systems and real systems.

Time resolved transient grating spectroscopy for in the study of protein dynamics.

M. Plazanet*, J.P. Ogilvie, G. Dadusc and R.J.D. Miller.
University of Toronto, Department of Chemistry, 80 St George Street, Toronto M5S 3H6, Canada.
*Institut Laue Langevin, BP 156, 38042 Grenoble, France.

Introduction

An important problem in the functionality of proteins is the efficient transport of ligands into and out of the protein. A dynamical pathway must exist that leads to large correlated motions that permit the ligand to access the protein site. Time resolved optical techniques enable the characterisation of dynamics over of a very wide time range (from 10^{-15}s to months). Transient (phase)-grating spectroscopy (TG), a non-linear technique, offers the possibility to observe density modulations following a triggered event. In Carboxy-Myoglobin (MbCO), after photodissociation of the ligand (CO), the technique enabled the full and direct observation of the ligand escape out of the protein.

Methods

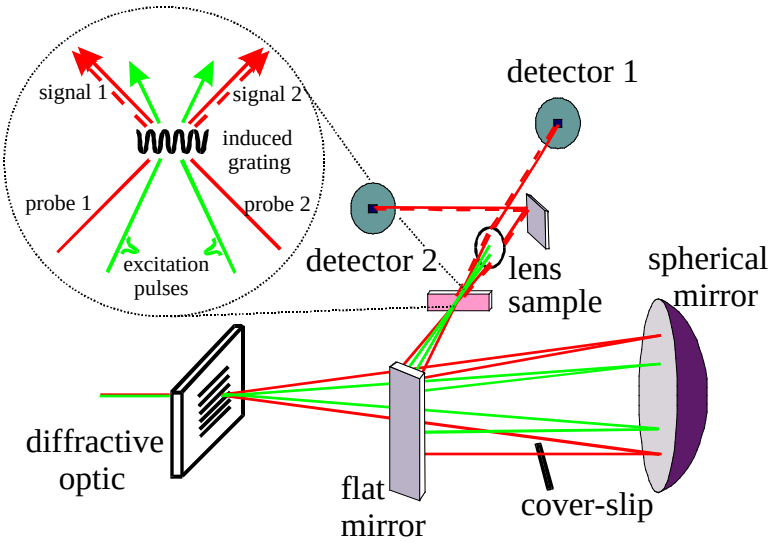

Figure 1. : Experimental setup for diffractive optics-based heterodyne-detected transient grating.

The grating image is formed at the sample by the interference of two excitation pulses, at a resonant wavelength. The optical interference pattern writes into the sample a diffraction grating with spatial period Λ, which depends on the angle between the two excitation beams. The index grating is probed by a cw beam or delayed pulse, that diffracts on the grating. The time-dependence of the diffracted probe reflects the variations in the grating, induced by the change in optical density and real part of the index of refraction [1].
The signal is proportional to the diffraction efficiency η of the sample, and for a protein in solution and suitable grating parameters, it can be written as[2]:

$$\eta \quad \left|\left(\Delta n_{protein} + \Delta n_{Th} + \Delta n_{ex}\right) + i\Delta k_{ex}\right|^2$$

The real part is made from several contributions, related to density and refractive index fluctuations:

- $\Delta n_{protein}$ contains the desired information about the protein dynamics, ie. density induced variations. This term is related to the material strain, or volume change that accompanies protein conformational change, as well as diffusion processes. Ideally, one would like to isolate $\Delta n_{protein}$.
- Contributions to the signal that arise from density changes due to heating, Δn_{Th}, can be isolated by varying the temperature, and removed by performing the studies at the zero-thermal expansion temperature of the protein solution.

- The terms Δn_{ex} is the electronic contributions of the real part of the modulated complex index of refraction. It arises from the difference in absorption giving also a phase component. It is related to Δk_{ex} by the Kramers Kronig's relations. It is also minimised far from resonance, or removed by tuning the probe wavelength to a zero-crossing point of Δn_{ex}.
- The imaginary part Δk_{ex} arise from the difference in optical density between the two populations, and can be avoided by performing the experiment with an off-resonant probe.

Temperature and fringe spacing dependence helps identifying the different components.

If heterodyne-detected, the signal is proportional to $\eta^{1/2}$ and is therefore linear in the refractive index changes. The linearization of the signal permits the separation of Real (Re) and Imaginary (Im) parts of the signal, made straightforward thanks to a differential detection setup [3].

Grating spectroscopies are capable of detecting changes in lattice temperature with energy deposition less than 10^{-4} °C for terms arising from $\left(\frac{\partial n}{\partial \rho}\right)_p$ for typical sample conditions (contained into $\Delta n_{protein}$), or changes in net volume of effective radius of less than 0.01Å.

Application to the study of protein dynamics.

One can find in the literature several systems where transient grating and related spectroscopies (photoacoustics, 3-Pulses Stimulated Photon Echo) have been successful in understanding the dynamics of proteins. Recently, Terazima and co-workers applied it to the Photoactive Yellow Protein and determined diffusion coefficients of transient species[4]. They could as well measure diffusion coefficients for various denatured conditions and compare it with transient states.

After calibration of the amplitude of the signal with a reference compound, thermodynamical measurements (volume changes, calorimetry) can also be extracted from the data. That has been done for example on octupus rhopospin[5] to determine relative energetic positions of the transient states; it also gave the volume variation between Mb and MbCO[6].

MbCO : real time observation of the ligand escape

Myoglobin has been extensively studied by optical techniques, as it enable the optical triggering of the ligand dissociation by visible light. We present in the following section our main results concerning the dynamics of MbCO[6,3].

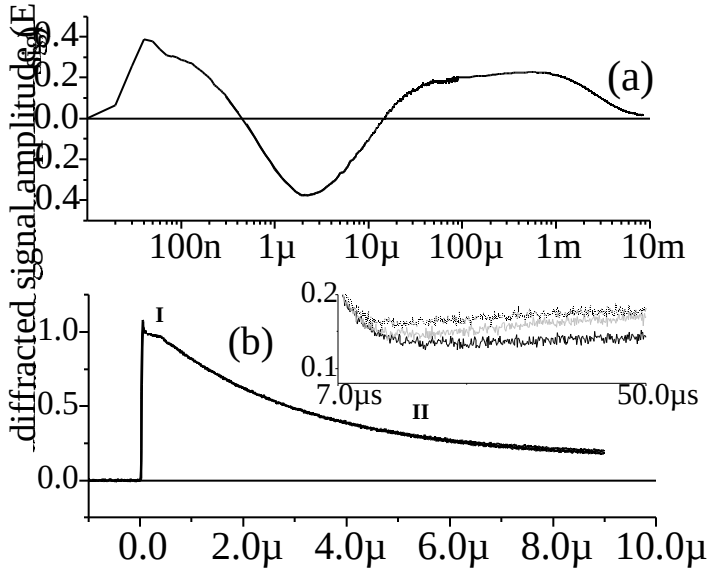

Figure2. . Dynamics of the real part of the refractive index following photodissociation of MbCO. (a) : 20°C, full range of the dynamics. (b): -1.5°C data, 2 µs timescale. The inset shows the dynamics on a longer timescale, where the fringe spacing dependence (7.5 µ, 15 µ, 30 µ) becomes distinguishable. This dependence demonstrates that the CO has escaped the protein.

The experimental setup, described with more details elsewhere[7], uses a 20 ns pulse at 527 nm to create the population grating, and probes with a cw beam at 1064 nm. Fig. 2a summarises the dynamics of Δn over the whole time scale after ligand dissociation at room temperature. Following the small peak observed within the first 20 ns due to induced structural birefringence, a barely perceptible plateau and a large decay that leads to a sign change in the signal are assigned to CO motions inside the protein and will be discussed bellow. After a few _s, the thermal relaxation of the grating is complete, followed by CO diffusion out of the grating, and finally the bimolecular recombination erases the fringes. Fig. 2b focuses on the 2 μs timescale at –1.5°C (zero-thermal expansion point of the protein solution) where the thermal component is absent in the signal. Two components can be clearly separated, labeled as parts I and II. The very simple (exponential) functional form of the decays suggests that the process involves the motion of the ligand along a well defined pathway i.e. thermal hopping mechanism between discrete sites.
The time decays have been interpreted in agreement with the model proposed by Beece et.al[8], that analyse the CO escape as a four steps process. The two observed components of fig. 2b are assigned to the last two steps (they are the only steps within the time-resolution of the experiment): motions between internal cavities of the protein, and escape to the solvent. They are associated to exponential decays of 49±10 ns and 725±15 ns respectively at room temperature, slowing down to 390 ns and 2.86 _s at –1.5°C. This work[6] was the first to fully resolve the ligand escape from a protein and is in good agreement with estimates made in previous studies[9].

The offset of the signal, at 10μs, is interpreted as Δn_{ex}. We extended the technique to the use of an on-resonant probe, with the aim of definitely identifying the Δn_{ex} contribution and remove it from the signal. The Kramers-Kronig relation expresses the relation between the real and imaginary parts of the electronic contribution to the complex index of refraction: due to the presence of isobestic points in the absorption difference spectrum, we expect the term Δn_{ex} to cross zero at several wavelengths.

We used as a probe a cw dye laser with wavelength tuned between 550 and 630 nm, where Δn_{ex} presents two zero-crossing points. The experiment, in MbCO, is complicated by the presence of spectral shifts on the timescale of interest, as can be seen in the transient absorption spectra (figure 3). Indeed, the absorption $|\Delta k_{ex}|^2$ is disturbed by the CO motion around the heme, and exhibits a time dependence very similar to the one of Δn. This influences directly $\Delta n_{ex}(t)$, that has therefore been calculated from $\Delta k_{ex}(t)$.

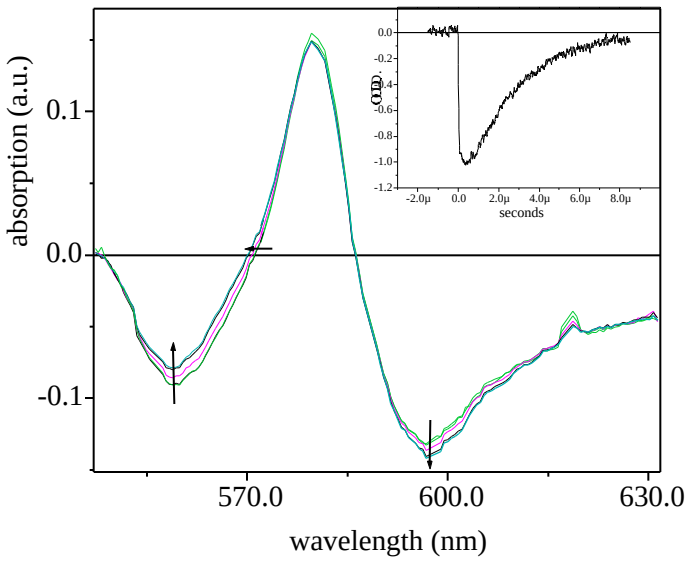

Figure 3. Transient absorption in the Q-band. (a): wavelength spectrum at –1.5°C at 100 ns, 500 ns, 2 μs, 5 μs, and 7.5 μs after photodissociation The inset shows the time-resolved signal at 570.5 nm, close to the isobestic point, where the amplitude of the spectral shift is the largest and the most sensitive to structural changes.

On figure 4 are presented the transient grating signal for several wavelength around at the zero-crossing point 579 nm: the amplitude of the offset for different wavelengths follows the calculated $\Delta n_{ex}(\lambda,$

10µs), and clearly shows the origin of the contribution. This effect was not distinguishable at 1064nm, where the amplitude of the time dependence of Δn_{ex} is negligible compared to its equilibrium value. The time dependence of $\Delta n_{ex}(t)$ was then removed from the signal : we were able to obtain the previously measured signal, without the Δn_{ex} contribution.

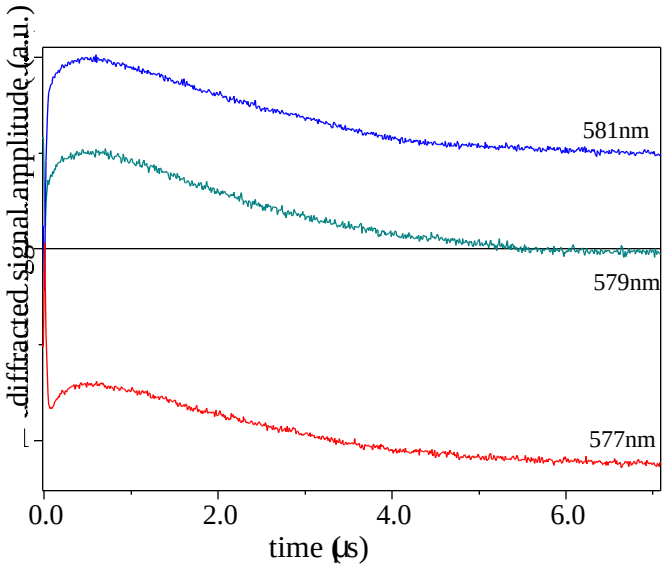

Figure 4 : Real part of the heterodyne-detected transient grating signal for MbCO at –1.5°C for wavelengths near the zero-crossings in Δn_{ex} at 579 nm.

Limitations and Perspectives

This work enabled the characterisation of the protein dynamics on the timescale of ns to ms, in distinguishing the CO and/or heme dynamics through its influence on the electronic transition (Δn_{ex}, Δk_{ex}), and the exponential form of the globin relaxation through $\Delta n_{protein}$. Earlier dynamics can obviously be investigated by the same technique using shorter pulses. Such kind of work can be easily extended to any kind of photoinduced dynamics: chemical reaction, pH jump, anisotropy…

Optical techniques present a great sensitivity and time resolution. They cover the wider time range, provide both time and frequency domains measurements and enable transient states observation. They need very small sample, but can be restricted to low concentration, though this can be overcome by reducing the concentration of chromophore (ex. Myoglobin heme-less) or adding crowding agents. By combining different techniques, one can focus on a very specific part of the macromolecule, the chromophore, or observing density fluctuations in the time domain (with TG). The techniques are often complementary with neutrons. Low energy processes (from µeV to meV, tunneling or diffusive processes) are easier to measure with neutrons. Neutron scattering, using deuteration contrast, enables the focusing on a well chosen hydrogenated part of the sample. Finally, neutrons directly probe nuclear measurements, while optics provides only indirect methods.

---

[1] R.J.D. Miller, In *Time resolved spectroscopy* (1989), ed. R.J.H. Clark, R. E. Hester, 18:1. Chichester, Engl :Wiley.
[2] R.J.D. Miller, Ann. Rev. Phys. Chem (1991) **42**:581-614.
[3] J.P. Ogilvie, M. Plazanet, G. Dadusc and R.J.D. Miller, J. Phys. Chem. B, in press.
[4] K. Takeshita, Y. Imamoto, M. Kataoka, F. Tokunaga and M. Terazima, Biochemistry (2002) **41**:3037-3048.
[5] Y. Nishioku, M. Nakagawa, M. Tsuda, and M. Terazima, Biophys. J. (2001) **80**: pp. 2922-2927.
[6] G. Dadusc, J.P. Ogilvie, P. Schulenberg, U. Marvet and R.J.D. Miller, Proc. Natl. Acad. Sci. (2001) **98**: p. 6116-6120.
[7] G.D. Goodno, G. Dadusc and R.J.D. Miller, J. Opt. Soc. Am. B (1998) **15**: p. 1791.
[8] D. Beece, L. Eisenstein, H. Frauenfelder, D. Good, M.C. Marden, L. Reinisch, A.H. Reynolds, L.B. Sorenson and K.T. Yue, Biochem. (1980). **19**(23): p. 5147-5157
[9] T.A. Jackson, M. Lim, and P.A. Anfinrud, Seventh International Conference on Time-Resolved Vibrational Spectroscopy (1995) 9-13.

Effects of disorder on the electrical conductivity of conjugated polymers

L.D.A. Siebbeles, IRI, Delft University of Technology, Mekelweg 15, 2629 JB Delft, The Netherlands

Introduction

The conductive properties of conjugated polymers (see Fig. 1) have attracted a great deal of interest in recent years due to their (potential) applications in organic light-emitting diodes, solar cells or field-effect transistors. Furthermore, single polymer chains might be used in the future as "molecular wires" in nanoscale electronic circuits. In their pure states conjugated polymers are insulators. They can become conducting on introduction of charge carriers by e.g. chemical doping, photo-excitation or injection of charges from electrodes. The mobility of charge carriers in conjugated polymers is one of the key parameters determining the performance characteristics (e.g. switching times and maximum current) of organic opto-electronic devices. A thorough understanding of the factors that govern the mobility in conjugated polymers is essential for the development of devices based on these materials.

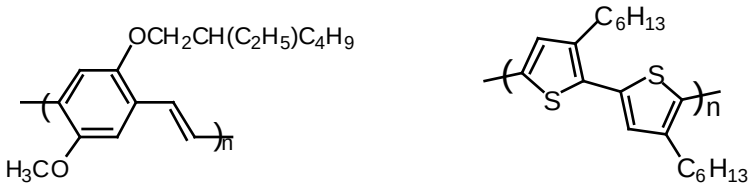

MEH-PPV **P3HT**

Figure 1: Molecular structure of MEH-PPV and P3HT

In carbon based π-bond conjugated polymers the conduction bands are mainly composed of the $2p_z$-orbitals on the carbon atoms. For perfectly ordered polymer chains the calculated widths of the conduction bands are typically 5 - 10 eV.[1] On basis of such bandwidths the effective mass of a charge carrier would be ~0.07 times the free electron mass. This effective mass is comparable to that of charge carriers in inorganic semiconductors (e.g. GaAs or InP), which have mobilities of the order of 5000 $cm^2V^{-1}s^{-1}$. The mobility of charges along perfectly ordered conjugated polymer chains could thus be expected to be comparable to that in inorganic semiconductors. However, typical values of the mobility of charge carriers in conjugated polymers are at least four orders of magnitude smaller. This is not surprising, since conjugated polymers are non-crystalline disordered materials. The polymer chains exhibit kinks and chemical defects that reduce the effective conjugation and hinder charge transport. Further, mobilities are usually obtained from DC measurements in which the transport of charges involves relatively slow steps such as motion from one polymer chain to another and across grain boundaries in the sample.

To avoid the difficulties in DC conductivity measurements on solid samples we have investigated the mobilities of charges on isolated polymer chains in dilute solution. Comparison of the experimental results with theory suggests that the measured mobility is limited by torsional disorder along the polymer chains and by the occurrence of chemical defects and/or chain ends.

Experiments on the conduction of isolated polymer chains

In the experiments the polymer chains are isolated from each other by dissolving them in benzene. Excess electrons and positive charges (holes) are produced in the solvent by pulsed irradiation with high-energy electrons from a van de Graaff accelerator. In the presence of oxygen the electrons are rapidly scavenged so that they do not undergo charge transfer to the polymer chains. The positive charges undergo charge transfer to the polymer chains. The mobility of the holes on the polymer chains is determined from time-resolved measurements of the change in the microwave (34 GHz) conductivity of the sample after irradiation. The results obtained show that there are significant differences in the ability of MEH-PPV and P3HT (see Fig. 1 for the structure) to transport positive charges. The hole-mobility on MEH-PPV was found to be 0.43 cm^2/Vs whereas for poly-3-hexylthiophene a value of ~0.02 cm^2/Vs was obtained.[2,3]

Theoretical model for charge transport

The calculations of charge transport are based on the tight-binding approximation combined with static torsional disorder along the chain.[4] A polymer is modeled by a chain of sites that correspond to the monomer repeat-units, and charge migration on this chain is described by the Hamiltonian

$$H_q = \sum_n \left[\varepsilon_n a_n^+ a_n - b(\Delta\theta_{n,n+1}) \left(a_{n+1}^+ a_n + a_n^+ a_{n+1} \right) \right] \quad (1)$$

In this equation ε_n is the energy of the charge at the *n*-th site, while a_n^+ and a_n are the creation and annihilation operators for a charge at this site. The charge transfer integral $b(\Delta\theta_{n,n+1})$, which is measure of the electronic coupling between neighboring sites, depends on the inter-unit angle, $\Delta\theta_{n,n+1}$, between the *n*-th and *(n+1)*-th monomer units in the polymer and is calculated using quantum chemical methods. The energy of a positive charge localized on a singly polymer unit, ε_n, is essentially the ionization potential of such a unit. The inter-unit angles were sampled from a Boltzmann distribution using the potential energy profiles for torsional motion between the monomer units as obtained from Hartree-Fock plus second order Møller-Plesset perturbation theory.

The wave function, $|\Psi(t)\rangle$, of a hole is expressed as a superposition of states $|n\rangle$ located on the different sites with coefficients c_n:

$$|\Psi(t)\rangle = \sum_n c_n(t) |n\rangle \quad (2)$$

For hole transport the states $|n\rangle$ were taken as the highest occupied orbitals in the neutral monomer units. At t=0 a positive charge is localized on a single unit; i.e. $c_i(t=0)$=1 and all other coefficients are zero. The time-dependent coefficients, $c_n(t)$, are obtained by numerical integration of the first-order differential equations that follow from the substitution of the wavefunction in Equation 2 into the time-dependent Schrödinger equation.

The frequency dependent mobility of the charge carriers can now be obtained from the mean-square displacement of the charge $\Delta^2(t)$ using the Kubo formula

$$\mu(\omega) = \frac{-e\omega^2}{2k_B T} \mathrm{Re}\left[\int_0^\infty \Delta^2(t) \exp(-i\omega t)\, dt \right], \quad (3)$$

in which e is the elementary charge, k_B is the Boltzmann constant, T is the temperature, ω is the radian frequency of the probing electric field, and 'Re' denotes that the real part of the integral is taken.

Results and discussion

The measured mobility of holes on MEH-PPV chains is much higher than has ever been obtained from DC measurements on thin films or bulk material. This is due to the fact that in the present AC conductivity experiments the motion of holes along the polymer chains is probed an relatively slow charge tranfer processes involved in DC measurements do not play a role. However, the mobility is orders of magnitude smaller than the typical values for inorganic semiconductors. As discussed below, the mobility is most likely limited by torsional disorder and chemical defects. The much lower mobility of holes along polythiophene chains is attributed to a larger degree of torsional disorder and the relatively short lengths of the polymer chains.

The potential energy profiles for torsional motion around the bonds between the monomer repeat units in the polymers investigated are presented in Fig. 2. In PPV the torsional degree of freedom involves variation of the angles between adjacent phenyl and vinyl groups. Therefore a styrene molecule was taken as a model system to calculate the torsional potential. For polythiophene a bithiophene molecule was taken as a model system to obtain the torsional potential. The results in Fig. 2 show that the barrier for torsional motion in polythiophene is significantly lower than the barrier found for PPV. Consequently, the probability of deviations from a coplanar alignment of monomer repeat-units within a polymer chain in solution is higher in polythiophene than in PPV. The calculated electronic coupling, $b(\Delta\theta_{n,n+1})$, is maximal for a planar arrangement of adjacent monomers and decreases when the angle is increased. The electronic coupling becomes (almost) zero at a perpendicular geometry and in that case motion of a charge between the repeat units involved is impossible. Hence, the larger torsional angles in polythiophene cause the mobility of holes to be smaller than in PPV.

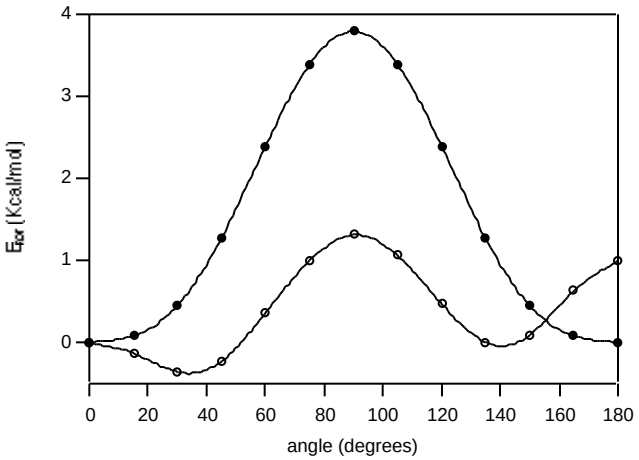

Figure 2: Potential energy profiles for torsional motion of structural units in PPV (filled circles) and polythiophene (open circles) chains. Calculations were performed at MP2/cc-pVDZ level.

Fig. 3 shows the calculated frequency dependence of the mobility of holes on PPV and polythiophene chains. The chains were taken sufficiently long so that chain end effects do not play any role. The mobility increases with the frequency of the probing electric field, since at high frequencies a charge carrier can follow the oscillating field by motion between points at which the torsional angles are large and the charge transfer rate is small. At all frequencies the calculated mobility of holes on infinitely long PPV chains is approximately 30 times higher than for polythiophene chains within the entire frequency range investigated. This is due to the more planar structure of the PPV chains.

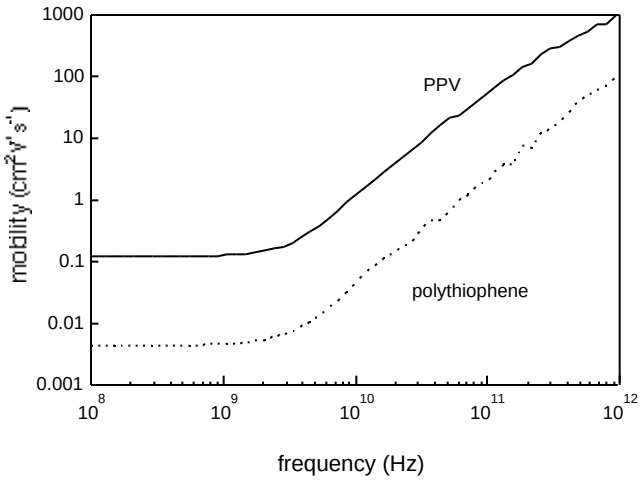

Figure 3: Calculated frequency dependence of the mobility of holes along PPV and polythiophene chains.

The theoretical mobility values in Fig. 3 for infinitely long polymer chains at 34 GHz are 12 $cm^2V^{-1}s^{-1}$ for PPV and 0.5 $cm^2V^{-1}s^{-1}$ for polythiophene. These values largely exceed the experimental mobilities of 0.43 $cm^2V^{-1}s^{-1}$ and 0.02 $cm^2V^{-1}s^{-1}$. This large difference is most likely due to the finite lengths of the polymer chains and the occurrence of polymerization defects. In particular, due to side reactions, polymer macromolecules can contain single or triple bonds instead of the normal double bonds. These polymerization mismatches disrupt the conjugated π-system and can act as reflecting boundaries for charge transport. The measured mobility of holes on PPV chains could be reproduced by taking chains consisting of 180 PV units. This effective (chemical) conjugation length is reasonable. Although the PPV chains used in the experiments consist of 800±400 phenylenevinylene units, they could contain up to ~2% polymerization defects, leading to a limited effective chain length for charge transport. The experimental hole mobility on polythiophene chains can be reproduced by calculations on chains consisting of 135 thiophene units. This chain length is not very different from those in the polythiophene sample, which have an average length of 55 thiophene units and a poly-dispersity index equal to 1.4.

A more detailed quantitative comparison of the experimental and calculated mobilities is hampered by the lack of knowledge of the precise shape of the distribution of the effective conjugation lengths in the polymer samples used. It should be noted that dynamic fluctuations in the polymer chains may increase the mobility, since monomer units that are initially perpendicular may rotate to a more planar conformation, which enables a charge to pass such a point after some time. Finally, another factor that has been neglected in the calculations presented here is the effect of substituents, which are present in both polymers studied experimentally. Substituents will alter the potential energy profile, which will result in a different amount of torsional disorder. Furthermore, the ionization potential of the monomer units which enter the simulation as the site energy ε_n, see Eq. 1, will also be affected by the presence of substituents.

A detailed understanding of the conducting properties of conjugated polymers requires information about the dynamic structure of the polymer chains. This information together with reliable theoretical models for charge transport will be useful to guide the development of organic opto-electronic devices and molecular wires with improved performance.

[1] A. J. Heeger, J. Phys. Chem. B **105**, 8475 (2001).

[2] F. C. Grozema, L. D. A. Siebbeles, J. M. Warman, S. Seki, S. Tagawa, and U. Scherf, Adv. Mater. **14**, 228 (2002).

[3] R. J. O. M. Hoofman, M. P. de Haas, L. D. A. Siebbeles, and J. M. Warman, Nature **392**, 54 (1998).

[4] F. C. Grozema, P. T. van Duijnen, Y. A. Berlin, M. A. Ratner, and L. D. A. Siebbeles, J. Phys. Chem. B **106**, 7791 (2002).

Sub-nano-second dynamics of proteins. MD simulations and inelastic neutron scattering

Mounir Tarek[¶] and D.J. Tobias[§]
[¶]*Equipe de chimie et biochimie théoriques,*
Unité mixte de recherche CNRS/UHP 7565, Université Henri Poincaré,
B.P. 239, 54506 Vandœuvre-lès-Nancy cedex, FRANCE.
[§]*Department of Chemistry, University of California*
Irvine, California 92697-2025 USA

Introduction

Detail understanding of the function of several proteins requires a good knowledge of their structure, energetics and dynamics at the atomic level. To probe the latter, inelastic neutron scattering (INS) has emerged as a powerful tool allowing the time-resolved study of motions taking place in the protein on the pico- to nano-second time scale. Because of experimental limitations, the technique has mainly been used to investigate the dynamics of proteins in powder environments. Usually, powder samples are used to balance the trade-off between maximal scattered neutrons flux and minimal data collection times. Recently, INS technique has been applied to probe the dynamics of proteins in solution. Pérez et al.(1) have shown that it is possible, through careful data processing to get information on the motions taking place in globular proteins for solution samples. Not long after, other authors have used neutrons to probe the dynamics of unfolded proteins(2, 3) and of protein complexes in solution(4)**.**

Pérez et al. (1) proposed an original treatment of the quasi-elastic neutron data (QENS) from proteins in solution. The authors take into account the overall motion of the protein - *i.e.* its overall translation and rotation- and assume that it is decoupled from the internal motion –motions and fluctuations taking place in the protein. The analysis of the data appears to indicate that at the length scale ($0.5\,\text{Å} \le Q \le 2.0\,\text{Å}$) and time scale ($\mathbf{t} \le 100\,\text{ps}$) covered by the experiment, the scattering contains a contribution from the motion of the protons due to the global motion of the protein. While some authors have considered such treatment of the INS data, the validity of the assumptions made remains unclear. For instance, the contribution from the overall motion has simply been ignored in several other subsequent studies (2).

We have recently used molecular dynamics (MD) simulations in comparison to INS experiments along the lines of previous simulations (5). We have considered powder samples and have shown that it is possible to reproduce quantitatively the neutron data, assessing hence the ability of current generation force-fields to capture the essence of protein internal dynamics, as well as their hydration water on the ~ 100 picosecond time scale(6-9). Here we present an extension of previous work to investigate the dynamics of proteins in solutions, at low to moderate concentrations. The aim is two fold: (1) provide support of the assumptions made in experiment for data reduction and (2) investigate in detail the protein internal dynamics. Ultimately, one would like to use the MD results to discuss the simple models used to fit the QENS data.

Methods

MD simulations produce phase-space trajectories that consist of the positions and momenta of all the atoms in the system as a function of time. Here, we focus on quantities related to incoherent neutron scattering measurements that probe motions of hydrogen atoms on picosecond time scales. Neutron spectroscopy experiments essentially measure the total dynamic structure factor, $S_{tot}^{meas}(\mathbf{Q},\omega)$, in which $\mathbf{Q}$ and $\hbar\omega$ are the momentum and energy transfers, respectively (10). For the systems under study, and because the incoherent scattering length of hydrogen is an order of magnitude larger than the scattering lengths of all

the other atoms in proteins and water molecules, $S_{tot}^{meas}(\mathbf{Q},\omega) = S_{inc}^{meas}(\mathbf{Q},\omega)$, the incoherent dynamical structure factor. $S_{inc}(\mathbf{Q},\omega)$ may be written as the Fourier transform of a time correlation function, the "intermediate scattering function," $I_{inc}(\mathbf{Q},t)$:

$$S_{inc}(\mathbf{Q},\omega) = \frac{1}{2\pi}\int_{-\infty}^{\infty} I_{inc}(\mathbf{Q},t)e^{-i\omega t}dt \quad (1); \qquad I_{inc}(\mathbf{Q},t) = \frac{1}{N}\sum_j \left\langle e^{i\mathbf{Q}\cdot\mathbf{r}_j(t)} e^{-i\mathbf{Q}\cdot\mathbf{r}_j(0)} \right\rangle$$

(2)

Here $\mathbf{r}_j$ is the position operator of atom *j*, or, if the correlation function is calculated classically, as in an MD simulation, $\mathbf{r}_j$ is a position vector, and the angular brackets denote an average over time origins and scatterers. $I_{inc}(\mathbf{Q},t)$ is computed from a MD trajectory and Fourier transformed (FT) to afford $S_{inc}(\mathbf{Q},\omega)$, taking into account the instrumental resolution.

Specification of $S_{inc}^{diff}(Q,\omega)$ requires models for the diffusive motions. QENS spectra for proteins and other disordered, condensed phase systems are often interpreted in terms of diffusive motions that give rise to an elastic line with a *Q* dependent amplitude, and a series of Lorentzian quasielastic lines with *Q* dependent amplitudes and widths, *i.e.*,

$$S_{inc}^{diff}(Q,\omega) = A_0(Q)\delta(\omega) + \sum_{i=1}^{n} A_i(Q)L_i(\Gamma_i(Q),\omega), \qquad L_i(\Gamma_i(Q),\omega) = \frac{1}{\pi}\frac{\Gamma_i(Q)}{\Gamma_i(Q)^2+\omega^2}$$

(3)

$L_i(\Gamma_i(Q),\omega)$ is a Lorentzian centered at ω = 0 with half-width-at-half-maximum $\Gamma_i(Q)$.
The amplitudes of the elastic scattering, $A_0(Q)$, the elastic incoherent structure factor, *e.g.* EISF, provides information on the geometry of the motion, while the line widths are related to the time scales (broader lines correspond to shorter times). The *Q* and ω dependence of these spectral parameters are commonly fitted to dynamical models for which analytical expressions for $S_{inc}^{diff}(Q,\omega)$ have been derived, affording diffusion constants, jump lengths, residence time scales, etc. characterizing the motion described by the models. (10)

We present results obtained for 4 globular proteins (Ribonuclease, Myoglobin, Lysozyme, α-lactobalbumin) in solution. The simulations were all initiated from crystal structures. For each system, the protein monomers were first solvated in a well-equilibrated water box. After energy minimization, a constant volume and temperature (300K) equilibration run was followed by constant pressure (1atm) and constant temperature (300K) runs.

Table1. Summary of the protein systems simulated.

Protein	PDB chain	Number of protein atoms	Protein molecular weight	Number of α helices domains	Number of β sheet domains	System size (X,Y,Z) [Å]^3	Number of water molecules
Ribonuclease A	7RSA (124)	1144	13674	3	9	57×52×40	3453
Lysozyme	194L (129)	1141	14296	4	3	56×48×78	6461
Myoglobin	1MBC (153)	1404	17184	9	0	57×52×40	3290
α-lactalbumin	1HML (142)	1102	16208	4	3	58×50×80	4655

Results

To estimate the contribution from the overall motion of the protein to the total scattering measured in the 100 ps time scale, we have calculated, for a wide range of *Q* values, $I_{inc}^{tot}(\mathbf{Q},t)$, the intermediate scattering functions computed directly from the

trajectories and $I_{inc}^{int}(\mathbf{Q},t)$, the intermediate scattering functions computed by taking-off the translational and rotational motion of the protein in the solvent, *i.e.* singling out the internal motion. The FT of $I_{inc}^{tot}(\mathbf{Q},t)$ and $I_{inc}^{int}(\mathbf{Q},t)$ correspond respectively to the spectra measured by experiments, and to the spectra resulting from the relative motion of the protons with respect to the protein (termed thereafter internal motion). The results reported in Figure 1 show that, in the hundred picosecond time scale, $I_{inc}^{tot}(\mathbf{Q},t)$ decay much more rapidly than $I_{inc}^{int}(\mathbf{Q},t)$, and that the corresponding structure factors are much broader.

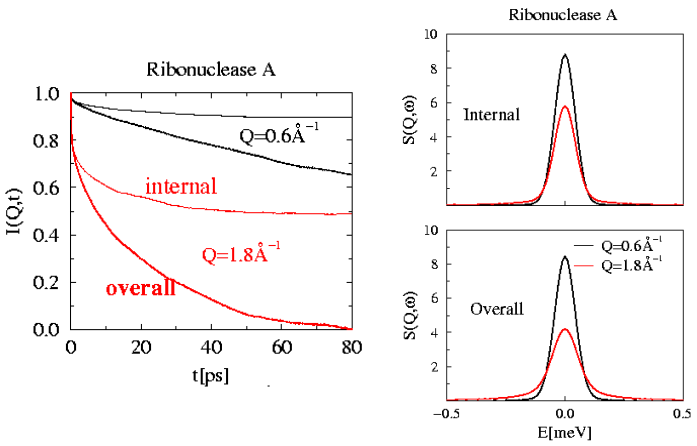

Figure 1. Total and internal intermediate scattering functions and corresponding dynamical structure factors $S_{inc}^{tot}(\mathbf{Q},t)$, *and* $S_{inc}^{int}(\mathbf{Q},t)$ *computed from the MD simulations of Ribonuclease A in solution at 300K, at Q = 0.6 and 1.8 Å^{-1} corresponding to overall and internal proton motion.*

Provided that the simulations reproduce quantitatively the overall motion of the protein in the solution, the present results show clearly that the scattering from a protein in solution, at the length and time scale studied here contains a substantial fraction due to the overall motion of the protein. The contribution from this motion may be analyzed by considering *R*, the ratio $I_{inc}^{tot}(\mathbf{Q},t)/I_{inc}^{int}(\mathbf{Q},t)$. For all proteins under study, the results indicate that in the 100 ps time scale, *R* decays exponentially *i.e* $R=\exp(\nu t)$. As ν displays a linear dependence on Q^2, the overall motion may be described as an effective diffusive motion with its corresponding diffusion coefficient, $D_{eff}=\nu/Q^2$. Therefore, the results support the model used by Perez *et al.* (1). Estimates from MD of the effective diffusion reported below are in good agreement with experiment (8.2 ± 0.2 10^{-7} for myoglobin, and 9.1 ± 0.2 10^{-7} cm^2/s for lysozyme).

Table2. Effective diffusion coefficients from MD simulations.

Protein	Mol. Weigth	D_{eff} (10^{-7}cm^2/s)
Ribonuclease A	13674	12.43
Lysozyme	14296	15.33
Myoglobin	17184	7.20
α-lactalbumin	16208	14.52

The internal dynamics has further been analyzed in terms of the gaussian-lorentzian model generally adopted by experimentalists (Eq. 3). Overall, we find that the MD results agree rather well with neutron data analysis by Perez *et al.* (1). The calculated EISF are very similar for all four proteins, and agree quantitatively with experiments mostly for the large *Q* values. For the initial Q range (0.5 Å^{-1}<*Q*<1 Å^{-1}), the EISF values are slightly larger (1-5 %) than those extracted from the QENS data.

Problematic and perspectives

One cannot confidently claim from the above results that the simulation did reproduce quantitatively the experiment. This may of course be related to the accuracy of the force field used, or to the simulation setup (sampling of multiple conformations for the protein,…). One should also keep in mind however the experimental limitations. Errors due to data treatment may contribute equally to the discrepancy. Indeed, one recalls that the measured spectra result from the scattering from the protein and from the solvent. It turns out that subtraction of the latter is rather complicated and often user-dependent. Bearing in mind this shortcoming, and based on previous results obtained for low hydration powder, where contributions from the solvent and from the overall protein diffusion are not an issue, one can claim that the simulations are rather "satisfactory".

The second step is now to afford a "real space" description of the motions of the protein atoms, and investigate how the models adopted by experimentalists are appropriate to describe such motion. In a typical experiment, it is difficult to "label" different protons to monitor independently their motion. It follows that one probe the motion of all non-exchangeable protons (the protein is immersed in a D_2O bath). On the other hand, the structure factor is an intensive quantity representing a scattering by atoms. Therefore, most if not all models used to describe the protein dynamics assume that mobile protons (those that give rise to a quasielastic signal in the time domain corresponding to the experimental resolution) have similar amplitudes and time scales of motion. The analysis of motion from MD simulations shows clearly that such model is inappropriate. Indeed, for proteins in solution, at room temperature, one finds that the protein is characterized by a very large heterogeneity of motions. In particular as shown in Figure 2, the amplitudes of motion (mean squared fluctuations) of different residues along the proteins can be as much as 5-10 fold different.

One interesting feature emerging from the simulation is the connection between the secondary structure and the amplitude of motions. Indeed, the results show, as expected, that the motions of atoms belonging to those residues implicated in highly structured regions of the protein (α-helices and β-sheets) are much less mobile that those attached to different part of the backbone, whether located at the surface of the protein or not. It is this kind of observation that should be somehow fed back in the experimental data analysis.

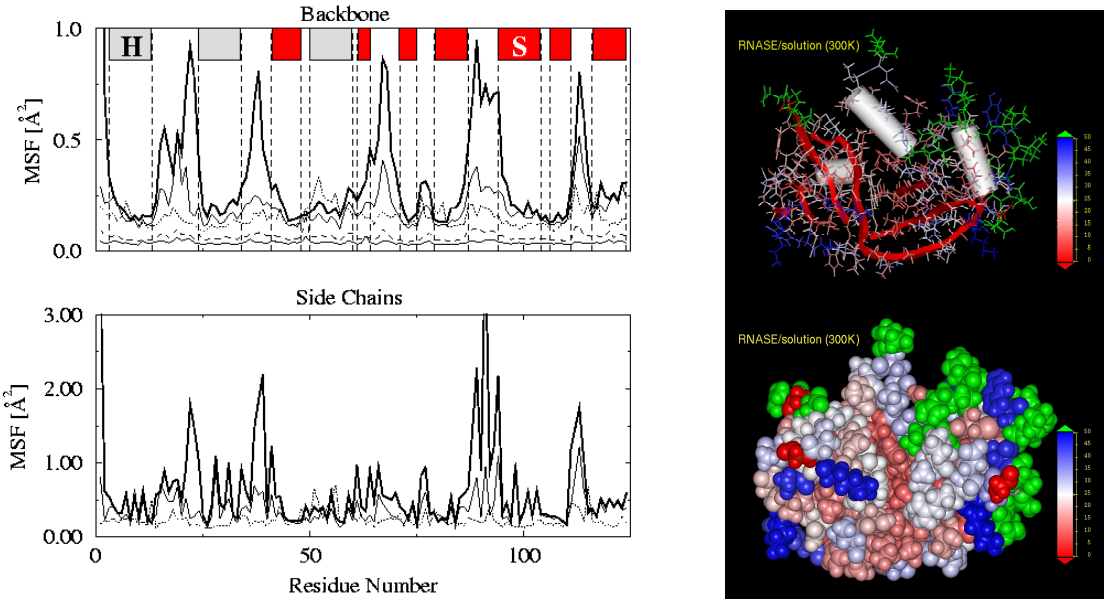

Figure 2. Mean squared fluctuations (MSF) of the backbone and the side chains atoms as a function of the residue number along the chain. From top to above the results for low temperature and low powder hydration simulations to high hydration powders at room temperature. The results for the solution simulations are reported in thick lines. The right panel represents a color code for the MSFs per residue for the Ribonuclease A in solution.

In summary, while classical MD simulations using current generation force fields allow to reproduce quite well the dynamics of proteins in a variety of environments, as probed by neutron scattering data, the full potential of such calculations is not yet taken advantage of. We have illustrated some examples where the simulation can be used to provide support for the models used by experimentalists and others where it is clear that further work is needed to extract the maximum information from QENS spectra. At any rate it is crucial that simulations and experiments on such complex systems go hand in hand, so that "raw data" may be compared, and all the experimental pitfalls overcome. It is only then that, based on comparison with neutron data on such complex systems, the "accuracy" of force fields used may be blamed for discrepancy, and intensive search for more sophisticated models (for instance by refinement of the force field parameters or by considering polarizable models) may be sought.

1. Pérez, J., Zanotti, J. M., and Durand, D. (1999) Evolution of the internal dynamics of two globular proteins from dry powder to solution. *Biophys. J.* 77, 454-469
2. Bu, Z., Neumann, D. A., Lee, S.-H., Brown, C. M., Engelman, D. M., and Han, C. C. (2000) A view of dynamics changes in the molten globule-native folding step by quasielastic neutron scattering. *J. Mol. Biol.* 301, 525-536
3. Bu, Z., Cook, J., and Callaway, D. J. E. (2001) Dynamic regimes and correlated structural dynamics in native and denatured alpha-lactalbumin. *J. Mol. Biol.* 312, 865-873
4. Gall, A., Seguin, J., Robert, B., and Bellissent-Funel, M. C. (2002) Membrane proteins in bulk solution can be used for quasielastic neutron scattering

studies: The case for the photochemical reaction center. *J. Phys. Chem. B* 106, 6303-6309

5. Smith, J. C. (1991) Comparisons of simulations with inelastic neutron scattering experiments. *Quart. Rev. Biophys.* 24, 227-291
6. Tarek, M., and Tobias, D. J. (1999) Environmental dependence of the dynamics of protein hydration water. *J. Am. Chem. Soc.* 121, 9740-9741
7. Tarek, M., Martyna, G. J., and Tobias, D. J. (2000) Amplitudes and frequencies of protein dynamics: an analysis of discrepancies between neutron scattering and molecular dynamics simulations. *J. Am. Chem. Soc.* 102, 10450-10451
8. Tarek, M., and Tobias, D. J. (2000) The dynamics of protein hydration water: a quantitative comparison of molecular dynamics simulations and incoherent neutron scattering experiments. *Biophys. J.* 79, 3244-3257
9. Tarek, M., and Tobias, D. J. (2001) Effects of solvent dumping on side chain and backbone contributions to the protein boson peak. *J. Chem. Phys.* 115, 1607-1612
10. Beé, M. (1988) *Quasielastic neutron scattering: principles and applications in solid state chemistry, biology, and materials science,* Adam Hilger, Bristol

Probing potential energy surfaces far from equilibrium

H.P. Trommsdorff

Laboratoire de Spectrométrie Physique, Université J. Fourier de Grenoble, CNRS (UMR5588), BP87, 38402 St Martin d'Hères Cedex, France

Introduction

The reliable establishment of potential energy surfaces (PES) of molecular systems is a central issue and a prerequisite for all molecular dynamics calculations. Minima of the PES represent equilibrium positions as observed in structural determinations, and the curvature around these minima determines the vibrational modes. To the extend that the harmonic approximation remains valid, the confrontation of data obtained from experiment and by numerical approaches is straightforward in these stable regions of the PES. This comparison is crucially important in order to establish the reliability of numerical methods as illustrated in the contribution of Mark Johnson [1].

The situation is more difficult far from equilibrium positions of the PES, in the regions of saddle points and of trajectories between stable configurations, important for all chemical dynamics. Here the harmonic approximation fails and the nuclear degrees of freedom are in general no longer separable. While calculations may still be performed for any nuclear configuration, the confrontation with experimental information is not direct. The observation of tunneling is the most sensitive and direct information available. For isolated small molecules high resolution vibration-rotation-tunneling spectra can be recorded, but even in this case, the calculation of spectroscopic data becomes complex beyond the first anharmonic corrections. For larger molecules and molecules in condensed phases, experimental data become more sparse, and the corresponding calculations less accurate.

Rigid body rotations, such as the reorientation of methyl groups, are notable exceptions in as far as these motions are often well described in a ID potential. In addition, coherent tunneling of methyl groups is readily measured, since the three-fold symmetry of the motion is due to the indiscernability of the protons and cannot be destroyed by any static or dynamic distortion of the environment. As the calculation of tunneling splittings in a 1D PES is straightforward, rotational tunneling has become an important probe of PES and a test of the quality of calculations of PES [2,3]. Deviations from 1D motions due to rotor-rotor coupling and rotation-nutation coupling are also well characterized [2,3,4]. Hardly any work, however, has been done on the coupling with other motions in excited rotational levels.

Theoretical approaches to tunneling in multidimensional PES

In general, the establishment of multidimensional PES, such as governing proton transfer between heavy atoms, is quite complex since the wide amplitude proton motion is coupled to a large number of small amplitude motions. This problem has been tackled in a recent novel theoretical approach using instanton methods [5]. This approach is based on the partitioning of the vibrational Hamiltonian in a separable part and a perturbation, which includes all potential and kinematic interactions between coordinates describing the tunneling motion and other transverse modes.

Tunneling splittings of vibration-tunneling levels of wide variety of non-rigid molecules with one wide-amplitude (tunneling) coordinate are obtained by expressing the extreme tunneling trajectory (red in the figure below) and the Euclidean action along this trajectory in terms of power series over coupling constants. For the values of coupling constants encountered in most systems, these monotonic series converge quite rapidly, so that the second-order expansion is sufficiently accurate for most calculations. The accuracy of the perturbative expansions is established by the determination of upper as well as lower bounds of tunneling splittings, obtained by using the straight line (green) and the minimum energy (blue) paths as zero order trajectories. The relevant regions of the PES around the tunneling trajectory are obtained from the knowledge of the geometry of the equilibrium positions of the PES (ground and transition states) and the curvature of the PES around these points. For moderate size molecules, quantum chemical calculations provide this information with sufficient accuracy, as demonstrated in illustrative calculations for a few prototype molecules.

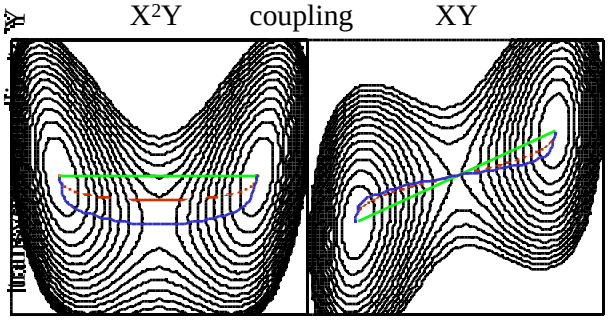

Representative 2D cuts of a multi-dimensional PES with two equivalent potential wells

In fact, even fairly low level calculations seem to reproduce the shape of the PES quite well, provided that the energy is scaled via a fit of the calculated to the experimentally observed ground state tunneling splitting.

The description becomes more complex, when several wide amplitude motions are involved [6]. The construction of any complete PES, is therefore still an area of active research in all these situations.

Experimental observations of tunneling in multidimensional PES

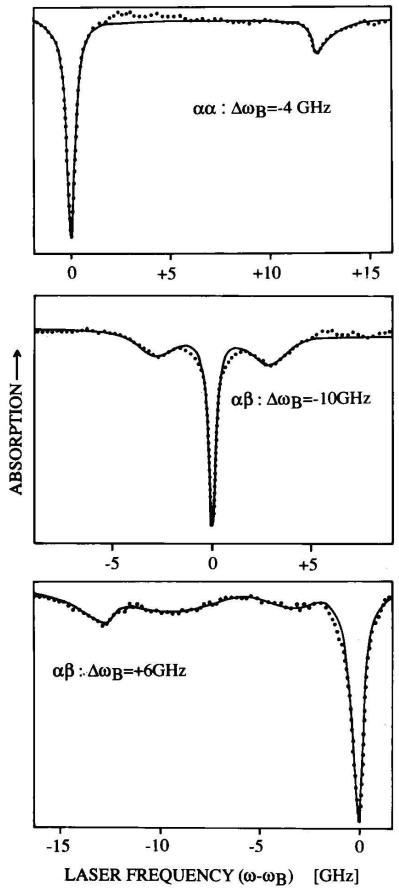

Aside from rigid body rotations, coherent tunneling is very rarely observed in condensed phases, since the environment induced asymmetry of an otherwise symmetric PES nearly always dominates the tunneling splitting. At low temperatures, the system is thus localized in the most stable configuration and tunneling splittings are no longer observable. At higher temperatures, dynamic fluctuations make the observation of small energy splittings altogether impossible. To my knowledge, the benzoic dimer crystal remains the only case in which coherent tunneling has been clearly observed and tunneling splittings were measured for intermolecular proton transfer [7].

Measurement (dots) of coherent proton tunneling in benzoic acid dimers by spectral hole burning. These spectra are analogous to inelastic scattering (e.g. Raman) spectra. The deep negative peak (central hole at zero frequency offset) marks the position of the exciting laser and the tunneling level structure is reflected in the side holes. From a fit (continuous line) of these spectra, the value of the tunneling splitting for one benzoic acid dimer is obtained as 8.4 GHz.

At higher temperatures, incoherent tunneling is readily measured in benzoic acid crystals by NMR methods and quasi-elastic neutron scattering, and this is the main reason why this system has become a prototype benchmark for proton transfer along hydrogen bonds [8,9,10].

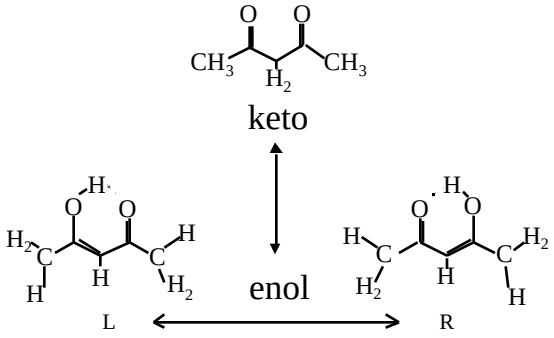

In the cyclic enol structure of acetyl-acetone, the interchange of the two tautomers involves in addition to an intramolecular proton transfer between the oxygen atoms a reorientation of the methyl groups, so that the reaction path involves three coupled wide-amplitude motions. In the crystal, intermolecular coupling of these coordinates leads to a low temperature phase transition, the full analysis of which is still an subject of investigation [11,12]. The size of the simulation

box required in any numerical analysis and the number of possible configurations to be considered, makes *ab initio* approaches impractical, while the accuracy of conventional force fields is insufficient.

Similar limitations are reached when investigating guest molecules in host crystals, such dimethyl-s-tetrazine in host lattices of durene and alcanes, for which rotational tunneling had also been characterized by laser hole burning techniques [13]. In these measurements information about the rotational potential of the methyl groups is also obtained for the excited electronic state of the guest. Even though in this case the intramolecular contribution to the potential is negligible and the main change of the potential stems from the geometry change of the guest, calculations fail to reproduce the data.

References

[1] M.R. Johnson, this workshop.
[2] M.A. Neumann, PhD Thesis, University of Grenoble (1999).
[3] M.R. Johnson, G.J. Kearley, Ann Rev Phys Chem. **51** (2000) 297.
[4] P. Schiebel, G.J. Kearley, M.R. Johnson, J. Chem. Phys. **108** (1998) 2375; G.J. Kearley, H.G. Buttner, P. Schiebel, Physica B: Cond. Matt. **276-278** (2000) 258.
[5] V.A. Benderskii, I.S. Vetoshkin, H.P. Trommsdorff, Chem. Phys. **271** (2001) 165, and references therein.
[6] V.A. Benderskii, E.V. Vetoshkin, E.I. Kats, H.P. Trommsdorff, Phys. Rev. A submitted.
[7] A. Oppenländer, Ch. Rambaud, H.P. Trommsdorff, J.C. Vial, Phys. Rev. Letters, **63** (1989) 1432.
[8] M. Neumann, D.F. Brougham, C.J. McGloin, M.R. Johnson, A.J. Horsewill, H.P. Trommsdorff, J. Chem. Phys. **109** (1998) 7300.
[9] M. Plazanet, N. Fukushima, M.R. Johnson, A.J. Horsewill, H.P. Trommsdorff, J. Chem. Phys. **115** (2001) 3241.
[10] M.R. Johnson, H.P. Trommsdorff, Chem. Phys. Letters, **364** (2002) 34.
[11] A. Geis, N. Jones, M.R. Johnson, A.J. Horsewill, H.P. Trommsdorff, ILL Annual Report 2001, 84-85, ILL (2002).
[12] M.R. Johnson, N.H. Jones, A. Geis, A.J. Horsewill, H.P. Trommsdorff, J. Chem. Phys. **116** (2002) 5694.
[13] M. Plazanet, A. Geis, M.R. Johnson, H.P. Trommsdorff, J. Lum. **98** (2002)197.

Recent advances in structure determination from low quality powder diffraction data

Steffen Wilke, Accelrys Ltd, 334 Cambridge Science Park, Cambridge CB4 0WN, GB

Introduction

Crystal structure determination frequently is a prerequisite for the rational understanding of the solid state properties of new materials. Moreover, many substances can crystallise in different polymorphic modifications – a subject of immense interest to pharmaceutical and petrochemical companies, since the control of biological and physical properties, and even patentability, depend critically on a thorough understanding of possible crystal structures. Even though single crystal diffractometry is the method of choice when it comes to crystal structure determination, this approach is often impractical because of the difficulties involved in growing single crystals of appropriate size. Sufficient quality powder samples, on the other hand, are much easier to obtain. Using direct-space structure solution techniques, increasingly complex crystal structures can nowadays be solved directly from powder diffraction data. Combined with the availability of easy-to-use software tools for model building and visualisation, crystal structure solution from high quality powder diffraction data has become more and more a routine task. In a number of important cases, however, powder data may be of low quality and structure solution using those standard techniques becomes significantly more difficult. In this contribution we discuss recent advances in structure determination achieved within the framework of Accelrys' Molecular Crystallisation Consortium. In particular, we concentrate on a new robust indexing algorithm X-Cell and on enhancements to the structure solution engine.

Methods

Direct space techniques for structure solution from powder diffraction data, such as Powder Solve [1] or other direct-space methods [2-6] are now well established. The Reflex Plus package [7], which Powder Solve is part of, is widely used in the pharmaceutical industry and has been thoroughly validated since its introduction in 1998 [1,8].

Direct space methods of structure solution from powder diffraction data generally proceed along the following steps: First, unit cell parameters have to be derived from the diffraction peak positions, a step known as indexing. Then, peak profile parameters, background parameters and the zero point shift of the diffraction pattern must be determined by Pawley refinement, since these parameters are required for the simulation of powder diffraction patterns from trial structures. In addition, a list of likely space groups needs to be established and the molecular fragments or atoms in the asymmetric unit have to be defined. In the structure solution process generated driven by a global optimisation algorithm, tens of millions of trial crystal structures are generated in order to locate the crystal packing optimising the agreement between the simulated and experimental diffraction pattern. After a structure solution has been found it is usually subjected to a final Rietveld [9] refinement to optimise all diffraction and structural parameters. In the following we discuss two steps in more detail: Indexing and structure solution.

Indexing

With the development of more and more powerful direct-space algorithms for structure solution, powder indexing increasingly becomes the new bottleneck for crystal structure determination from powder diffraction data. A variety of indexing algorithms are currently in use: some of the most common are ITO [10], TREOR [11] and DICVOL [12]. Most of them have been developed many years ago and were designed for the relatively limited computer resources available at the time. Different indexing programs have different strength and weaknesses. It is not uncommon that some are able to index a pattern while others fail. To increase the overall chance of success, often a powder pattern is indexed with a number of different algorithms. While this

approach certainly has its merits, it is by no means equivalent to an exhaustive and systematic search of the space of possible unit cells.

It is important to understand the reasons why existing indexing algorithms frequently fail. One more obvious reason is the zero-point shift, a constant offset of the experimentally observed peak positions. If the zero-point shift is too large, it needs to be taken into account explicitly or indexing is impossible. Impurity peaks, i.e. reflections that cannot be attributed to the unit cell of the main crystalline phase, present another obvious difficulty. While TREOR and ITO are able to tolerate impurity peaks, a single impurity peak is often sufficient to make indexing with DICVOL impossible. One important reason for failure is rarely addressed. Due to strong peak overlap, preferred orientation or poor statistics, decisive reflections may not be observed experimentally and/or accurate peak positions may be difficult to obtain. In such cases, which occur rather frequently in an industrial working environment, the correct unit cell is hidden among a mass of incorrect solutions with similar figures of merit.

In order to address those difficulties, a completely new algorithm has been developed and implemented in the X-Cell program package [13]. X-Cell makes use of systematic absences to facilitate the search for possible indexing solutions. It performs a complete search of unit cell space, going from cells with low numbers of calculated reflections to cells with high numbers of calculated reflections. A choice of impurity tolerance levels allows to specify the maximum number of reflections which may not be indexed. The search is carried out such that more likely solutions are considered first. For a given number range of reflections, a given pattern of systematic absences and a given impurity tolerance level, an exhaustive search is performed using a successive dichotomy procedure. The zero-point shift is determined as part of the indexing process. All indexing solutions are fully optimised, compared and ranked according to a special figure of merit. A multi-step procedure can be used to index long and flat unit cells.

All validation results obtained so far indicate that X-Cell has a high success rate and copes very well with the various difficulties that are typically encountered in powder indexing, including contamination with impurity phases, strong peak overlap, peak positioning errors, zero-point shifts and extreme cell geometry. Many powder diffraction patterns have been indexed with X-Cell over the past few months at Accelrys that could not be indexed previously.

Using X-Cell, some fundamental reasons remain why indexing may still fail. If the data quality is too low, the correct unit cell may be hidden far beyond the feasibility limit among a mass of incorrect solutions and never be reached. Even if the correct unit cell is generated by X-Cell and added to the list of indexing solutions, it may not be recognised as the correct solution. New methods, likely to be based on full-profile comparison and probability theory, need to be developed to identify the correct unit cell among a limited number of possible solutions. Even if the data quality is excellent and virtually all diffraction peaks are observed, indexing with the current implementation of X-Cell will fail if the amount of impurity peaks exceeds the allowed maximum of about 50%.

Structure solution

Structure solution with Powder Solve has been shown to be successful for a wide variety of molecular compounds, including solvates, salts and crystals with more than one molecule in the asymmetric unit [1,8,14]. In our initial validation work [1], 14 known crystal structures with up to 18 degrees of freedom were solved again from powder diffraction data. In an independent study, Powder Solve was used to solve the previously reported structures of papaverine hydrochloride and erythromycin A dihydrate [8].

Despite this success the method could not be applied in cases where the powder showed a large degree of preferred orientation. When solving crystal structures from powder diffraction data, it is usually assumed that the orientations of the crystallites in the powder sample are randomly distributed. However, this is not always true. Many compounds form plate- or needle-like crystals that tend to align with respect to the walls of the sample holder, thus leading to a loss of isotropy. This effect, known as preferred orientation, modifies the intensity distribution of the observed diffraction peaks. If not corrected for, even a moderate degree of preferred orientation can make structure solution impossible. To enable structure solution in the presence of preferred

orientation, the Powder Solve algorithm has been modified and it is now possible to determine preferred orientation parameters and structural degrees of freedom simultaneously.

The feasibility of the approach was verified by solving the crystal structures of three polymorphs of (E)-2-(4,6-Difluoroindan-1-ylidene) acetamide from powder diffraction data [14]. The crystal structures of the three polymorphs, previously determined by single crystal diffractometry, reveal pronounced one-dimensional hydrogen bonding schemes, thus explaining the tendency to form plate- or needle like crystals. Diffraction patterns were recorded using Cu K_α radiation and a flat spinning sample holder. All three powder diffraction patterns were strongly affected by preferred orientation, certain peak intensity ratios being modified by as much as a factor of 50.

Another common reason for failure of structure solution from powder data is that the powder pattern does not contain sufficient information for a successful structure solution. This may not only be due to the poor quality of the powder pattern showing a large number of broad, overlapping peaks. Preferred orientation of crystallites as discussed above obviously reduces diffraction information from certain spatial directions. Other reasons are the existence of a large number of structural degrees of freedom or high symmetry of the crystal packing reducing the number of peaks due to systematic absences. If structure solution is attempted in those cases using just powder data, typically a large number of solutions with similar good agreement between the simulated and experimental powder pattern are obtained. Some of these solutions (often those with the best agreement) will be chemically unreasonable. For example they may contain a large number of undesirable close contacts between structural fragments.

A possible way to overcome this problem is to add additional chemical information to the structure solution process [15,16]. The correct solution now has to simultaneously meet two different (and possibly conflicting) objectives: (i) the simulated pattern has to match the experimental diffraction data and (ii) the potential energy associated with the chemical information has to be close to its global minimum. One of the most basic pieces of chemical information that can be incorporated into a structure determination is the fact that viable solutions will not contain overlapping atoms. More complex requirements (connected with a significant computational cost), as for instance expressed by a low potential energy of a simple force field, may be considered equally well. Currently, Powder Solve allows adding a close contact penalty to the figure of merit. During the global optimisation step a combined figure of merit is optimised. It is defined as a linear combination of the normally used R_{wp} factor and an energetic contribution expressing a close contact penalty. Using this new combined figure of merit during structure optimisation removes configurations with bad contacts from the set of possible solutions very effectively. As a result, it may be possible to solve crystal structures, even in cases where the powder data alone do not contain sufficient information to locate the correct solution.

Perspectives

Over the last five years structure solution from powder diffraction pattern has made significant progress. It has evolved from an expert tool applicable to a small number of model systems to a routine method accessible to non-expert modellers and capable of solving the structure of a wide variety of commercially relevant substances. The obvious challenge is to extend its applicability to crystal structures of larger and more flexible molecules.

However, this technique has its fundamental limitations. It cannot be applied if only very poor powder diffraction data are available or in the case of polymorph screening, where the existence of all metastable crystal structures is not even known. The latter case is of extreme commercial importance: a particular drug substance may crystallise into multiple crystal structures which differ in important material properties such as colour, taste, solubility, rate of dissolution etc [17]. Ab-intio prediction of possible polymorphs using computational techniques is notoriously difficult and only recently reached a stage where it becomes applicable to a selected range of commercial interesting structures. Over the years, Accelrys developed the Polymorph Predictor technology [7,17] to aid polymorph screening. It is based on force-field energies and searches for energetically favourable packing arrangements. Even in cases where no experimental powder

pattern is available, or where the powder pattern is of poor quality, this approach can often elucidate the crystal structure and/or a limited number of potential polymorphic modifications. We feel that one of the greatest challenges in structure determination of molecular crystals over the next years is to further progress polymorph prediction [18].

Acknowledgement

The work presented in this contribution summarizes the efforts of a large team of researches and developers at Accelrys. The work has been greatly supported by the members of Accelrys' Molecular Crystallisation Consortium.

References

[1] G. E. Engel, S. Wilke, O. König, K. D. M. Harris and F. J.J. Leusen, *J. Appl. Crystallogr*., **32**, 1169-1179 (1999).

[2] K. D. M. Harris, R. L. Johnston and B. M. Kariuki, *Acta Cryst.* **A54**, 632-645 (1998).

[3] W. I. F. David, K. Shankland and N. Shankland, *J. Chem. Soc. Chem. Commun*., 931-932 (1998).

[4] A. A. Coelho, *J. Appl. Cryst*., **33**, 899-908 (2000)

[5] H. Putz, J. C. Schön and M. Jansen, *J. Appl. Cryst*, **32**, 864-870 (1999)

[6] Y. G. Andreev, P. Lightfoot and P. G. Bruce, *J. Appl. Cryst*., **30**, 294-305 (1997)

[7] Reflex Plus, Powder Solve, X-Cell and Polymorph Predictor are products of Accelrys Inc., 9685 Scranton Road, San Diego, CA 92121-3752 USA.

[8] G. A. Stephenson, *J. Pharm. Sci.*, **89**, 958-966 (2000).

[9] H. M. Rietveld, H.M., J. Appl. Cryst., 2, 65-71 (1969).

[10] J. W. Visser, *J. Appl. Cryst.* **2**, 89-95 (1969).

[11] L. Eriksson and M. Westdahl, *J. Appl. Cryst.* **18**, 367-370 (1985).

[12] A. Boultif, and D. Louër, *J. Appl. Cryst.* **24**, 987-993 (1991).

[13] M. A. Neumann, *J. Appl. Cryst*., submitted (2002).

[14] M. A. Neumann, F. J. J. Leusen, G. E. Engel, S. Wilke and C. Conesa-Moratilla, *Int. J. Modern Physics B* **16**, Nos. 1&2, 407-414 (2002).

[15] H. Putz, J.C. Schoen, and M. Jansen, *Journal of Applied Crystallography*, **32**, 864-870 (1999).

[16] O.J. Lanning, S. Habershon, K.D.M. Harris, R.L. Johnston, B.M. Kariuki, E. Tedesco and G.W.Turner, *Chemical Physics Letters*, **317**, 296-303 (2000).

[17] P. Verwer and F.J.J. Leusen, in Reviews in Computational Chemistry, K.B. Lipkowitz and D.B. Boyd, Eds, Wiley-VCH:New York, Volume 12, pp.327-365 (1998).

[18] J. P. M. Lommerse, W. D. S. Motherwell, H. L. Ammon, J. D. Dunitz, A. Gavezzotti, D. W. M. Hofmann, F. J. J. Leusen, W. T. M. Mooij, S. L. Price, B. Schweizer, M. U. Schmidt, B. P. van Eijck, P. Verwer and D. E. Williams, *Acta Crystallogr., Sect. B* **56**, 697 (2000).